UNIVERSITY of OULU
OULUN YLIOPISTO

The Phosphatic chalk of the Mons Basin, Belgium

Petrography and geochemistry of the Ciply Phosphatic Chalk and implications on its genesis

Damien Jacquemin

2018

Acknowledgements

I would like to express my sincerest appreciation and gratitude to the following people and institutions that helped to make the completion of this study a possibility;

- Dr Sophie Decrée of the Geological survey of Belgium who assisted me during my two months of internship for the present study and guided me throughout the entire process of the study.
- Dr Jean-Marc Baele of the University of Mons who contributed to interesting discussion on the Mons Basin.
- Dr Michel Hennebert who helped in the retrieval of the Hyon borehole at the university of Mons.
- Thomas Goovaert of the Geological survey of Belgium who helped and assisted me for the preparation of the samples and the X-ray diffraction analyses.
- Dr Vincianne Debaille and the G-time laboratory of the University of Brussels for overseeing the geochemical analyses of the samples of this work.
- Dr Kari Strand of the University of Oulu who reviewed and commented my work.
- My wife for her support and caring love.

Abstract

The Ciply Phosphatic Chalk (CPC) has been exploited for its enrichment in phosphorus in the early part of the twentieth century to produce fertilisers. Regained interests stimulated new research to characterise the potential for rare earth elements endowment and propose a genetic model for the formation of this phosphate deposit. This work studied the CPC using scanning electron microscopy, X-ray diffraction, cathodoluminescence and geochemical analyses. New insights into the formation of the deposits have been obtained regarding the mode of formation of the deposit. First, the deposit clearly shows evidence of alternating phase of phosphatisation and reworking giving rise to the formation of phosintraclasts which are the dominant phosphatic grains of the deposit. Weak or moderate upwellings brought nutrients to the Mons Basin during a period of sea-level highstand. Negative Ce-anomaly and the presence of bioturbation strongly argue against the development of an important oxygen-minimum zone indicating a low-productivity system. In these conditions, Fe-oxyhydroxides might have played an important role in scavenging phosphorus from the water column to the sediment. Phosphatisation seems to have occurred in the sediment when supersaturation relative to francolite was reached in the sediment pore water. Reworking processes probably consisted of wave action during storms. The REE are hosted in francolite and possess an average ΣREE of 350 ppm for the Hyon borehole. Their shale-normalised patterns are similar to other Cretaceous phosphate deposits but also to Cambrian deposits of China which typically display negative Ce-anomaly and HREE depletion. Post-depositional processes are only evident for the "phosphatic sands" which are strongly enriched in both phosphorus and REE. Further studies should aim to better constrain the paleoenvironmental conditions of deposition using stable isotopic studies. LA-ICP-MS studies should be able to give interesting insights into the compositional variations of the phosintraclasts thus giving elements to better characterise the genetic model of the CPC.

Table of contents

1. Introduction:

The Ciply Phosphatic Chalk of the Mons area (southwest Belgium) was a significant source of phosphate for Belgium in the 20th century. The exploitation took place from the end of the 19th century until World War II. The "phosphatic sands" - with grades attaining 30-35 % P_2O_5 - were the first parts of the deposit to be used. They resulted from a weathering process of weak intensity (De Putter et al., 1999). Then, the phosphatic chalk with 8-10 % P_2O_5 was extracted in underground galleries and open quarries. Between 1880 and 1945, more than three million tons were mined from the entire phosphatic basin.

The phosphatic basin has an area of about 23 km². The phosphatic chalk generally exceeds 20 m in thickness and in some places attains 76 m. Resources were evaluated at 960 million tons of phosphatic chalk at a grade comprised between 5 and 10% P_2O_5. Out of those resources, 20 to 30 million tons with an average grade of 5-8 % P_2O_5 were considered a seemingly easy workable area (Robaszynski and Martin, 1988).

Phosphorus, rare earth elements (REE), phosphate rocks and 24 other materials are considered critical by the European Commission (European Commission, 2017). In this context, the Mons Basin and its potential as a phosphate and REE source regained interests. There has not been any study up to this day whose aim was the characterisation of the REE of the Mons Basin. Little effort has been made to produce a model of the formation of the deposit. The only published model existing is the one of Poels and Robaszynski (1988). Robaszynski and Martin (1988) put forward important elements for the source of phosphorus for the Mons Basin. However, there is a lack of a convincing model for the formation of the Ciply Phosphatic Chalk. Extensive scanning electron microscopy (SEM) accompanied by X-ray diffraction (XRD), cathodoluminescence (CL) and geochemical analyses of this study are part of the effort to better characterise the genesis of the deposit and its economic potential especially in REE.

This study includes a brief review of the mineralogy, geochemistry and sedimentology of sedimentary phosphorites followed by the existing data for the Ciply Phosphatic Chalk, the results of this study and the ensuing discussion.

2. Phosphorites and their mineralogy:

Phosphorus is present in most rocks in minor amounts. However, some rocks may possess unusual amounts of this element. Those that contain more than 18 % P_2O_5 are called "phosphorites" and may reach concentrations of up to 40 % (Glenn et al., 1994). The term "phosphate rock" is used for rocks with P_2O_5 smaller than 18 % (see Trappe, 2006).

2.1. Mineralogy of phosphorites:

Among more than 200 minerals species, the apatite family represents the most common form of minerals containing phosphorus. The apatite family is a calcium phosphate occurring in igneous, metamorphic and sedimentary rocks capable of various substitutions. Magmatic apatite is typically dominated by fluorapatite (Pufahl and Groat, 2017). In sedimentary rocks, the dominating mineral phase among the apatite family is francolite, a carbonate fluorapatite (CFA). Carbonate fluorapatite mostly displays cryptocrystalline to microcrystalline texture in sediments (Trappe, 2006). McConnell (1973) defined francolite to be a carbonate fluorapatite with more than one percent fluorine and appreciable amounts of CO_2.

The following formula has been used to represent CFA: $Ca_{10-a-b}Na_aMg_b(PO_4)_{6-x}(CO_3)_{x-y-z}(CO_3.F)_{x-y-z}(SO_4)_zF_2$ (Jarvis et al., 1994). Unaltered francolite typically contains 32 % P_2O_5, 52 % CaO, and 4 % F. It includes as well 1.2 ± 0.2 % Na, 0.25 ± 0.02 % Sr, 0.36 ± 0.03 % Mg, 6.3 ± 0.3 % CO_2, and 2.7 ± 0.3 % SiO_2 (Jarvis et al., 1994).

Along with francolite, minerals such as quartz and calcite are major components in most phosphorites deposits. Silica commonly occurs as opal-CT and chalcedony in the form of porcelanites and cherts (Jarvis et al., 1994). Numerous other phases are commonly present in phosphorites such as dolomite, glauconite, sulphides (pyrite), sulphates (gypsum), clinoptilolite, clay minerals (kaolinite, illite, smectites, palygorskite) and organic matter (Jarvis et al., 1994). The presence of these accessory phases has important implications for the extraction and beneficiation of a deposit.

2.2. Substitutions in francolite and substitution mechanisms in apatite:

A wide range of substitutions is made possible by the structure of sedimentary apatite. Therefore, they may potentially reflect the geochemical environment of precipitation or subsequent alteration during diagenesis or weathering (Trappe, 2006). Figure 1 presents the possible substitutions occurring in francolite. Of particular interest are the REE that substitute Ca^{2+}.

Constituent ion	Substituting ion
Ca^{2+}	**Na^{+}**, K^{+}, Ag^{+} **Mg^{2+}**, **Sr^{2+}**, Ba^{2+}, Cd^{2+}, Mn^{2+}, Zn^{2+} Bi^{3+}, Sc^{3+}, Y^{+}, REE^{3+} U^{4+}
PO_4^{3-}	**CO_3^{2-}**, **SO_4^{2-}**, CrO_4^{2-} **$CO_3 \cdot F^{3-}$**, $CO_3 \cdot OH^{3-}$, AsO_4^{3-}, VO_4^{3-} SiO_4^{4-}
F^{-}	OH^{-}, Cl^{-}, Br^{-} O^{2-}

Figure 1. Possible substitutions in francolite. Compositionally significant substitutions are indicated in bold (Jarvis et al., 1994).

It was reported that apatite crystals may contain up to 21 wt. % REE_2O_3 (Hoshino et al., 2015; Hughes et al., 1991; Roeder et al., 1987). There are four main mechanisms that have been proposed for the compensation of charges that accompanies the substitution of Ca^{2+} by REE^{3+} (and Y^{3+}) in apatite (Chen et al., 2002a, b; Cherniak, 2000; Comodi et al., 1999; Felsche, 1972; Fleet and Pan, 1995; Ito, 1968; Roeder et al., 1987; Rønsbo, 1989; Serret et al., 2000).

$$REE^{+3} + X^{2-} = Ca^{2+} + F^{-} \quad (1)$$

$$2\ REE^{3+} + (\text{vacancy}) = 3\ Ca^{2+} \quad (2)$$

$$REE^{3+} + Na^{+} = 2\ Ca^{2+} \quad (3)$$

$$REE^{3+}\ SiO_4^{4-} = Ca^{2+} + PO_4^{3-} \quad (4)$$

While mechanisms (1) and (2) are reported only in synthetic compounds, mechanisms (3) and (4) are generally observed in nature.

2.3. Geochemistry of francolite:

2.3.1. Major elements:

The geochemistry of unaltered francolite in sedimentary phosphate particles gives clues to the chemical environment of formation (Trappe, 2006). Because the major elements in francolite display only little variations compared to the unaltered francolite composition (see section 2.1 for details on the composition), they cannot be used in order to determine the environmental conditions during phosphogenesis (Trappe, 2006).

2.3.2. Trace elements:

Unlike major elements, trace elements have been used to determine trends to specific geochemical environments (see Trappe, 2006 and references therein). However, studies have shown that in non-reworked phosphorites trace element incorporation is distinctively controlled by fractionation processes during phosphate fabric formation. There is usually a significant difference between trace element composition of the phosphate components and the host sediment (Trappe, 2006).

In phosphorites deposits, uranium and phosphorus present a positive correlation (Burnett and Veeh, 1977). U^{4+} and Th^{4+} substitute Ca^{2+} in the apatite lattice (Gilinskaya 1991,; Gilinskaya et al., 1993). The incorporation of uranium is thought to occur in the initial phase of phosphogenesis (Jarvis et al., 1994). The contents of uranium were shown to be indicator of diagenesis (Starinsky et al., 1982) and a paleo-redox marker (Burnett and Gomberg, 1977). However, it has been pointed out that the U(IV) concentrations do not necessarily indicate anoxic conditions during precipitation (Jarvis et al., 1994).

2.3.3. Rare earth elements:

It was noted very early that phosphorites were enriched in REE (Trappe, 2006). The REE patterns were initially thought to reflect geochemical characteristics of the environment during formation (Trappe, 2006). Only a few of the phosphate occurrences display one of the natural seawater distributions described by Elderfield and Greaves (1982) and Bertram and Elderfield (1993) Ce- or Eu-anomaly and a heavy REE enrichment. This is true for both granular phosphorites and concretionary phosphorites. Three sources of REE have been

pointed out by Piper and Medrano (1995) for phosphorites: detrital, biogenic and authigenic. The discussion of this study deals more extensively on REE.

2.4. The source of phosphorus for phosphorite formation:

Although hydrothermal activity and submarine weathering of basalts at mid-ocean spreading centres directly provide phosphorus, it is in negligible amounts (Baturin, 1982). Instead of acting as a net input of phosphorus, these processes actually have a net output of phosphorus and act as a sink for marine dissolved phosphate. This proceeds from the scavenging of dissolved phosphate onto suspended iron oxyhydroxides derived from hydrothermal activity, and direct uptake of phosphate through reaction with basalt (Froelich et al., 1977; Froelich et al., 1982; Feely et al., 1990).

Weathering of continental rocks is the most important pre-anthropogenic source of phosphate (figure 2; Föllmi, 1996) and provides phosphorus to the oceans in two forms, dissolved and particulate (Benitez-Nelson, 2000; Filippelli, 2008, 2011). Once removed from rocks through mechanical and (bio-) chemical weathering, phosphate is transported by water through river systems. Phosphorus adsorbed on eolian dust is also an important supply in arid climates (figure 2; Drummond et al., 2015). Eolian phosphate occurs in the forms of mineralic dust particles, insect remains, pollen and spores, and leaf fragments. Once in the marine environment, about 15 to 50 % of total eolian phosphate is, or is made, bioavailable (Bentor, 1980; Duce et al., 1991).

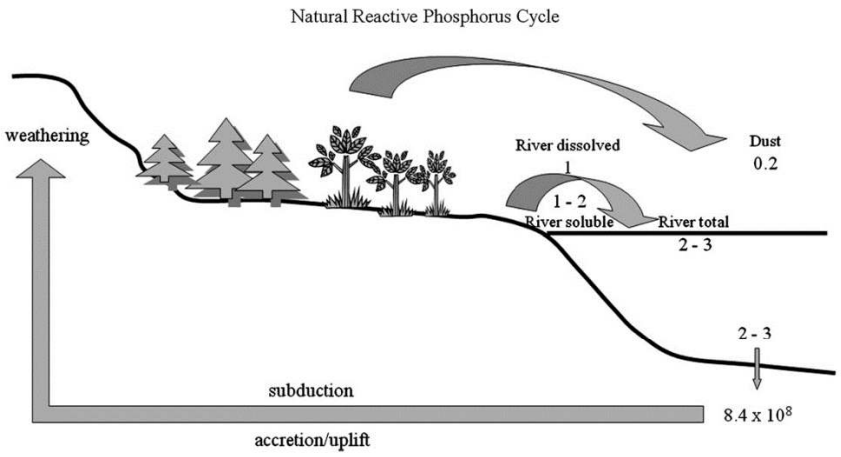

Figure 2. Natural cycle of reactive phosphorus. The phosphorus input to the oceans is from riverine and dust sources, output via sedimentation, and recycling via tectonics. Fluxes are in Tg P/year and sedimentary reservoir in Tg P (Filippelli, 2011).

Most of the particulate fraction of phosphorus consists of grains of insoluble igneous and metamorphic phosphatic materials that do not take part in the biogenic cycling of P, since it is not bioavailable. The particulate fraction that delivers bioavailable phosphorus consists of detrital organic matter, clay minerals and Fe-oxyhydroxides with adsorbed phosphorus (Filippelli, 2008). Redox changes and oxidation processes lead to transformation from particulate into dissolved phosphate phases and vice versa. This is frequently observed during temporary burial in river sediments and consequent reworking (Föllmi, 1996). The dissolved phosphate fraction, both organic and inorganic, appears usually in low quantities (around 10-25 µg/L; Meybeck, 1993).

Upon arrival to the marine environment, almost all reactive and bioavailable phosphate from river and eolian sources is used in the surface zone of primary productivity and incorporated into organic matter (Föllmi, 1996). Phosphate is then transferred to the deep ocean as partly aggregated organic matter and as dissolved inorganic phosphate. Most phosphate is reintroduced to the photic zone by upwelling processes where it is used by ecosystems. Only a small fraction, amounting to about 5 %, is removed from the ocean by sediment burial by incorporation into authigenic phosphate-bearing minerals among other forms (Berner et al., 1993).

Coastal upwellings have long been thought as the major process involved in phosphorite formation. It was first proposed that upwellings were the cause of direct precipitation of phosphate from seawater (Kasakov, 1937). Kazakov argued that during oceanic upwelling, a decrease in the partial pressure of CO_2, and an accompanying increase in pH of near-surface water, resulted in a decrease in the solubility of these waters with respect to marine apatite.

Although Kazakov suggested that phosphorites were formed in association with upwelling along continental margins, the underlying process of phosphorites formation is not generally accepted (Glenn et al., 1994). It is now widely believed that CFA precipitation is an indirect consequence of upwelling in modern settings, as well as in the rock record. Phosphorus is transferred to the sediment via organic matter or Fe-oxyhydroxides. It is then released from the organic matter by diagenetic degradation through microbial breakdown (Föllmi, 1996). Phosphorus is progressively concentrated in the pore water of the sediment and eventually CFA precipitates as an *in situ* diagenetic phase (Glenn et al., 1994).

2.5. Sedimentology of phosphorites:

2.5.1. Phosphogenesis:

The term 'phosphogenesis' takes into account all the processes of apatite precipitation which give rise to the formation of pristine (or orthochemical, *in situ*) phosphate fabrics (Trappe, 2006). Phosphogenesis occurs at the sediment/water interface and/or during diagenesis (Glenn et al., 1994). In most cases, apatite is not precipitated directly from seawater. Phosphogenesis is to be distinguished from the processes of phosphorites formation. These require additional processes such as winnowing, reworking, and sediment transport (Trappe, 2006). They typically lead to enrichment in P_2O_5.

Trappe (2006) describes phosphogenesis in sedimentary environments as a sequence of four succeeding main events. The first step is the supply of phosphorus and its liberation from organic matter. Because the availability of phosphorus in natural environments is very limited, an increased supply of phosphorus is required. The majority of the phosphorus is bound in organisms and in dead organic matter or is dispersed in shallow marine sediments. Moreover, phosphogenesis requires a decoupling of the phosphorus from organic matter to take place. The liberation of phosphorus from organic matter is the result of microbial degradation. Organic matter degradation occurs through a series of microbial-mediated redox reactions that are organised beneath the sea floor in order of decreasing energy production (Jarvis et al., 1994). Among those reactions, bacterial sulphate reduction is the most efficient (Arning et al., 2009).

The second step consists of the removal of phosphorus from biologic recycling. This can be done in a number of ways: (1) by rapid burial or microbial overgrowth (forming a seal at the sediment surface), (2) seasonal changes which affect the rate of bioproductivity and P-consumption, (3) shuttling of phosphorus into a deeper sediment layer (via Fe-pumping; see figure 3), or (4) phosphorus-fixation within microbial mats (Trappe, 2006). *Beggiatoa* and *Thioploca* are sulphur-oxidizing bacteria that trap phosphate that would otherwise escape from pore water to the seafloor (Reimers et al., 1990; Jarvis et al., 1994).

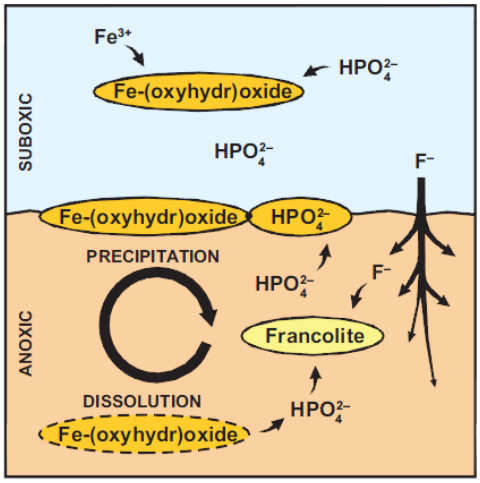

Figure 3. Cyclic precipitation of Fe-oxyhydroxide and its dissolution below the Fe-redox boundary during burial maintain high phosphate concentration. Francolite precipitation is limited by the availability of F (Pufahl and Groat, 2017). Pyrite may also form due to the release of Fe^{2+}.

The third step is the formation of a storage environment for phosphorus. For this environment to form, microbial decomposition rate needs to exceed the oxygen recharge. Oxygen depletion leads to decreasing bioproductivity and reduced phosphorus consumption. High organic matter deposition and stratification (to reduce oxygen recharge) are factors initiating the process. If these two driving processes are intensively developed, supersaturation with respect to francolite is reached relatively rapidly. If these conditions are poorly developed, supersaturation is reach through time (Trappe, 2006). When organic matter deposition is low, Fe-redox pumping can concentrate phosphorus to the state of supersaturation (figure 3; O'Brien et al., 1990; Heggie et al., 1990). Upon burial below the Fe redox boundary, adsorbed phosphate is released when Fe-oxyhydroxides dissolve in anoxic pore water. High phosphate levels are maintained by the re-adsorption of phosphate onto Fe-oxyhydroxides above the suboxic redox interface, which are then buried and dissolved to again release phosphate (Pufahl and Groat, 2017).

The fourth and last step is the formation of a precipitation site, and precipitation of solid-phase phosphate. There are two different reaction pathways that lead to apatite deposition in sediments (Van Cappellen, 1991). The first results in slow formation of apatite dispersed throughout the sediments. This is the result of the direct nucleation of apatite crystals, a kinetically very inefficient process (Krajewski et al., 1994). Phosphorite bodies on the other hand are explained by the initial, localized precipitation of a metastable precursor, creating a large number of crystallization sites. It is then replaced by apatite over time. It is not clear

whether microbial activity plays a role in the formation of apatite. However, the transformation of particulate phosphorus into active dissolved phosphate is presently the only unambiguous level at which microbial mediation is clearly driving apatite precipitation in sediments (Krajewski et al., 1994).

2.5.2. Phosphate depositional systems:

Several phosphate depositional systems exist and are subdivided based on the nature of their sedimentary environments (figure 4). Unique to the Precambrian are the peritidal phosphate deposits in coastal environments where thin stratiform orebodies formed parallel to the paleoshoreline (Nelson et al., 2010; Drummond et al., 2015). There is no Phanerozoic equivalent for this low-grade deposit type and was produced by microbial and abiotic phosphogenetic processes on tidal flats (Pufahl and Groat, 2017).

In the late Neoproterozoic and continuing into the Phanerozoic, phosphate deposits show higher P concentrations that were related to P-rich upwelling. Continental margin phosphate deposits formed when coastal upwelling was focused on the distal shelf (Pufahl, 2010). In this environment, bacterial processes both release and incorporate phosphate from pore water driving francolite precipitation in organic-rich sediment beneath the upwelling front (Froelich et al., 1979; Jarvis et al., 1994; Arning et al., 2009). Today, continental margin phosphatic sediments accumulate where favourable trade winds induce upwelling along western America, South America, and southern Africa. Along these coasts, economically significant Pleistocene and Miocene deposits formed under these conditions are exposed (Pufahl and Groat, 2017). Epeiric sea phosphate deposits formed in shallow inland seas with current systems that transported dissolved phosphate away from the entire platform. Among important eperic sea phosphorites are included the late Neoproterozoic Doushantuo Formation of China, the Permian Phosphoria Formation of the United States, and the Late Cretaceous-Eocene South Tethyan phosphorites province (Pufahl and Groat, 2017).

On Cenozoic carbonate atolls, insular phosphate occurrences formed in organic-rich lagoonal sediment and guano from nesting birds (Hill and Jacobson, 1989; Trichet and Fikri, 1997). Small high-grade deposits were formed by degradation of organic matter by bacterial processes and meteoric-water leaching of P (Pufahl and Groat, 2017). Ore grades are exceptionally high in these deposits, reaching on average 38 wt % P_2O_5 (Van Kauwenberg,

2010). Seamount phosphorites are formed when insular phosphorites are submerged beneath the sea surface. However, in most cases they form independently from insular phosphorites at low latitudes in response to equatorial upwelling.

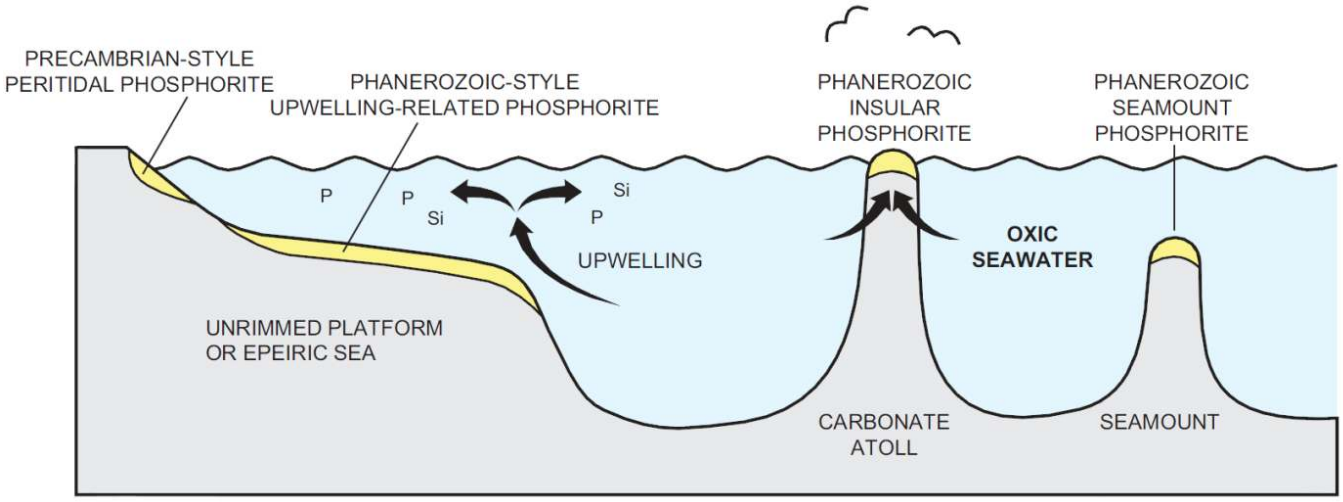

Figure 4. Phosphorite depositional environments. Large deposits form on passive continental margins with associated coastal upwelling. From Pufahl (2010).

2.5.3. Primary phosphorites:

In the sedimentology of phosphorites and phosphate rocks, two main types are distinguished based on the genetic processes that formed them (figure 5). First, primary phosphate rocks or phosphorites are defined as precipitates composed of CFA minerals formed physico-chemically or biochemically *in situ* in the marine environment and show little evidence for significant transportation (Glenn et al., 1994). They can occur in different forms such as primary phosphorites mud, hardgrounds, concretions or nodules, micro-concretions in mud and as lenses and layers in encasing sediments (see Glenn et al., 1994 and references therein). Most pristine facies are subeconomic containing around 2 and 10 wt % P_2O_5 (Pufahl and Groat, 2017).

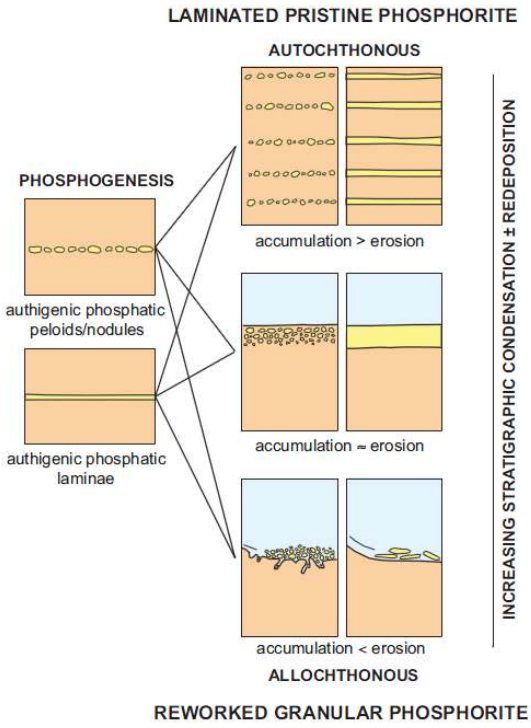

Figure 5. Classification of phosphorites. Granular phosphorites result from stratigraphic condensation and redeposition of *in situ* authigenic phosphatic peloids/nodules derived from pristine/primary phosphorites. From Pufahl and Groat (2017).

A way phosphate commonly precipitates is as stratiform and/or concretionary association of microcrystallite (Glenn et al., 1994). This is attested by the occurrence of "mudstone phosphorites" in Vendian deposits of Mongolia (Ilyin and Ratnikova, 1981), Middle Cambrian phosphorites of Georgina Basin, Australia (Soudry and Southgate, 1989), in the Miocene of Florida (Riggs, 1979a, 1979b), etc.

2.5.4. Granular phosphorites:

Granular phosphorites (figure 5) consist of variously cemented phosphorites siltstones, sandstones and sometimes conglomerates, composed mainly of phosphatic particles, many of which show some evidence of transport and deposition under the influence of bottom currents (Glenn et al., 1994). Syndepositional processes such as winnowing, transport, and redeposition of phosphatic peloids and grains produce P-rich grainstones and lags that are primary exploration targets, reaching up to 35 wt % P_2O_5 (Van Kauwenbergh, 2010).

The most desirable phosphate deposits consist of the amalgamation of granular storm beds that form the thickest sequences (Grimm, 2000; Pufahl et al., 2003). Storm strength, duration, and frequency are critical for controlling the grade and thickness of many high-grade granular phosphorites beds (Pufahl and Groat, 2017). In deeper environments that are below the storm-wave base, the only reworked lithofacies other than winnowed lags from contourites are phosphatic turbidites (Grimm and Föllmi, 1994).

2.6. Worldwide phosphorites distribution, production and reserves:

Phosphate deposits can be found worldwide as igneous and sedimentary deposits (figure 6). The world's largest igneous phosphate deposits are the Devonian Khibina Alkaline Complex in Russia's Kola Peninsula. There are four operating mines that produced 12.50 Mt or 58 % of all igneous phosphate rock production in 2015 (Pufahl and Groat, 2017). Around 31 % of igneous phosphate rock production was produced in Brazil and 10 % in South Africa in 2015 (Jasinski, 2016). Interestingly, South Africa hosts the largest reserves of igneous phosphate rock (1500 Mt; table 1) while being a rather small P producer.

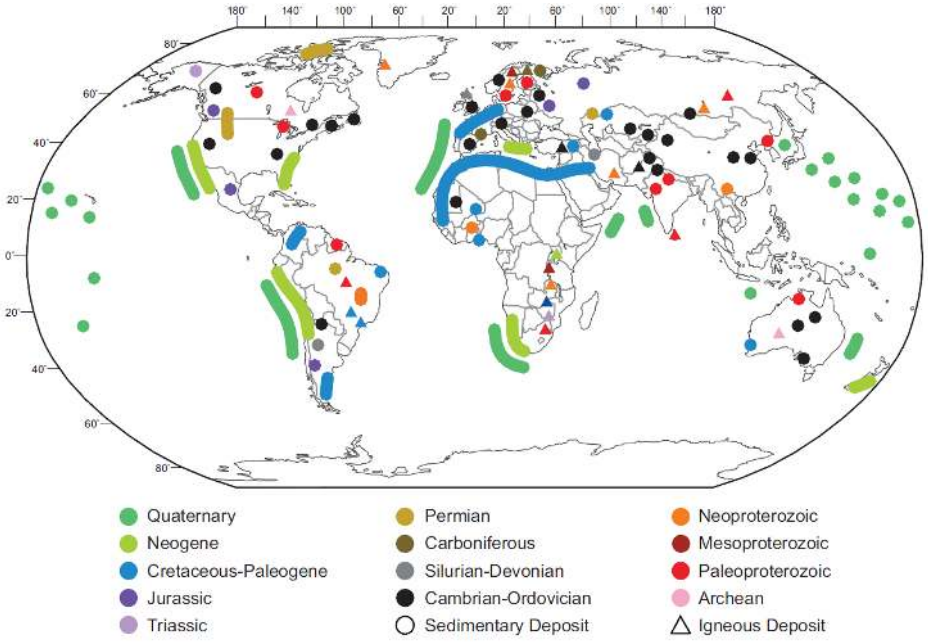

Figure 6. Worldwide distribution of igneous and sedimentary phosphorites with respective ages. From Pufahl and Groat (2017).

Sedimentary phosphate deposits are by far the most exploited phosphate rock type (table 1; Jasinski, 2016; Pufahl and Groat, 2017). The largest economic sedimentary deposits occur in North Africa and the Middle East, China, and the United States (table 1). The Late

Cretaceous-Eocene South Tethyan phosphogenic province, which includes the North African and Middle Eastern phosphorites, is the largest accumulation of phosphate on Earth and host to over 85 % of the world's known P reserves (Pufahl et al., 2003; Jasinski, 2016). The late Neoproterozoic Doushantuo Formation accounts for 45 % of the world's P production while possessing only around 5 % of global reserves (Jasinski, 2016). The famous Permian Phosphoria Formation provides about 10 % of the United States' P production (Pufahl and Groat, 2017).

	Mine production		
Country	2014 (Mt)	2015 (Mt)	Reserves (Mt)
Igneous phosphorites			
Brazil	6.04	6.70	315
Russia	11.00	12.50	1,300
South Africa	2.16	2.20	1,500
Total	19.20	21.40	3,115
% of world	8.80	9.59	4.53
Sedimentary phosphorites			
Algeria	1.50	1.20	2,200
Australia	2.60	2.60	1,030
China	100.00	100.00	3,700
Egypt	5.50	5.50	1,250
India	1.11	1.10	65
Iraq	0.20	0.20	430
Israel	3.36	3.30	130
Jordan	7.14	7.50	1,300
Kazakhstan	1.60	1.60	260
Mexico	1.70	1.70	30
Morocco/W. Sahara	30.00	30.00	50,000
Peru	3.80	4.00	820
Saudi Arabia	3.00	3.30	956
Senegal	0.90	1.00	50
Syria	1.23	0.75	1,800
Togo	1.20	1.00	30
Tunisia	3.78	4.00	100
United States	25.30	27.60	1,100
Vietnam	2.70	2.70	30
Other countries[1]	2.37	2.60	380
Total	198.99	201.65	65,661
% of world production	91.20	90.41	95.47
World total, all sources	218.19	223.05	68,776

Table 1. World phosphate production and reserves. From Pufahl and Groat (2017).

3. Geology of the Mons Basin:

3.1. Geological settings :

The Ciply Phosphatic Chalk (CPC) represents a facies developed during Cretaceous times in the Mons Basin, which was a gulf at the north-eastern margin of the then Paris Basin Sea (Robaszynski and Martin, 1988). Its direction is parallel to that of the Variscan front and is lying on the folded and eroded Westphalian Brabant Parautochthon (Robaszynski and Martin, 1988). The CPC is preserved in two areas: the Ciply area and the Baudour area. They are generally covered by Late Cretaceous and Tertiary-Recent sediments (Robaszynski, 1984).

The Paleozoic basement consists of thick Carboniferous formations of the Brabant Parautochton and Haine-Sambre-Meuse Overturned thrust sheets dipping to the south. Dinantian carbonates lie at ca. 2000 m under the Mons Basin and outcrop to the north. On the northern rim of the basin, Namurian siliciclastics are exposed and most of the overlying >1500 m-thick Westphalian coal measures are concealed under the Meso-Cenozoic cover. Lower Devonian siliciclastics (Ardennes Allochthon) are uncomformably overlying the Carboniferous (Midi fault) to the south of the Mons Basin (Baele and Hennebert, 2016).

It is a subsiding area where up to 300 m thick sediments accumulated during the Meso-Cenozoic. Subsidence mechanisms are attributed to evaporite dissolution (Visean evaporites have been discovered in the borehole of Saint-Ghislain; Baele and Hennebert, 2016). Moreover, the subsidence of the Mons basin coincides with the Hainaut Trough in which, during the Dinantian, thick evaporites were accumulated (Dupuis and Robaszynski, 1986). Some suggested that the Mons basin underwent a pull-apart process. This mechanism was observed in the “La Malogne” underground quarry, where synsedimentary tectonic features are well developed (Vandycke et al., 1991).

Different pulses of transgression-regression phases are recorded by the Meso-Cenozoic lithological sequence of the Mons Basin. The first pulse consists of the Haine Group (Barremian – Aptian, or “Wealden” facies) with continental siliciclastics. The maximum flooding occurred in the Turonian where there is good lateral and vertical continuity, and more carbonate in the sedimentation. The thickest sedimentary sequence in the Mons Basin is the Chalk Group (Coniacian to Maastrichtian). The sedimentation was dominated by

shallow carbonate and then by siliciclastics during the Cenozoic (Baele and Hennebert, 2016).

In the Ciply area, the CPC occurs as a lens lying on the southern flank of a syncline and dipping to the north (figure 7). Its thickness varies from several meters at the southern border to a little more than 70 m at the axis of the lens (figure 8). One hundred meters separate the surface from the top of the Phosphatic Chalk at the axis of the synclinal structure. The CPC lies generally on the Spiennes white chalk and is overlain by the Saint Symphorien Tuffeau (a calcarenite of Late Maastrichtian age; Robaszynski and Martin, 1988).

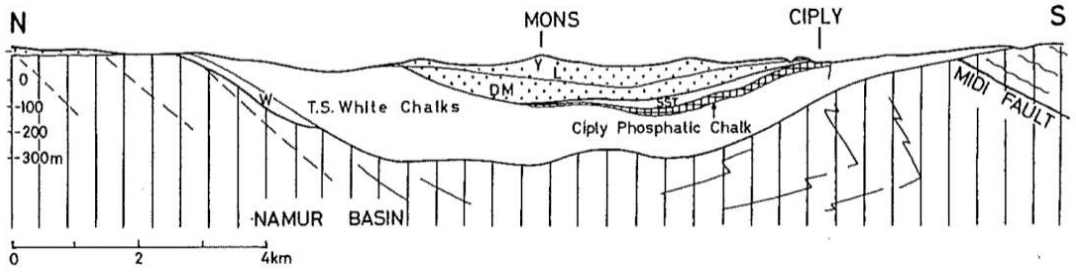

Figure 7. North-south geological section of the Mons Basin. W: Wealden facies; TS: Turonian-Senonian white chalk; SST: Saint-Symphorien Tuffeau; DM: Danian and Montian; L: Landenian; Y: Ypresian. From Robaszynski and Martin (1988).

Figure 9 presents details about the variation in thickness of the phosphatic formation based on seven old quarries and the Hyon drill hole. We observe an increase of the thickness from the south to the north. It can also be noted that chert beds are present in the thickest part, but they are not present in the southern part (Robaszynski and Martin, 1988).

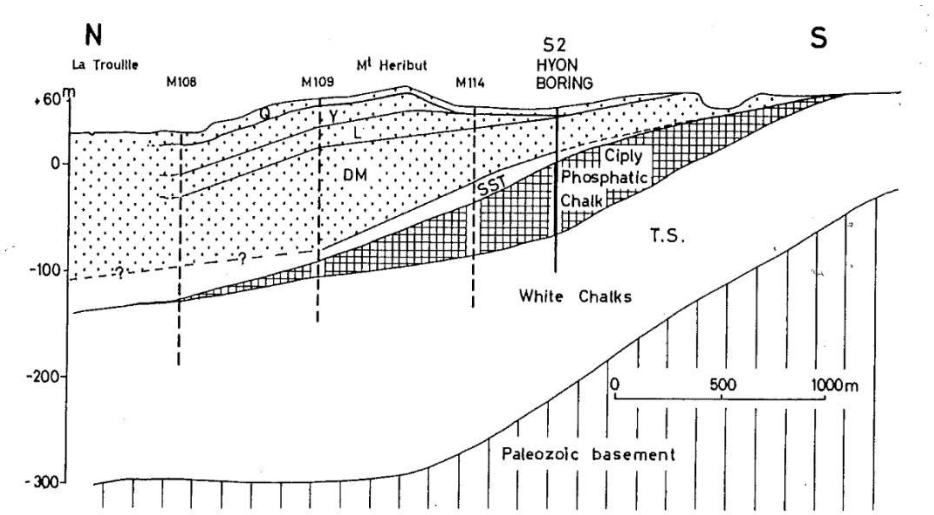

Figure 8. Details of the southern part of the section presented based on data given by three old borings (M108 to 114) and the Hyon boring and showing the lenticular feature of the phosphatic basin. From Robaszynski and Martin (1988).

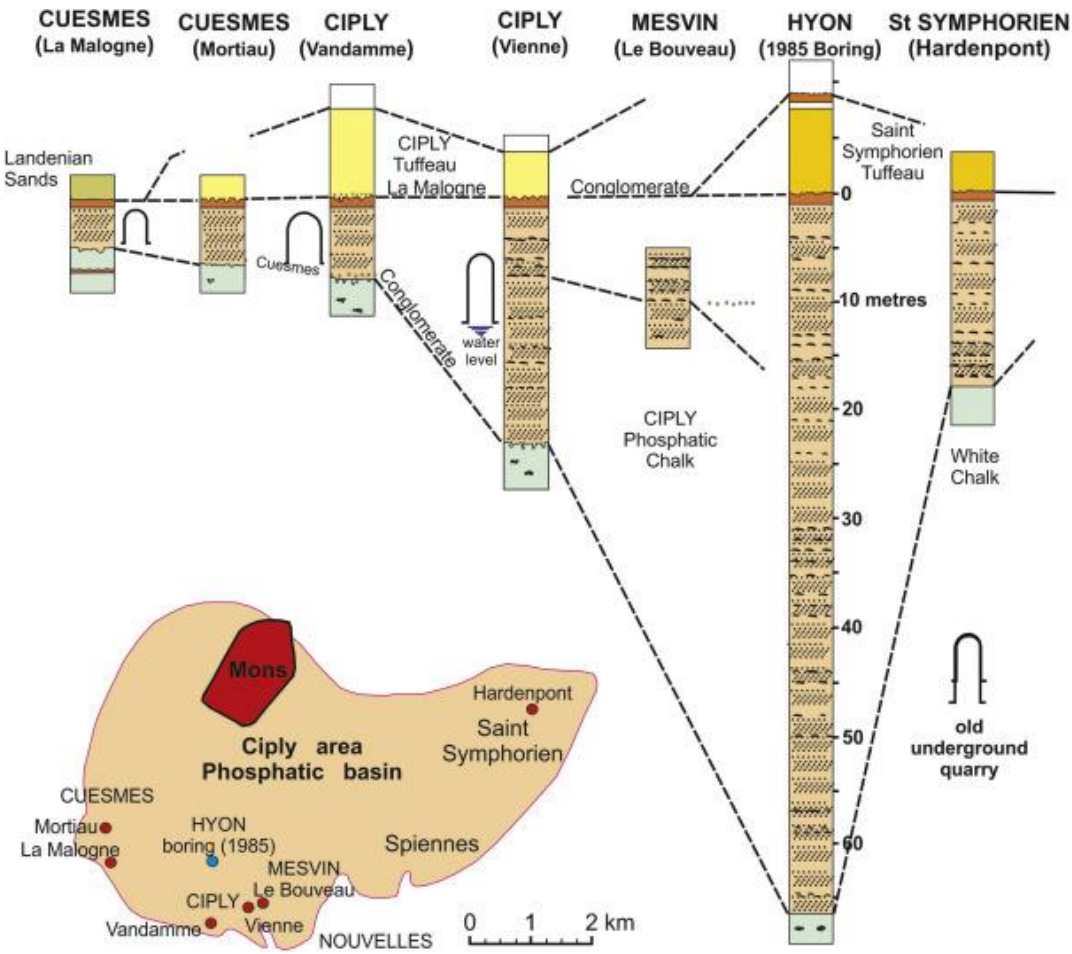

Figure 9. Variation in thickness of the Ciply Phosphatic Chalk from six lithological outcropping sections and one borehole from the southern to the eastern border of the Ciply area. From Mortimore et al. (2017).

3.2. La Malogne underground quarry:

La Malogne underground quarry is located on the border of the Mons basin to the west (figure 9). The Ciply-Malogne Formation is overlying the Spiennes Formation. Between these two formations is intercalated the Cuesmes Conglomerate (figure 10; Baele and Hennebert, 2016). Kilometres of galleries are spreading through the Maastrichtian phosphatic chalk. Flints are virtually absent from the Malogne Quarry. A thick hardground caps the phosphatic chalk. It is intensely burrowed and covered with a fossiliferous phosphatic conglomerate (*Poudingue de la Malogne*). Its thickness varies laterally, and it can grade into a firmground (the cemented zone is no longer continuous but nodular). The geometry of the galleries reflects the discontinuity of the hardground. Where the hardground is well-developed, the gallery shows a square cross section whereas when the hardground grades into a firmground, the cross section of the gallery is ogive-like (Baele and Hennebert, 2016).

Cryptokarsts are observed where the galleries intersect them presenting glauconitic sand of Thanetian age (Baele and Hennebert, 2016). De Putter et al. (1999) studied those cryptokarsts and showed that the weathering process was of low intensity and recent (Quaternary). These “phosphatic sands” are brownish and comprise some pebble-sized phosphatic nodules.

The Ciply-Malogne Formation forms a massive succession of phosphatic chalk where no stratification is visible (figure 11), except where conglomeratic beds are present. Many signs of bioturbation can be observed on the walls of the galleries. The rock consists roughly of very fine to fine sand-sized phosphatic grains embedded in a chalky matrix. The phosphatic grains are irregularly concentrated in the rock, sometimes probably related to bioturbations. These concentrations sometimes form irregular laminae.

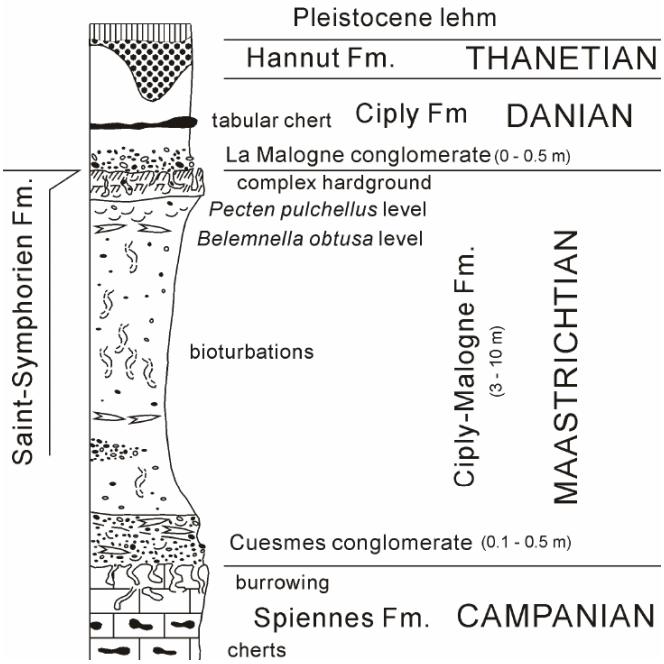

Figure 10. Stratigraphic section of the La Malogne underground quarry. From Baele and Hennerbert, (2016).

Above the Cuesmes Conglomerate, decimetric to pluri-decimetric conglomeratic beds with pebble-sized phosphatic nodules are present, displaying variable thicknesses laterally and showing lenticular geometry in some places (figure 11). Oblique stratifications are visible in the lenticular bodies and some concentrate the phosphatic nodules. The occurrence of conglomeratic beds is uncommon.

Figure 11. Conglomeratic lens with high concentration of phosphatic grains (red arrow) of the La Malogne underground quarry. No stratification is present in the phosphatic chalk enclosing this conglomeratic bed.

3.3. Lithology of the Ciply Phosphatic Chalk:

The Ciply Phosphatic Chalk is not a phosphorite, which is defined as containing more than 18 % P_2O_5 (Slansky, 1980). It is a light brown phosphatic calcarenite with P_2O_5 grades around 10% (Robaszynski and Martin, 1988). The rock is generally friable and can be broken down between the fingers. It is made up of mostly two types of particles: (a) very fine carbonate particles (such as intraclasts, bioclasts and coccoliths; size less than 0.05 mm, with a P_2O_5 content of about 1.5 to 2%); and (b) coarser carbonate and brown phosphate particles (0.100-0.270 mm, with a P_2O_5 content of about 14 %) consisting mainly of microfossil fragments, rounded granules of more or less phosphatic white, yellow to brown grains, faecal pellets, bioclasts, intraclasts and small calcite crystals (Robaszynski and Martin, 1988).

Robaszynski and Martin (1988) identified four classes of phosphatic grains for the (b) type particles based on light microscope and scanning electron microscope (SEM) studies: brown to grey grains, and white grains are the most abundant and are accompanied by some amber-coloured and spherical grains. The brown to grey and white grains are grouped under the term 'peloids' and constitute more than 90 % of the phosphatic particles (Poels and Robaszynski, 1988). They were first believed to be internal moulds of foraminifera by analogy with the phosphatic grains of Picardy (Renard and Cornet, 1891). Cayeux (1939) refuted this interpretation. He noted that the majority of the phosphatic grains did not show any sign of biologic precursor. However, no alternative explanation was given for the origin of the phosphatic grains. Poels and Robaszynski (1988), who studied the phosphatic grains of the Mons Basin the most, did not propose a model for their origin but merely called them "peloids". Nonetheless, they did put forward a mechanism for the phosphatisation of the peloids (see section 3.5).

Poels and Robaszynski (1988) identified the porous internal structure of a chalky calcarenite in the brown to grey grains, the white grains and their intermediates (i.e. peloids). The former grains are the most affected by a centripetal phosphatisation. Almost all the grains are more or less coated with a transparent phosphate which constitutes a brain-like cortex. In the special case of grey grains, a phyllitic structure with iron content seems to be mixed with the porous chalky structure. The amber-coloured grains correspond to phosphatic bone

fragments. The spherical grains seem to have an oolitic structure with a nucleus and concentric zones.

Robaszynski and Martin (1988) undertook granulometry studies that revealed the following results: (1) most of the phosphatic grains have a size between 0.073 and 0.177 mm; (2) thin particles less than 0.063 mm are abundant (about 25%) and contain very little phosphate.

3.4. Mineralogy and chemical composition:

Robaszynski and Martin (1988) determined the "a" and "c" lattice parameters using X-ray analysis of phosphate particles from the Vienne Quarry and the Hyon borehole. The a and c parameter values of 9.321 and 6.896 Å respectively show that phosphate is mineralogically a member of the carbonate-fluorapatite or francolite group with an apatitic CO_2 content of 5.17%. Such an apatitic CO_2 content indicated good phosphate solubility in acids (Slansky, 1980).

3.5. Phosphogenesis in the Mons Basin:

Poels and Robaszynski (1988) were the only to propose a phosphogenetic model for the Mons Basin. As part of their work, they first established a series of phenomena associated with the phosphatisation of the peloids.

- Phosphatisation is accompanied by the progressive reduction of primary porosity of the peloids.
- As phosphatisation proceeds, progressive dissolution of microfossils and micritic particles that are part of the peloids takes place. A secondary porosity is formed.
- The secondary porosity is also affected by the reduction of porosity as phosphatisation continues. The preservation of secondary porosity if highly variable.

The successive precipitations and dissolutions took place centripetally, leading to the progressive transformation of porous micritic peloids in massive phosphatic peloids. However, few peloids are completely phosphatized. Most of them are in an intermediate stage owing to the partial character of the phosphatisation in the Mons Basin.

Poels and Robaszynski (1988) go on to describe the evolution of the phosphatisation of the peloids from non-phosphatised micritic peloids to completely phosphatised peloids.

According to Lamboy (1976), the conditions of semi-confinement were favourable for the creation of a phosphatisation cell in the peloids.

The phosphogenetic model proposed by Peols and Robaszynski (1988) indicates that several factors controlled the phosphatisation of the peloids.

- Phosphorus, Ca^{2+} and CO_3^{2-} are limiting factors for apatite precipitation.
- The permeability of the grains affects the speed and the amplitude of phosphatisation. Permeable peloids are susceptible to become more strongly phosphatised than more impervious ones.
- The duration of phosphatisation is another important factor and depends on the sedimentation rate and bioturbation. High sedimentation rates will isolate more quickly the peloids from the phosphatisation zone in the uppermost part of the sediment.

Finally, Poels and Robaszynski (1988) did not observe bacterial activity as a mechanism for the phosphatisation of the Ciply Phosphatic Chalk.

4. Samples and sampling localities:

The samples analysed came from two different localities. Most of them originated from the Hyon boring (see figure 9) that was retrieved in 1985. Out of the entire sequence, two-thirds could be sampled, which represent approximately 50 m of phosphatic chalk. The basal part of the formation was not available for the present study. Twenty-five samples were taken from the boring that was kept at the University of Mons. The samples were collected approximately every two meters. There was no need for specific sampling method given the continuous and homogeneous nature of the sequence that consists of phosphatic chalk. The chert beds were avoided as much as possible except for one sample (S2-76.02; table 2).

The remaining samples (six in total; table 2) were collected from the underground quarry of La Malogne (see map on figure 9). The hardground at the top of the Ciply-Malogne Formation was sampled (figure 12). Two samples from the phosphatic chalk were taken as well as one sample from the conglomeratic bed above the Cuesmes conglomerate (figure 11) which was itself sampled.

Figure 12. Picture of the hardground capping the Ciply-Malogne Formation. The hardground is directly overlain by the La Malogne conglomerate. Taken from the La Malogne underground quarry.

Eventually, the “phosphatic sands” were also collected from the La Malogne underground quarry. They represent a recent (Quaternary) weathering process of weak intensity (De Putter et al., 1999).

Table 2 compiles the different samples of the Ciply Phosphatic Chalk along with their facies description.

Table 2. Compilation of the samples studied with their locality and facies description.

Colonne1	Locality	Facies description
S2-52	Hyon	Matrix-supported carbonate rock with silt- and sand-sized peloidal phosphatic grains
S2-52.7	Hyon	Matrix-supported carbonate rock with silt- and sand-sized peloidal phosphatic grains
S2-56.76	Hyon	Matrix-supported carbonate rock with silt- and sand-sized peloidal phosphatic grains
S2-65	Hyon	Matrix-supported carbonate rock with silt- and sand-sized peloidal phosphatic grains
S2-76.02	Hyon	Silica cement enclosing silt- and sand-sized peloidal phosphatic grains
S2-79.06	Hyon	Matrix-supported carbonate rock with silt- and sand-sized peloidal phosphatic grains
S2-81.08	Hyon	Grain-supported carbonate rock with silt- and sand-sized peloidal phosphatic grains
S2-84.12	Hyon	Grain-supported carbonate rock with silt- and sand-sized peloidal phosphatic grains
S2-88.18	Hyon	Grain-supported carbonate rock with peloidal phosphatic grains
S2-90.2	Hyon	Grain-supported carbonate rock with peloidal phosphatic grains
S2-94.53	Hyon	Grain-supported carbonate rock with peloidal phosphatic grains
S2-98.4	Hyon	Matrix-supported carbonate rock with silt- and sand-sized peloidal phosphatic grains
S2-100.3	Hyon	Matrix-supported carbonate rock with silt- and sand-sized peloidal phosphatic grains
HARD	La Malogne underground quarry	Well-cemented carbonate rock containing phosphatic pebbles and silt- and sand-sized peloidal phosphatic grains. Bioturbation is abundant.
ECH1	La Malogne underground quarry	Matrix-supported carbonate rock with silt- and sand-sized peloidal phosphatic grains
ECH 2	La Malogne underground quarry	Matrix-supported carbonate rock with silt- and sand-sized peloidal phosphatic grains
ECH 3	La Malogne underground quarry	Unconsolidated to very weakly consolidated silt- and sand-sized peloidal phosphatic grains. Carbonates almost totally absent.
ECH 4	La Malogne underground quarry	Weakly consolidated conglomeratic carbonate rock with abundant phosphatic pebbles.
Cuesmes Poudingue	La Malogne underground quarry	Weakly consolidated conglomeratic carbonate rock with abundant phosphatic pebbles.

5. Methodology and analytical techniques:

5.1. Analytical techniques:

The objectives of this study are to document the petrography, mineralogy and rare earth elements geochemistry to have a better knowledge and understanding of the Ciply Phosphatic Chalk. The information gained will be used to better constrain the conditions of formation of the phosphatic chalk of the Mons Basin. In order to accomplish this task, several analytical techniques were used. They include :

- Scanning electron microscopy (SEM) using a Quanta 20 ESEM (FEI), coupled with energy dispersive spectroscopy (Apollo 10 silicon drift EDS detector; EDAX) at the Royal Belgian Institute of Natural sciences.
- X-ray diffraction (XRD). The powders are then analysed using a diffractometer PANanalytical Empyrean (copper tube λ: 1,5418Å with a nickel filter, 45KV and 40 mA detector x'celerator. The powders are first loaded in a steel holder and measured in a Bragg-Brantano configuration. The studied area was between 6 and 69 degrees 2-theta. The semi-quantitative interpretation is done using Visual Crystal 6 software.
- Cathodoluminescence (CL) studies were performed at the University of Mons (Belgium) using a cold-cathode CL unit model Mk5 operated at 15 kV beam voltage and 500 µA current (Cambridge Image Technology Limited). Cl spectra were recorded with CITL optical spectrometer model COS8200 allowing acquisition from 380 to 1100 nm at 3.7 nm resolution and a set of bandpass interference filters.

5.2. Samples preparation:

In order to be analysed by any of the analytical technique mentioned above, the samples need to be treated in a specific manner. For both the SEM and CL, the samples were prepared in the same way. However, for the XRD the treatment was different.

The first step for all the samples was sawing to retrieve smaller and more easily workable samples. Once they were in the suitable dimension, the samples were put in Epoxy resin mixed with a hardener and placed in a vacuum to remove the air for about 24 hours. After the resin had solidified, the samples were cut with a sectioning saw. Some were damaged in the process due to the very high friability of the rock. Those which were too damaged were

not used for SEM and CL analyses. However, enough samples in good condition were produced. The samples were then polished with a series of sandpapers down to a granulometry of 1 µm.

For XRD analyses, powders had to be produced from the samples. To obtain representative results, the samples were first reduced in size using a hammer and steel plate (wrapped inside paper to reduce contamination). Afterwards they were crushed using a Fritsch Laboratory Planetary Mono Mill through which the materials were homogenized. The powder was crushed and ground by agate grinding balls in a grinding bowl. Afterwards the powder was passed through a 53µm sieve.

Major elements were obtained on powder aliquots after alkaline fusion, on a Thermo Scientific iCAP ICP-OES. For that, around 50 mg of samples were mixed with high purity lithium metaborate and tetraborate flux in a graphite crucible and heated for 10 minutes at 1000 °C. After cooling, the bead was dissolved for several hours using a stirring magnet in 5% HNO3. After dilution and addition of Y as internal standard, the samples were measured along with USGS standards BHVO-2 that were used as unknown standards to evaluate precision, which is better than 2% (2RSD) for each element.

Trace elements were analysed on the same solution with an Agilent 7700 Q-ICP-MS at the Laboratoire G-Time (ULB). After dilution and addition of In as internal standard, analyses were conducted using a He collision cell and samples were introduced with 5% HNO3. Standards BHVO-2 and BCR-2 were used as international reference material, providing an external precision better than 10 % (2RSD).

6. Petrography and mineralogy of the Ciply Phosphatic Chalk:

This section presents the petrography and mineralogy of the phosphatic chalk of the Mons basin from the samples collected from the Hyon boring and the La Malogne underground quarry. General macroscopic descriptions are followed by observations using a scanning electron microscope (SEM), an energy dispersive spectrometer (EDS), X-ray diffraction (XRD), and cathodoluminescence (CL).

6.1. Phosphatic chalk of the Hyon boring:

The Ciply Phosphatic Chalk is a phosphatic calcarenite, a clastic limestone consisting predominantly of sand-grade calcitic or aragonitic particles (allochems; Folk, 1959). It is composed of various coarse silt-sized and very fine sand-sized phosphatic grains embedded in a chalky matrix. The Ciply Phosphatic Chalk is mostly a phosclast-wackestone, that is, a mud-supported rock with structureless phosphatic grains (see nomenclature in Trappe (2006)). The colour of the rock is directly linked to the abundance of phosphatic particles, varying from a white-yellow colour for samples with low contents of phosphatic particles (figure 13), to a brownish colour for samples rich in phosphate (figure 14). Figure 15 presents the lithological log of the Hyon borehole compiled by Robaszynski and Martin (1988) and indicates the location of the samples for this study.

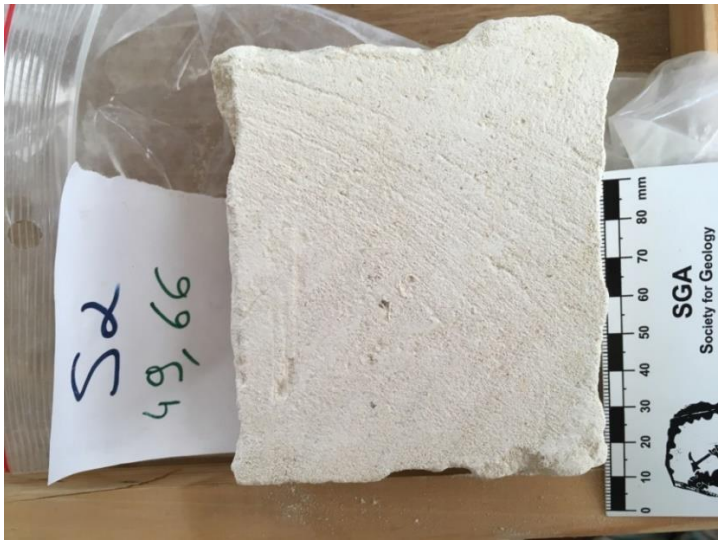

Figure 13. Whitish phosphatic calcarenite of the Hyon boring (sample S2-49.66) with very low content of phosphatic particles. This sample represents the transition from the Saint-Symphorien Tuffeau and the high-grade part of the Ciply Phosphatic chalk at a depth of approximately 49.66 m from the surface (see figure 15).

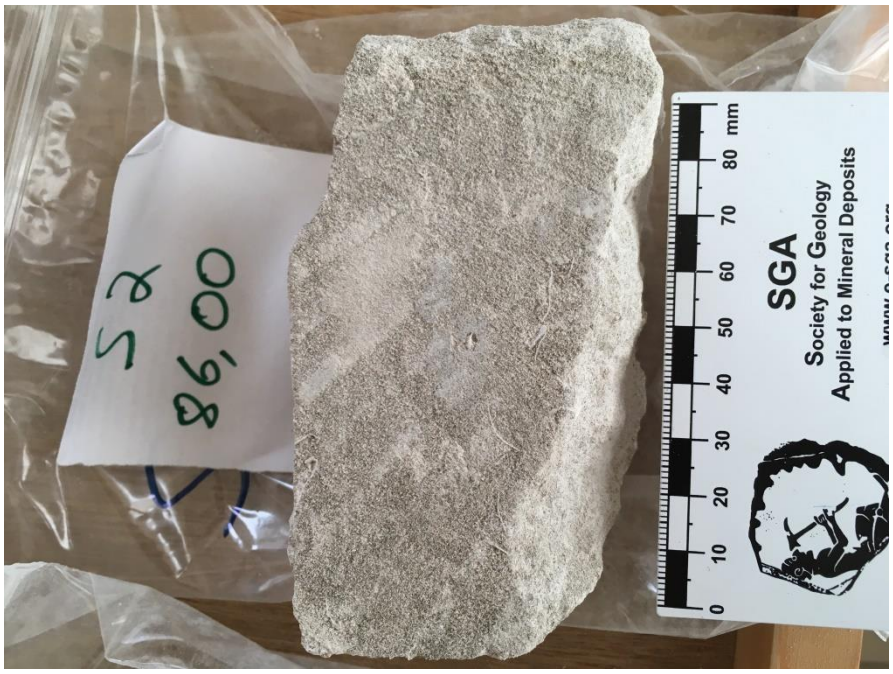

Figure 14. Brownish phosphatic calcarenite (sample S2-86.00) with high content of phosphatic particles (mainly peloids). This sample represents the richest part of the high-grade section of the Ciply Phosphatic Chalk at a depth of 86 m (see figure 15).

The Ciply phosphatic chalk is abundantly bioturbated. The phosphatic grains are disseminated or concentrated in laminae. Concentrations of phosphatic grains may also be linked to bioturbation. Few medium to very coarse sand-sized (i.e. 0.25 to 2 mm) well-rounded glauconite grains are present throughout the sequence studied (i.e. from approximately 49 m to 100 m deep). Silicification is observed as nodular chert beds. The importance of silicification varies throughout the section. It induces a hardening of the rock, making it much more resistant than an otherwise very friable phosphatic calcarenite.

As observed by Robaszynski and Martin (1988), the faunistic assemblage is dominated by neritic and relatively shallow marine water benthic organisms such as Ostreids and Pectinids. Some nektonic forms (e.g. *Belemnella obtuse*) indicate a Maastrichtian age to the formation (Robaszynski and Martin, 1988).

The X-ray diffraction analyses performed confirmed the previous results obtained. The phosphate mineral corresponds to carbonate-fluorapatite (i.e. francolite); calcite is the major calcium carbonate mineral (figure 16). Quartz is also present. The results give homogeneous mineralogical compositions throughout all the section studied.

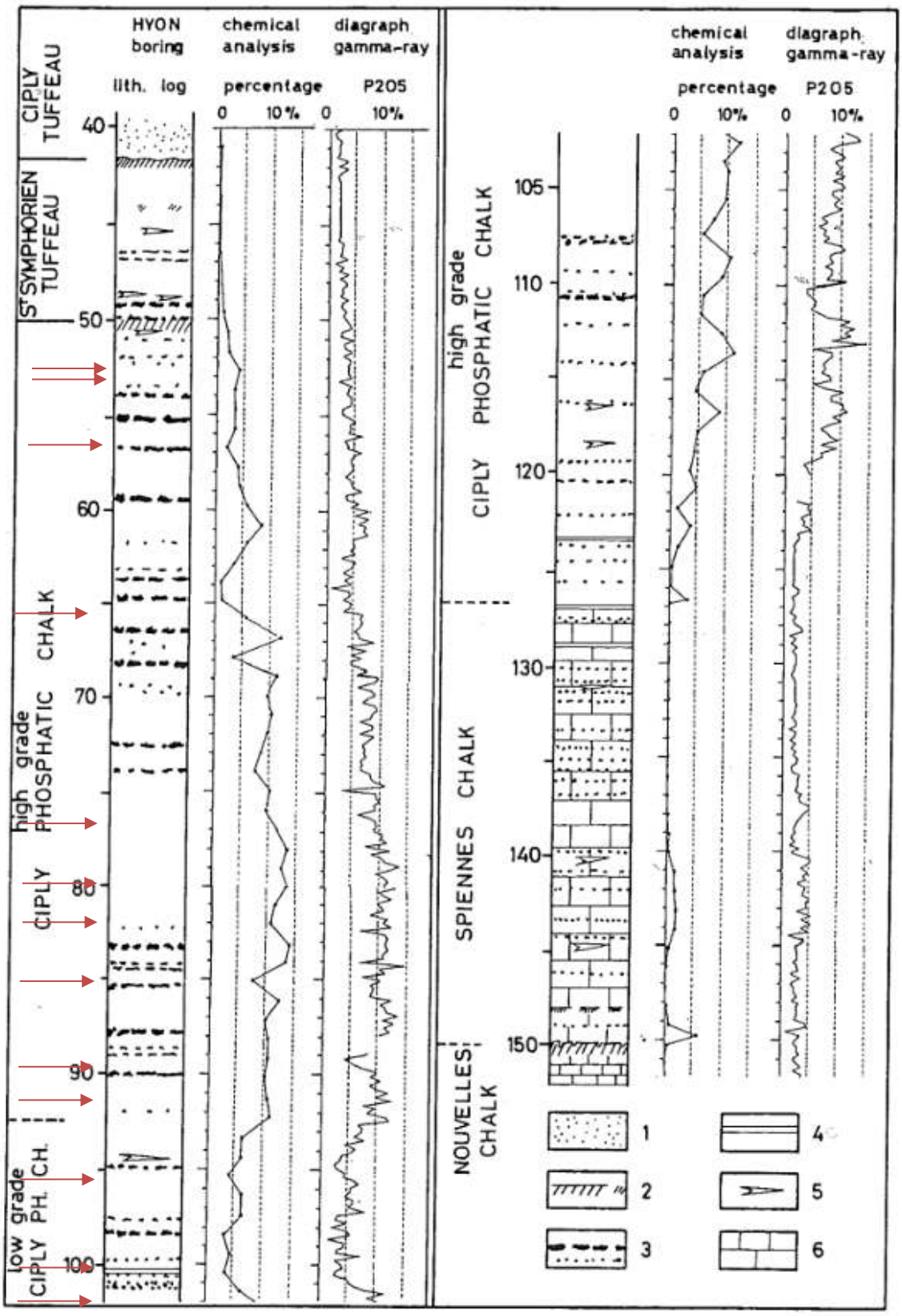

Figure 15. Lithological log of the Hyon boring between 40 to 152 m. 1 Tertiary Ciply Tuffeau; 2 hardground; 3 flint band; 4 grey, slightly marly level; 5 belemnite level; 6 white chalk. Modified after Robaszynski and Martin (1988). The red arrows show approximately the samples taken for this study (compiled in table 2).

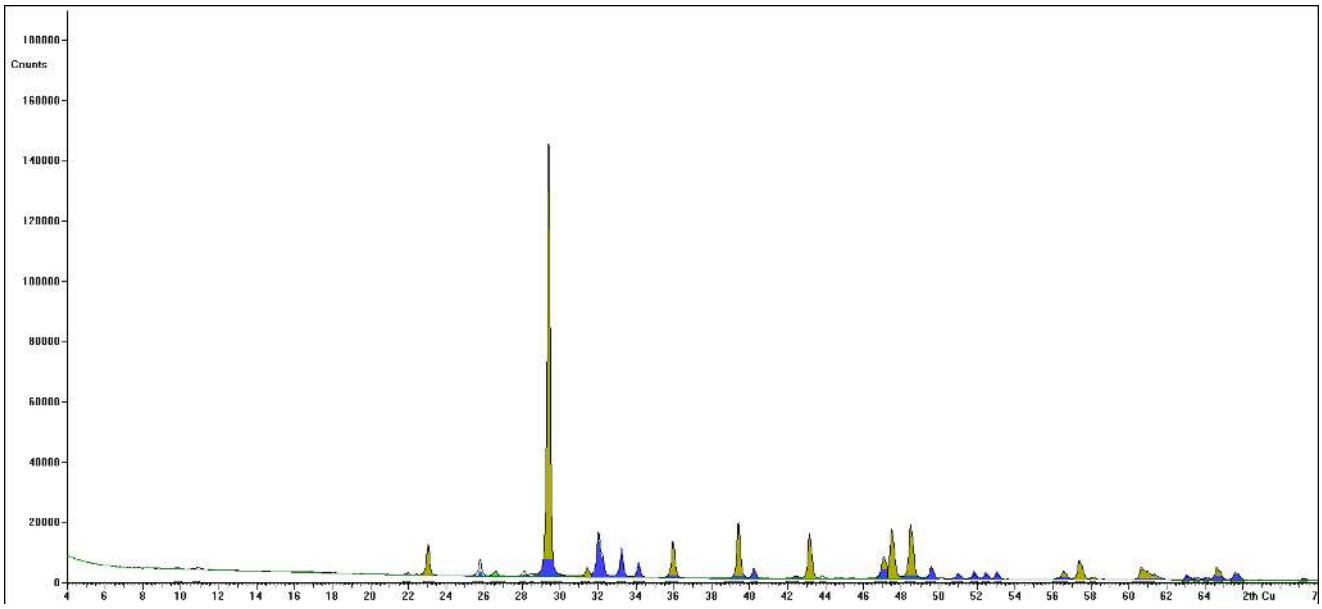

Figure 16. X-ray diffraction results for sample S2-84.12. Yellow corresponds to calcite, blue to carbonate fluorapatite, and green to quartz.

Scanning electron microscopy coupled with an energy dispersive spectrometer reveal much about the constituents of the rock as well as the phosphatisation process to some extent (figure 17). The majority of the phosphatic grains consist of irregularly shaped peloids showing various degrees of phosphatisation. In some grains, phosphatisation appears to be centripetal and most of the grains are not fully phosphatised but possess calcitic particles and porosity. Although the centripetal trend is clear, it is important to note that CFA is present in virtually all parts of the interstitial space of the peloids where it acts as cement binding the carbonate particles together.

Cathodoluminescence (CL) is a useful tool to locate the REE in the samples. Apatite often shows bright CL emission since Mn^{2+}, Eu^{2+} and REE^{3+} - which are activators - ubiquitously substitute for Ca^{2+} in the crystal lattice. REE (mainly Eu^{2+}, Dy^{3+}, Sm^{3+}) produce violet, blue, green to red CL colours (Waychunas, 2002). The phosphatic grains of the Hyon borehole display blue to violet CL colours in most of the cases (figure 18). Therefore, it is most likely that the REE are hosted in CFA. However, few grains possess green CL colour. They have been identified as biogenic phosphate grains.

Some grains seem to be brighter on their rims rather than in the core. This can be explained by the fact that some grains have a centripetal trend of phosphatisation. Therefore, the more phosphatised rims would produce brighter colours. The cortices are not necessarily

more enriched in REE based on CL observations. On the contrary, it appears that they are depleted in REE relative to the rest of the grains (see figure 18).

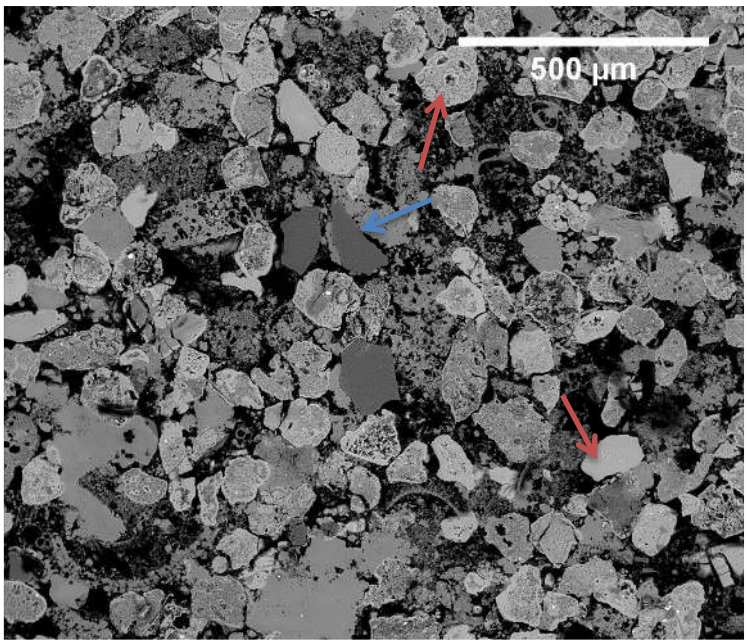

Figure 17. Back scattered electron SEM image of a representative view of the enriched part of the Ciply Phosphatic Chalk. The majority of the phosphatic grains are composed of peloids which show different degrees of phosphatisation (red arrows). The peloids usually have an intricate internal structure composed of CFA, micritic calcium carbonate, and quartz and glauconite in lesser amounts. Detrital quartz grains are also present (blue arrow) and rarely show signs of phosphatisation.

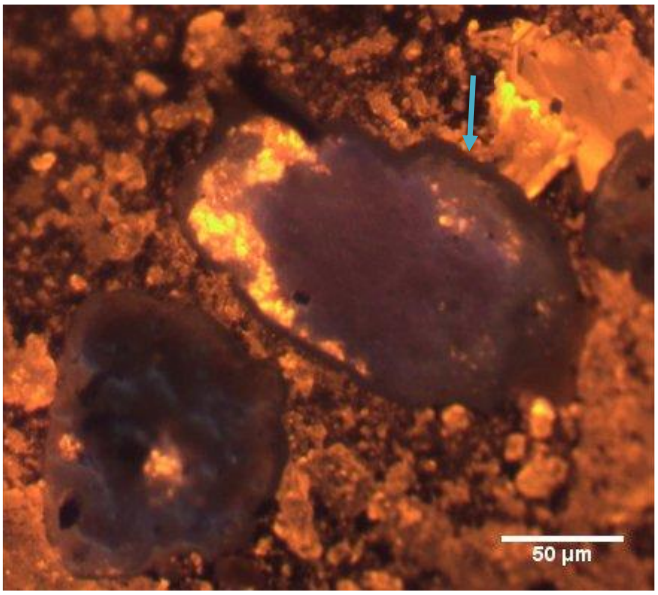

Figure 18. CL image of phosphatic peloids. The blue-violet colour indicates the presence of REE. The blue arrow indicates the cortex of the peloid.

Accompanying phosphatisation of the peloids is the formation of secondary porosity that results from the dissolution of calcitic debris. Interestingly, the peloids tend to preserve their calcitic components in weakly and moderately phosphatised peloids while strongly phosphatised peloids tend to exhibit secondary porosity in the form of moulds. However, this phenomenon is variable within a peloid. This is due to the variability of phosphatisation intensity at the micrometre scale (figure 19). This also reflects the centripetal trend of phosphatisation already noted by Poels and Robaszynski (1988). There is also evidence of apparent replacement of carbonate bioclasts by CFA in a weakly phosphatised peloid. However, this probably arose from the prior dissolution of calcite and the subsequent precipitation of CFA. This is suggested by the partial dissolution of some calcitic bioclasts (figure 19). The secondary porosity produced, at least in part, is filled by CFA. This is evidenced by the strongly phosphatised parts of peloids which do not exhibit the porosity they would exhibit if the calcite was dissolved - granted that initially there was a homogeneous distribution of calcitic debris within the peloid, which can be assumed given that weakly to moderately phosphatised peloids do have calcitic debris more or less homogenously scattered throughout them.

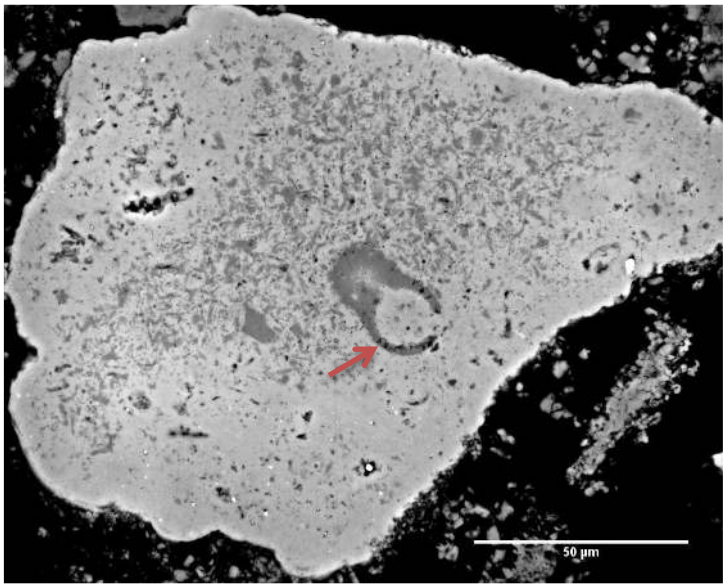

Figure 19. Back-scattered electron SEM image of a partially strongly phosphatised peloid. The margins of the peloid have undergone stronger phosphatisation than the core of the peloid where calcite debris is present. The near absence of calcite in the marginal parts is probably due to the dissolution of calcite and precipitation of CFA in the secondary porosity. This is suggested by the partial dissolution of some calcitic bioclasts (red arrow). Note that all the porosity is not filled.

Some peloids possess a phosphatic cortex. The cortex sometimes displays a well-developed brain-like texture (figure 20). This texture is probably due to the surface irregularities of the peloids. Indeed, it has been observed by Poels and Robaszynski (1988) that the cortex does not present a brain-like texture where the peloids have smooth surfaces. There is no apparent relationship between the presence of a cortex and the intensity of phosphatisation of the peloids.

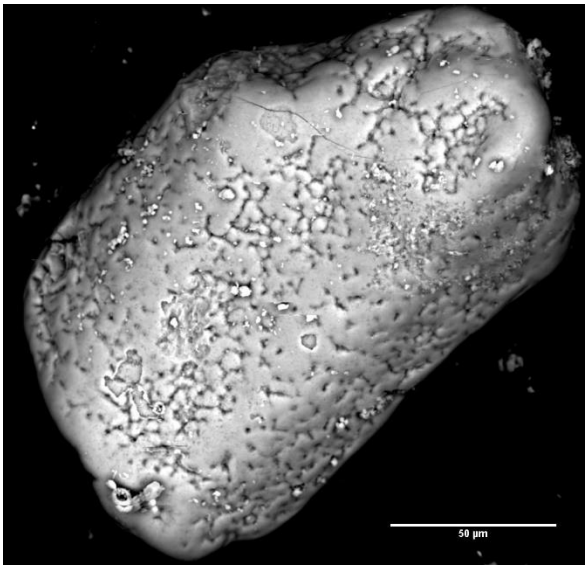

Figure 20. Back-scattered electron SEM image of a phosphatic peloid.

Some phosphatic grains of the Hyon borehole suggest that reworking processes affected the phosphatic sediment (figure 21). This is plainly shown by the truncation of the laminated structure present in the phosphatic grain of the left-hand side image of figure 21. The right-hand side image of figure 21 suggests that previously formed phosphatic grains redeposited in the sediment which experienced another phosphatisation event. The sharp contrast present supports the hypothesis that this grain was not produced by a single phosphatisation phase, but rather was fashioned by a series of processes involving phosphatisation and reworking.

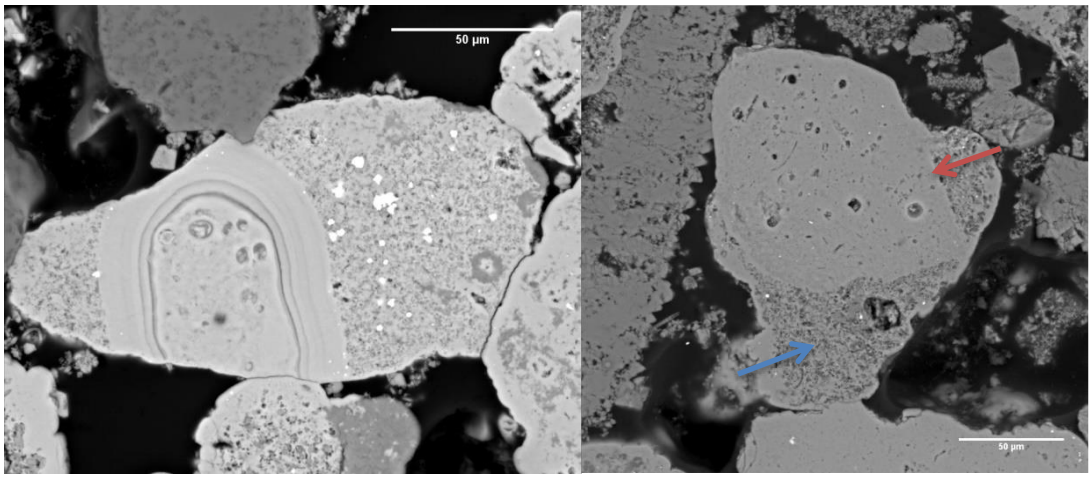

Figure 21. Back-scattered electron SEM images of two phosphatic grains (=peloids of Robaszynski and Martin (1988)) that attest that the previously formed phosphatic sediment was reworked and possibly underwent other events of phosphatisation and reworking. The right-hand side image suggests that a previously formed phosphatic grain (red arrow) was reworked and deposited. Then the sediment in which it deposited (blue arrow) underwent a phosphatisation event. Further reworking formed the present peloid. The left-hand side image clearly shows signs of reworking from previously formed phosphatic sediment. It also suggests different modes of phosphatisation. The shiny specks in the peloids are iron sulphide (probably pyrite) grains.

Peloids typically have dimensions of about 50-100 µm in diameter although this may vary. The compositions of the peloids consist of a few typical phases (figure 19 and 22). They consist primarily of CFA and calcite; their respective content varies according to the degree of phosphatisation. They also commonly show small amounts of iron sulphide (probably pyrite). The iron sulphide phase is almost exclusively present with CFA which indicates that its formation is linked with some stage of phosphatisation. Finally, a phase that has been identified as glauconite is sometimes present within the peloids. However, the identification of this phase as glauconite cannot be made certain with SEM observations and EDS analyses.

The matrix of the Ciply Phosphatic Chalk consists of numerous calcitic debris < 10 µm. It is also composed of diverse bioclasts such as foraminifers and other shells. It seems that some of the calcitic debris derives, in part at least, from these bioclasts. Others derive from coccoliths. All these particles are loosely packed together due to the scarcity of calcitic cements. Consequently, much of the porosity is preserved.

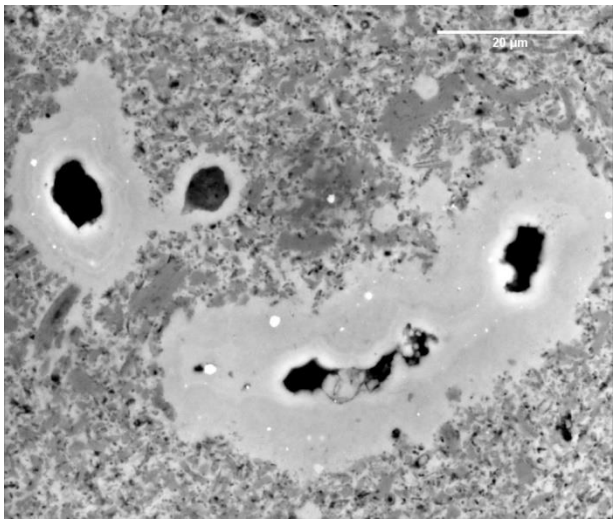

Figure 22. Back-scattered electron SEM image of the interior of a typical peloid found in the Ciply Phosphatic Chalk of the Hyon boring. It consists mostly of three phases, the major ones being calcite and CFA. Minor amounts of pyrite occur mainly with CFA. The calcite phase is made up of small debris usually < 5 µm. The CFA phase displays two modes of deposition: as interparticle cement, and as laminated infilling of pores.

Interestingly, the matrix and the calcitic phase of the peloids show many similarities. Indeed, some peloids are comprised of foraminifers and other calcitic debris comparable to the matrix of the rock. The foraminifers occasionally dictate the geometry of the peloids, but sometimes are simply a part of the peloids without having any effect on the geometry of the peloids (figure 23).

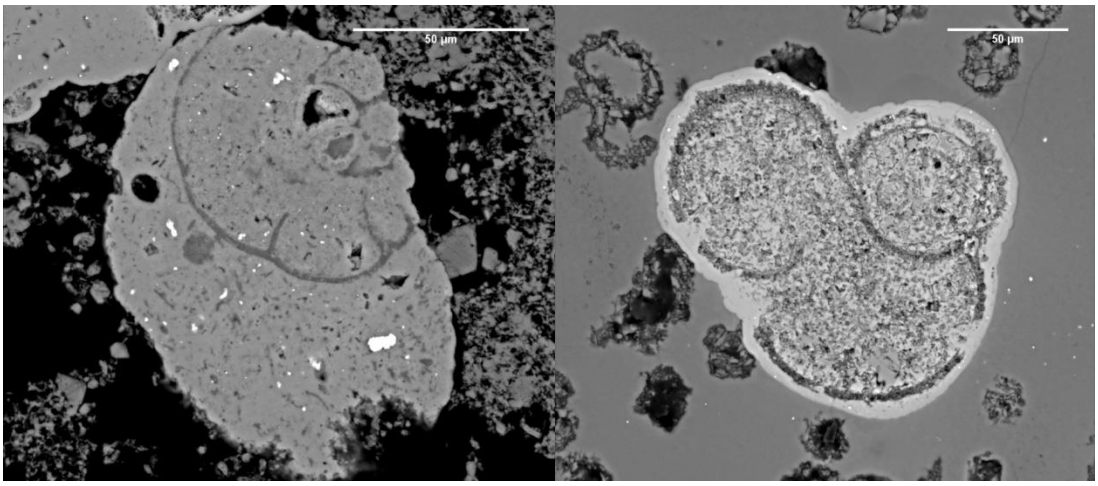

Figure 23. Back-scattered electron SEM images of peloids and foraminifers. The left-hand side image shows a foraminifer as a part of the calcite phase of a strongly phosphatised peloids. The right-hand side image shows a peloid whose shape is dictated by the geometry of the foraminifer. The interior is filled with small (< 5 µm) calcitic debris and CFA cement

At some levels of the Ciply Phosphatic Chalk, silicification may form nodular beds rich in silica which indurated greatly the rock. SEM observations show that silicification leads to the dissolution of calcium carbonate and even indicate signs of replacement of calcium carbonate (figure 24). This is made manifest by the partial centripetal replacement of carbonate bioclasts by silica. Silicification also affected the peloids by replacing calcite by silica. However, the peloids possessing a cortex tend to be unaffected by silicification because CFA played the role of a seal that protected the inner parts of the peloids. Because of silicification, the matrix is almost devoid of calcite which is mainly present in the inner part of unaffected peloids.

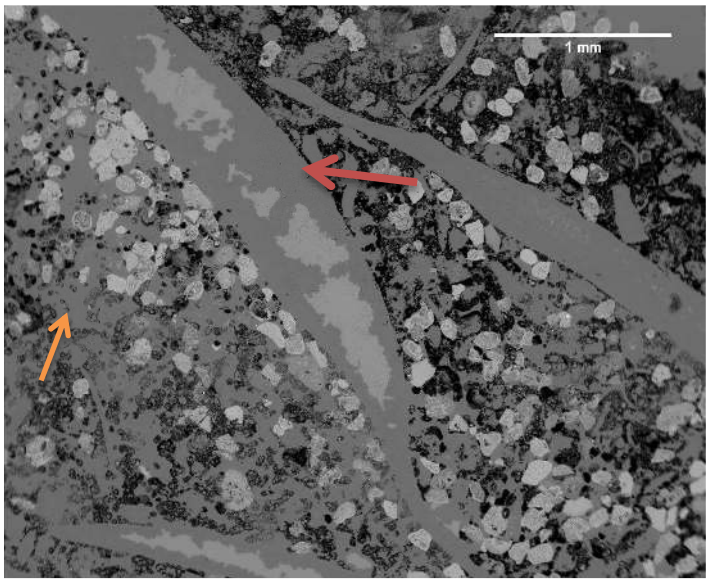

Figure 24. Back-scattered electron SEM image of silicification (red arrow) of the Ciply Phosphatic Chalk replacing bioclasts made up originally of calcium carbonate. The matrix is silicified (orange arrow) and is almost devoid of calcium carbonate. Only impervious peloids retain their calcium carbonate.

While phosphatised peloids form the majority of the phosphatic grains, other types of grains are also present. Bones and teeth fragments can also be found as well as pieces of scales. All these grains are present in rather small amount (about 5 % of the phosphatic grains). Some of these grains are marked by bioerosion in the form of perforation. The microborings are often partly or completely filled by a brighter phosphate phase which indicates that the precipitated phosphate phase is denser than the material of the original grains. This difference may be due to an enrichment of F in the newly precipitated micritic CFA (figure 25; Soudry and Nathan, 2000). There is no significant difference in brightness between the

cortex of phosphatic peloids and the CFA present in the peloids. However, other phosphatic grains, probably of biogenic origin, which possess a cortex often display a difference in brightness between the grain and the cortex. Poels and Robaszynski (1988) observed a bioeroded bone fragment enveloped by a CFA cortex which indicates that an event of phosphatisation took place after bioerosion.

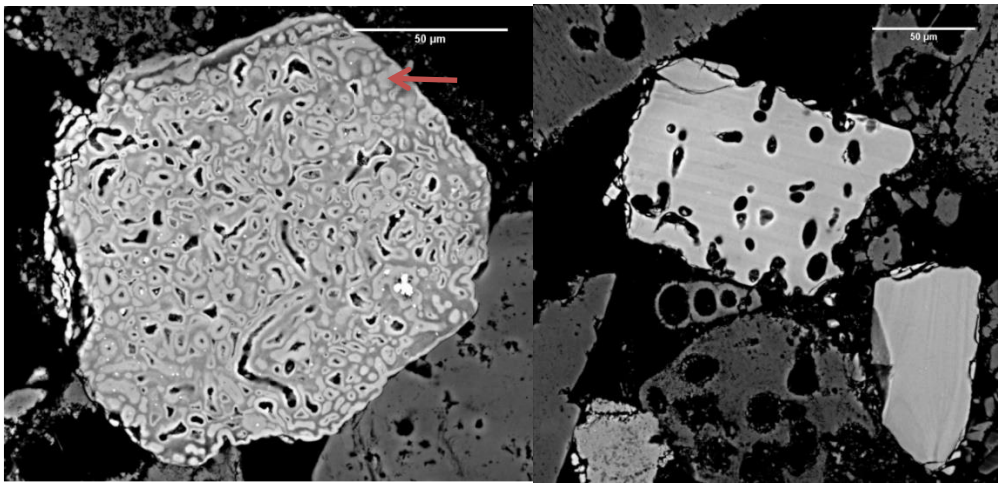

Figure 25. Back-scattered electron SEM image of bioeroded bone fragments. The perforations are sometimes coated with CFA that may fill completely the cavities (red arrow). Note the difference in brightness between the newly precipitated CFA and the bone fragment in the left-hand side image.

Well-developed phosphatic ooids are rarely found in the Ciply Phosphatic Chalk. They show alternation of phosphate and carbonate layers with a nucleus that varies in composition (figure 26).

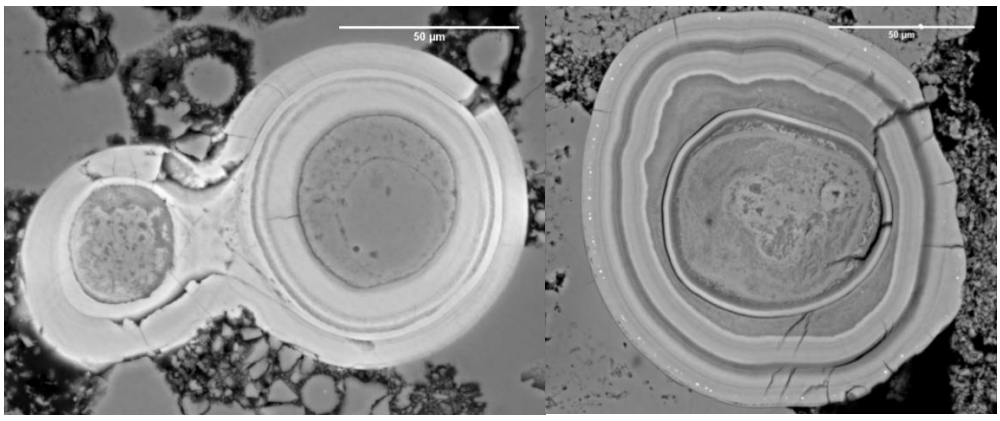

Figure 26. Back-scattered electron SEM images of phosphatic ooids. On the left-hand side image, the amalgamated ooids are composed of a phosphatic cortex with a nucleus of quartz. On the right-hand side image, the nucleus is essentially phosphatic. However, its origin is unknown. It may have a bacterial origin suggested by the presence of microspheres. The layers of the cortex seem to alternate between CFA and calcite.

Microsphere structures are rarely occurring (figure 27). They are approximately 1 µm in diameter. Where the interior of these structures is dissolved, a coating of CFA is present. These structures usually appear to compose most of the grain in which they are present. They form patches of microspheres of relatively homogenous size. They may occur within grains composed essentially of these structures, or in peloids and ooids (cf. figure 27).

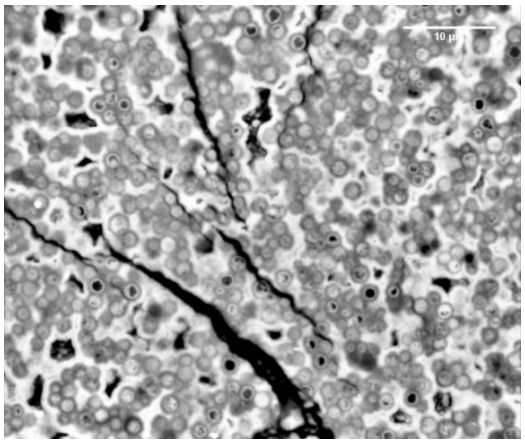

Figure 27. Back-scattered electron SEM image of microspheres enveloped in CFA. They may be of microbial origin.

Whether these structures are of bacterial origin or not, it is impossible to argue that phosphatisation arose from these structures based on the SEM observations. Other structures seem to represent relics of microbial mats even though there is no certainty regarding their origin (figure 28). In some instances, it seems that those mats were responsible for the bioerosion of some peloids. These structures are relatively rare.

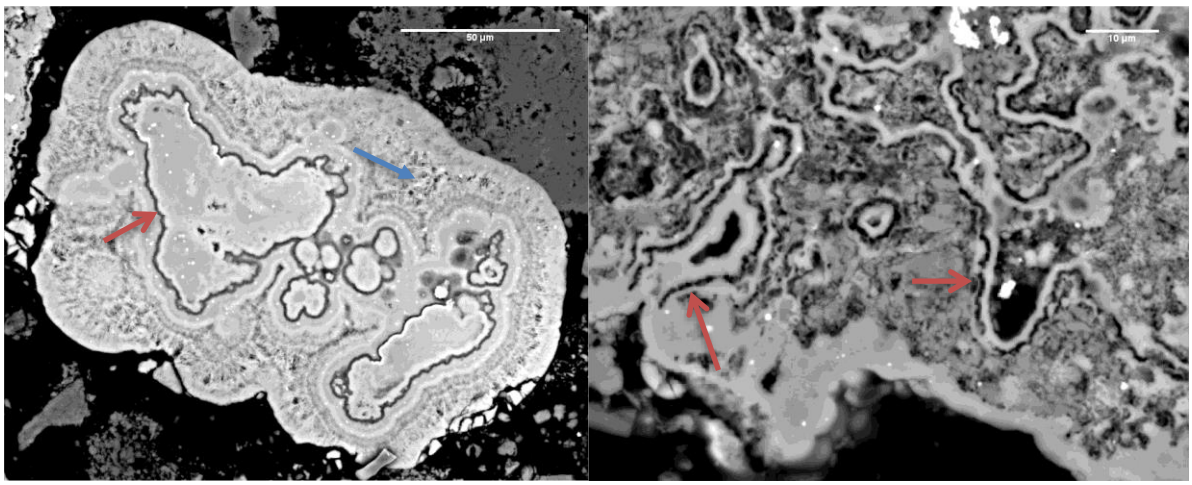

Figure 28. Back-scattered electron SEM images of supposed possible relics of microbial mats (red arrows) highlighted by CFA mineralisation. The left-hand side image displays fibrous CFA mineralisation (blue arrow).

6.2. La Malogne underground quarry:

The Ciply Phosphatic Chalk of the La Malogne underground quarry has many similarities with the phosphatic calcarenite of the Hyon borehole (figure 29). The peloids form the exceeding majority of the phosphatic grains followed by marginal bones and teeth fragments. The matrix is richer in foraminifer bioclasts. Coccoliths are also present in the matrix. Observations using cathodoluminescence indicate that corrosion has been more important on these rocks (figure 30). As shown by X-ray diffraction analysis results, the mineralogy is the same as the Hyon boring's (figure 31), that is, calcite, CFA and quartz.

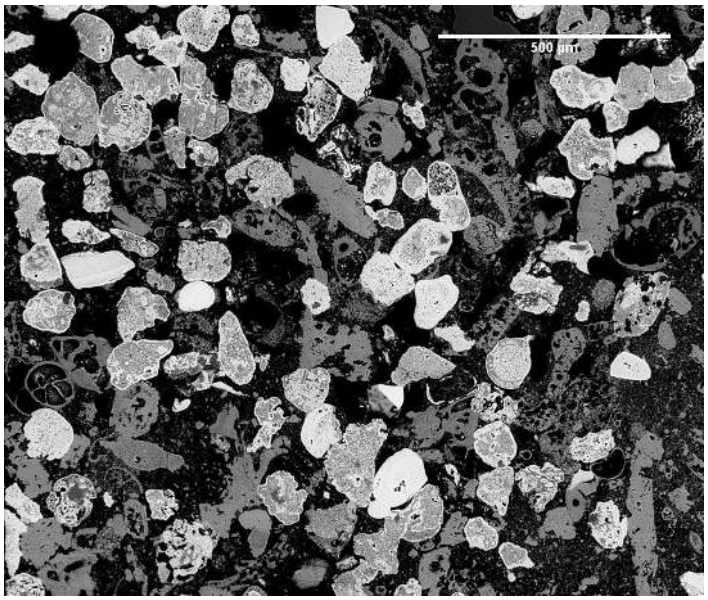

Figure 29. Back-scattered electron SEM image of a calcarenite from the La Malogne underground quarry. It is similar in many points to the calcarenite of the Hyon boring. Peloids are the main phosphatic grains. Bones and teeth fragments are present in low amounts. The matrix is composed of diverse calcitic debris comprising coccoliths. Foraminifers are more abundant than in the Hyon boring.

The "phosphatic sands" (i.e. sample ECH3) of the La Malogne underground quarry present very distinctive features (figure 32). They have a brownish colour and consist of unconsolidated sand-sized particles. They are found in funnel-shaped cavities that the galleries sometimes intersect. Very weak brownish pebble-sized nodules are present and can be very easily broken down with the fingers. X-ray diffraction indicates that the calcite originally present has been totally dissolved. SEM observations show that only a very small percentage of calcium carbonate has been preserved in some impermeable phosphatic grains. However, the vast majority of calcium carbonate has been removed (figure 32).

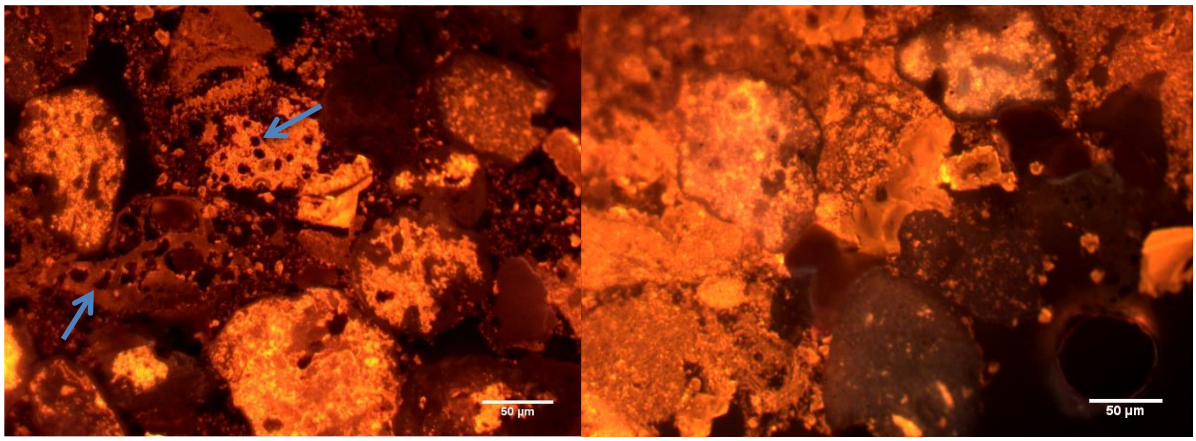

Figure 30. Cathodoluminescence images of the Ciply Phosphatic Chalk of the La Malogne underground quarry (left-hand side image) and the Hyon (right-hand side image). As a general trend, the calcarenite of the La Malogne underground quarry shows more signs of corrosion (blue arrows).

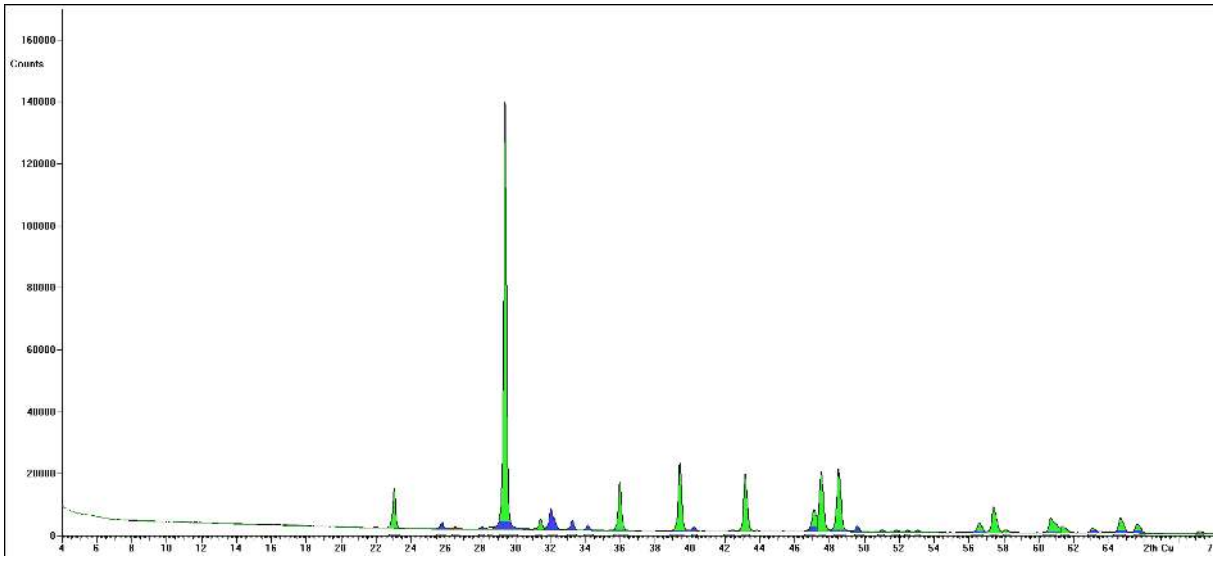

Figure 31. X-ray diffraction results for the phosphatic calcarenite of the La Malogne underground quarry (sample ECH 2). Green is calcite, blue is CFA and red is quartz.

A hardground caps the top of the Ciply Phosphatic Chalk. It grades laterally to a firmground and is overlain by a conglomeratic bed (figure 33). However, there may be remnants of a hardground at the top of the phosphatic formation present in the Hyon boring as well, but it cannot be made sure due to the fragmentary nature of this part of the boring (Robaszynski et al., 1988).

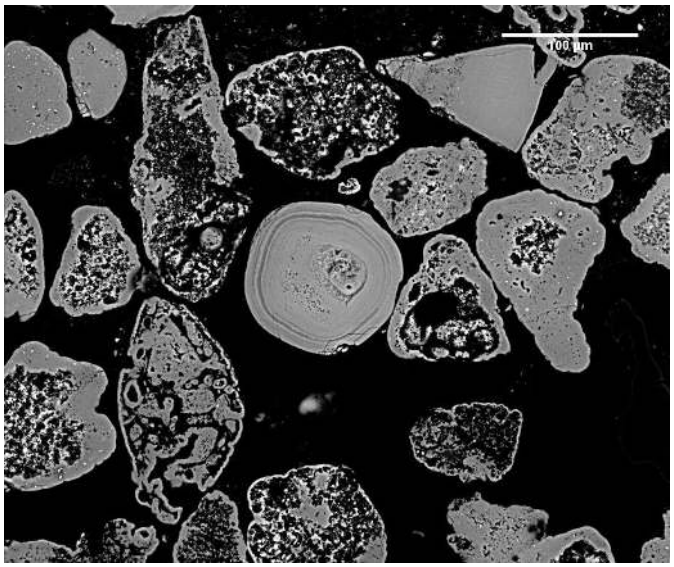

Figure 32. Back-scattered electron SEM image of weathered phosphatic calcarenite (sample ECH3) from the La Malogne underground quarry. The vast majority of calcium carbonate has been removed. The CFA is unaffected.

Figure 33. The hardground of the La Malogne underground quarry is capped by a conglomeratic bed. This hardground grades laterally into a firmground.

XRD results show that calcite and CFA are the dominant phases of the hardground accompanied by marginal quartz. SEM observations indicate that calcite acts as cement that binds phosphatic peloids, phosphatic granules and pebbles, and miscellaneous bioclasts (figure 34). The phosphatic pebbles of the hardground yield interesting observations (see figure 34). Indeed, the pebble observed is not homogeneously phosphatised but possesses zones of very advanced phosphatisation marked by the dissolution of calcium carbonate.

This feature clearly manifests the local and/or multi-stage nature of phosphatisation. In both strongly and moderately phosphatised zones CFA acts as cement.

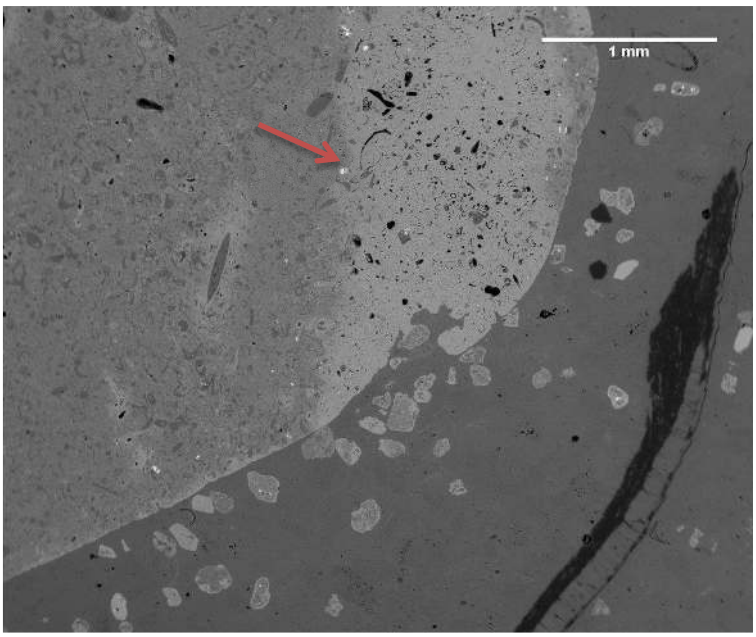

Figure 34. Back-scattered electron SEM image of the hardground of the La Malogne underground quarry. Phosphatic peloids, pebbles and miscellaneous bioclasts are enclosed in calcite cement. Note the discontinuous phosphatisation in the pebble (red arrow).

Conglomeratic beds of the Ciply-Malogne Formation are rich in phosphatic pebbles. They are generally rounded to well-rounded. Some pebbles are perforated by multiple borings of about 1 mm in diameter filled mainly by carbonate materials. Sand-sized grains of glauconite can be found in these pebbles. The presence of phosphatic granules in the pebbles is a clear indicator of reworking processes and multiple phosphatisation events.

7. Geochemistry of the Ciply Phosphatic Chalk:

This section presents the results for the major, minor and trace elements -including REE- of the Hyon boring and the La Malogne underground quarry.

7.1. Major and minor elements :

Table 3 compiles the major elements concentrations of the Hyon borehole and the La Malogne underground quarry. The P_2O_5 concentration ranges from 0.15 to 6.7 % for the Hyon boring. The La Malogne underground quarry has similar abundances with 3.7 % for the phosphatic calcarenite, 5.8 % for the conglomeratic bed, 0.81 % for the hardground, and 11 % for the 'phosphatic sands'.

For the Hyon borehole samples SiO_2 ranges from 0.66 to 15 %, Na_2O from 0.19 to 0.63 %, MgO from 0.27 to 0.44 %, Al_2O_3 from 0.11 to 0.47 %, Fe_2O_3 from 0.092 to 0.41 %, K_2O from 0.027 to 0.17 %. For the La Malogne samples SiO_2 ranges from 0.70 to 17 %, Na_2O from 0.32 to 0.83 %, MgO from 0.45 to 0.79 %, Al_2O_3 from 0.097 to 4.9 %, Fe_2O_3 from 0.24 to 14 %, K_2O from 0.035 to 0.60 %. The MnO and TiO_2 contents are insignificant and reach 0.14 % and 0.13 % respectively for the 'phosphatic sand' which is the sample with the highest concentrations of these elements (see table 3).

There is a good correlation between Na_2O and P_2O_5 (figure 35), and between Fe_2O_3 and P_2O_5 while there is only a weak correlation ($R^2 = 0.36$) between K_2O and P_2O_5. Al correlates slightly ($R^2 = 0.21$) with P. There is no significant correlation among the other major elements.

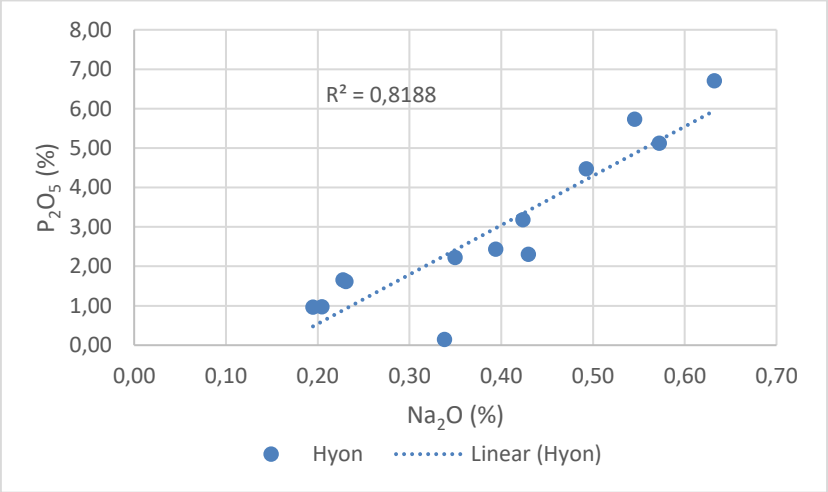

Figure 35. Plot of Na_2O vs P_2O_5. There is a very good correlation.

Table 3. Major elements concentrations in wt. % for the samples of the Hyon boring and the La Malogne underground quarry.

	Al2O3	CaO	Fe2O3	K2O	MgO	MnO	Na2O	P2O5	SiO2	TiO2
S2-52	0.13	57	0.25	0.052	0.32	0.0092	0.35	2.2	1.0	0.021
S2-52.7	0.11	60	0.18	0.032	0.44	0.011	0.19	0.97	0.66	0.010
S2-56.76	0.11	61	0.20	0.027	0.41	0.011	0.23	1.6	0.74	0.014
S2-65	0.19	60	0.14	0.035	0.42	0.0066	0.20	0.97	0.83	0.012
S2-76.02	0.15	58	0.25	0.068	0.32	0.011	0.39	2.4	1.6	0.020
S2-79.06	0.24	59	0.34	0.10	0.34	0.011	0.55	5.7	1.6	0.031
S2-81.08	0.21	59	0.24	0.075	0.33	0.011	0.43	2.3	1.6	0.022
S2-84.12	0.21	58	0.32	0.089	0.33	0.010	0.49	4.5	2.2	0.026
S2-88.18	0.31	59	0.30	0.10	0.33	0.011	0.42	3.2	2.5	0.028
S2-90.2	0.47	55	0.40	0.16	0.38	0.0085	0.63	6.7	6.2	0.039
S2-94.53	0.62	49	0.41	0.17	0.35	0.0079	0.57	5.1	15	0.043
S2-98.4	0.46	57	0.19	0.14	0.33	0.013	0.34	0.15	4.4	0.024
S2-100.3	0.22	57	0.092	0.076	0.27	0.015	0.23	1.7	2.1	0.012
ECH2	0.27	58	0.40	0.054	0.45	0.0078	0.36	3.7	1.3	0.018
ECH3	4.89	30	14	0.60	0.79	0.14	0.83	11	17	0.13
ECH4	0.31	58	0.61	0.10	0.50	0.012	0.49	5.8	1.7	0.034
HARD	0.10	61	0.24	0.035	0.51	0.011	0.32	0.81	0.70	0.0078

7.2. Trace elements:

The trace elements concentrations are compiled in table 4. The concentrations of trace elements are usually enriched in phosphorites compared to seawater, crustal abundances or average shales (Altschuler, 1980).

Several elements have a good correlation with P_2O_5 ($0.75 < R^2 < 0.85$) such as Y, U, Th, Pb, Zr, Ga, Ge, Sr, Rb, and Cr (figure 36).

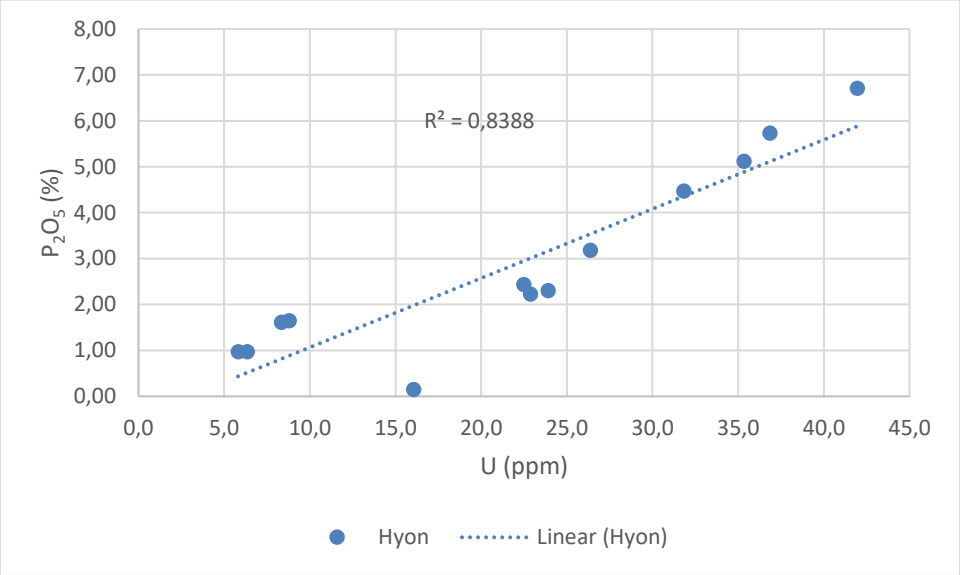

Figure 36. Plot of U (ppm) vs P_2O_5 (%). Other elements such as Y, Th, Pb, Zr, Ga, Ge, Sr, Rb and Cr display similar patterns.

Table 4. Trace elements concentrations in ppm for the samples of the Hyon boring and the La Malogne underground quarry.

	Cr	Co	Ni	Cu	Zn	Ga	Ge	Rb	Sr	Y	Zr	Nb	Ba	Pb	Th	U
S2-52	15	0.67	10	4.8	7.1	4.9	1.5	2.0	713	98	14	0.50	8.7	2.7	0.67	23
S2-52.7	5.5	0.77	11	4.4	12	1.0	0.35	1.4	624	19	4.3	0.21	7.7	1.6	0.24	6.3
S2-56.76	6.0	1.0	10	4.9	28	1.9	0.58	0.93	663	32	5.4	0.25	6.9	1.6	0.26	8.3
S2-65	6.2	0.86	8.6	2.7	15	1.2	0.29	1.2	528	21	4.3	0.29	8.9	1.3	0.32	5.8
S2-76.02	14	0.73	8.3	2.8	22	5.3	1.8	2.6	706	108	15	0.60	8.7	2.9	0.84	22
S2-79.06	20	0.83	12	2.3	18	8.8	2.9	3.7	945	172	26	0.88	18	4.5	1.3	37
S2-81.08	13	0.71	9.9	2.8	16	5.4	1.8	2.3	752	111	18	0.64	13	2.9	0.81	24
S2-84.12	19	0.79	11	2.6	14	7.7	2.6	2.9	887	149	19	0.72	14	3.5	1.1	32
S2-88.18	14	1.0	13	3.8	21	6.4	2.0	2.8	870	123	16	0.68	15	3.2	0.92	27
S2-90.2	23	1.3	13	2.7	23	11	3.3	5.1	1088	197	25	1.3	17	5.2	1.7	42
S2-94.53	20	2.1	12	7.7	32	9.5	2.9	4.9	1030	170	27	1.3	19	4.6	1.4	35
S2-98.4	10	1.0	11	3.7	32	4.0	1.2	2.5	797	72	11	0.81	13	2.6	0.72	16
S2-100.3	15	0.33	9.0	2.0	14	2.2	0.68	1.7	566	40	6.7	0.42	7.8	1.3	0.38	8.8
HARD	9.1	0.50	11	2.3	15	1.2	0.46	1.7	621	31	9.8	0.31	18	1.7	0.22	18
ECH 2	17	0.70	14	4.9	21	4.4	1.2	2.1	892	77	16	0.53	13	2.3	0.64	22
ECH 3	91	120	519	30	371	49	12	27	1101	283	73	3.9	139	11	3.7	65
ECH 4	19	1.8	18	3.1	17	3.0	0.83	3.5	1028	57	21	0.79	20	2.7	0.47	24

7.3. Rare earth elements:

The Hyon borehole samples show variable ΣREE contents, ranging from 63 to 696 ppm (Table 5). The ΣLREE (i.e. La, Ce, Pr, Nd, Sm) range from 37 to 408 ppm. The ΣHREE (i.e. Eu, Gd, Tb, Dy, Ho, Er, Tm, Yb, Lu, Y) range from 27 to 289 ppm. The LREEs account for about 60 % of the total REEs. The highest concentrations are found between 76.02 m and 94.53 m where the average ΣREE is 512 ppm. Their REE patterns (Figure 37) overall exhibit a MREE enrichment, with $(La/Sm)_{SN}$ and $(Gd/Yb)_{SN}$ ratios varying from 1.1 to 1.2, and 1.6 to 2.0, respectively. They overall show a LREE enrichment, with $(La/Yb)_{SN}$ ratios ranging from 1.2 to 1.3. These patterns present a strong Ce anomaly (0.25<Ce/Ce*<0.28, Table 5), with no significant Eu anomaly (0.92<Eu/Eu*<0.99; Table 4).

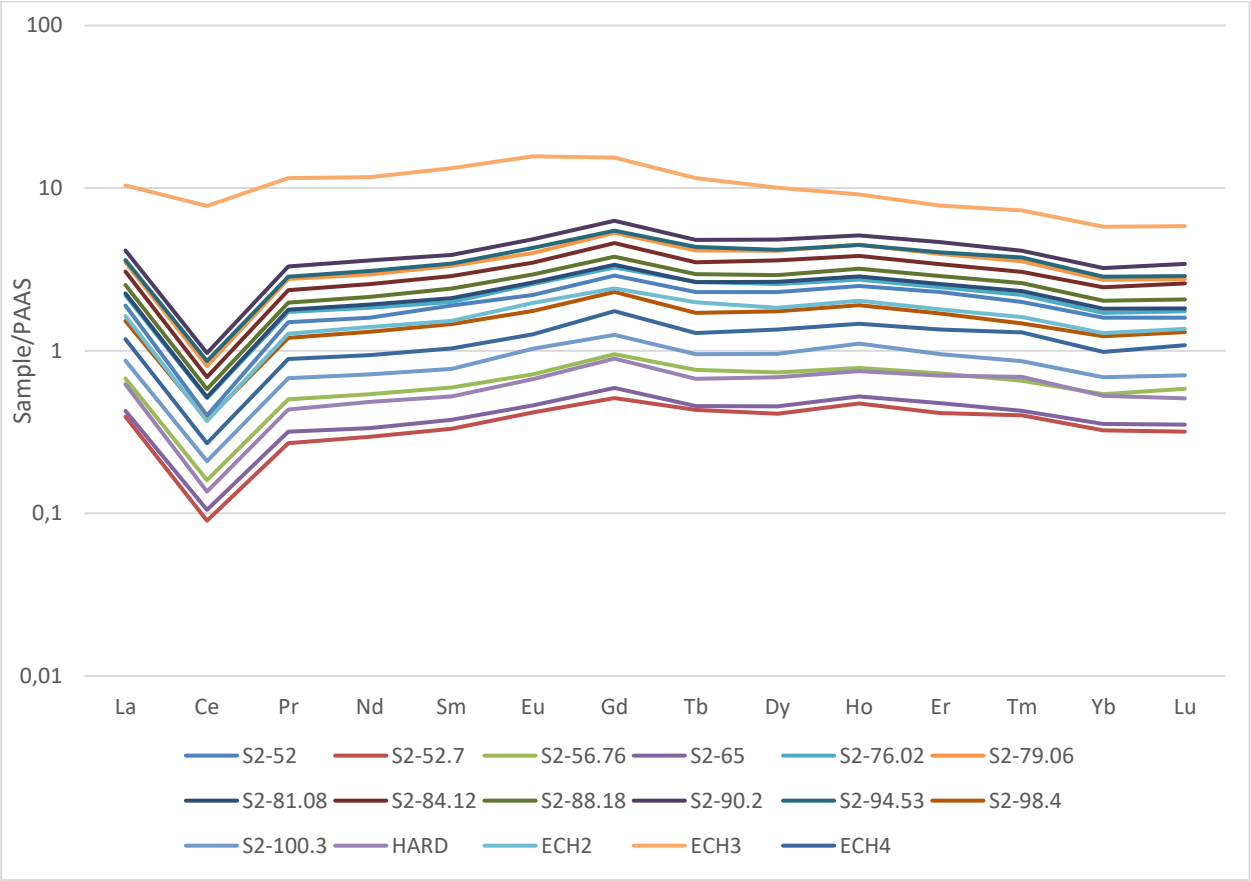

Figure 37. Shale-normalised REEs distribution spectra of the samples from the Hyon borehole. Regardless of the REE abundances, all samples show similar REEs patterns except ECH3.

The abundances for the samples of La Malogne with ΣREE ranging from 102 to 272 ppm (table 6). However, the 'phosphatic sand' possesses very high REE contents with ΣREE reaching 2070 ppm.

Table 5. REE concentrations in ppm for the Hyon boring samples. $(Ce/Ce^*)_{SN} = Ce_{SN}/(0.5\ La_{SN} + 0.5\ Pr_{SN})$ and $(Pr/Pr^*)_{SN} = Pr_{SN}/(0.5\ Ce_{SN} + 0.5\ Nd_{SN})$.

	S2-52	S2-52.7	S2-56.76	S2-65	S2-76.02	S2-79.06	S2-81.08	S2-84.12	S2-88.18	S2-90.2	S2-94.53	S2-98.4	S2-100.3	Average	PAAS
La	74	15	26	16	84	134	86	117	97	158	138	58	33	80	38
Ce	36	7.2	13	8.4	41	64	41	55	46	77	69	30	17	39	80
Pr	13	2.4	4.4	2.8	15	24	16	21	18	29	25	11	6.0	14	8.8
Nd	54	10	18	11	62	100	65	87	73	122	105	44	24	60	34
Sm	10	1.8	3.3	2.1	11	18	12	16	13	22	19	8.1	4.3	11	5.6
Eu	2.4	0.45	0.77	0.50	2.8	4.3	2.8	3.8	3.2	5.2	4.6	1.9	1.1	2.6	1.1
Gd	13	2.4	4.4	2.8	15	25	16	21	18	29	26	11	5.8	14.6	4.7
Tb	1.8	0.34	0.59	0.35	2.1	3.2	2.0	2.7	2.3	3.7	3.4	1.3	0.74	1.9	0.77
Dy	11	1.9	3.4	2.1	12	19	12	17	14	23	20	8.2	4.5	11	4.7
Ho	2.4	0.47	0.78	0.52	2.7	4.4	2.8	3.8	3.2	5.1	4.4	1.9	1.1	2.6	1.0
Er	6.5	1.2	2.1	1.4	7.0	11	7.3	9.7	8.2	13	11	4.8	2.7	6.7	2.9
Tm	0.81	0.16	0.27	0.17	0.89	1.4	0.94	1.2	1.1	1.7	1.5	0.60	0.35	0.85	0.41
Yb	4.5	0.91	1.5	1.0	4.8	7.7	5.1	6.9	5.7	9.1	8.0	3.5	1.9	4.7	2.8
Lu	0.71	0.14	0.25	0.15	0.76	1.2	0.79	1.1	0.9	1.5	1.2	0.56	0.31	0.74	0.43
Y	98	19	32	21	108	172	111	149	123	197	170	72	40	101	27
ΣREE	328	63	111	71	369	591	382	512	426	696	607	256	143	350	212
ΣLREE	187	36	65	41	213	341	220	296	247	408	356	151	85	204	166
ΣHREE	141	27	46	30	156	250	161	217	179	289	250	105	58	147	46
$(Eu/Eu^*)_{SN}$	0.94	0.99	0.93	0.95	0.98	0.92	0.96	0.93	0.95	0.95	0.96	0.94	1.0	0.96	1.0
$(Ce/Ce^*)_{SN}$	0.26	0.27	0.27	0.28	0.26	0.26	0.26	0.25	0.26	0.26	0.27	0.28	0.27	0.27	1.0
$(La/Sm)_{SN}$	1.0	1.2	1.1	1.1	1.1	1.1	1.1	1.1	1.0	1.1	1.1	1.0	1.1	1.1	1.0
$(Gd/Yb)_{SN}$	1.8	1.6	1.8	1.7	1.9	2.0	1.9	1.9	1.9	2.0	1.9	1.9	1.8	1.8	1.0
$(La/Yb)_{SN}$	1.2	1.2	1.2	1.2	1.3	1.3	1.2	1.2	1.2	1.3	1.3	1.2	1.3	1.3	1.0

Except for the phosphatic sand, the samples of La Malogne have similar features (see table 5 and 6). All the spectra exhibit similar trends expect the ECH3 which is significantly enriched in REEs compared to the other samples (figure 37). Moreover, the negative Ce anomaly is much less pronounced.

Table 6. REE concentrations in ppm for the La Malogne samples.

	HARD	ECH 2	ECH 3	ECH 4	Average
La	24	62	397	45	132
Ce	11	29	619	21	170
Pr	3.8	11	102	7.9	31
Nd	16	48	397	32	123
Sm	2.9	8.5	74	5.7	23
Eu	0.72	2.1	17	1.4	5.3
Gd	4.2	11	72	8.2	24
Tb	0.52	1.5	8.9	1.0	3.0
Dy	3.2	8.6	47	6.3	16
Ho	0.74	2.0	9.1	1.5	3.3
Er	2.0	5.1	22	3.8	8.3
Tm	0.28	0.65	3.0	0.52	1.1
Yb	1.5	3.6	16	2.8	6.1
Lu	0.22	0.59	2.5	0.47	0.95
Y	31	77	283	57	112
ΣREE	102	272	2070	195	660
ΣLREE	58	159	1588	112	479
ΣHREE	44	113	481	83	180
$(Eu/Eu^*)_{SN}$	0.56	0.99	2.93	0.76	1.3
$(Ce/Ce^*)_{SN}$	0.26	0.25	0.71	0.26	0.37
$(Pr/Pr^*)_{SN}$	1.4	1.4	1.2	1.5	1.4
$(La/Sm)_{SN}$	1.2	1.1	0.78	1.1	1.0
$(Gd/Yb)_{SN}$	1.7	1.9	2.7	1.8	2.0
$(La/Yb)_{SN}$	1.2	1.3	1.8	1.2	1.4

8. Discussion:

8.1. Apatite mineralisation in the Ciply Phosphatic Chalk:

For both the Hyon borehole and the La Malogne underground quarry, the same kinds of apatite mineralisation occur. CFA mostly plays the role of interparticle cement. Only in a few instances do we find laminated CFA mineralisation associated with the peloids or with other phosphatic grains that are rarely found. A cortex commonly coats the peloids. Another exceptional mineralisation type has been found in the phosphatic grain of unknown origin (figure 28) where CFA forms fibres.

A closer examination of the apatite mineralisation shows that CFA commonly appears to have a globular ultrastructure (figure 38). This is characteristically observed in pores where there is enough room to develop such structure as well as on the surface of some peloids. Lucas and Prévot (1981) conducted an experiment where bacterial decomposition of organic compounds liberated phosphate which subsequently precipitated with calcium to produce mostly fluorapatite. The ultrastructure obtained suggests its formation via amorphous-like precursor phases. Therefore, the globular ultrastructure of the apatite reflects the rapid formation of a poorly ordered precursor phase involving a high concentration of nucleation sites (Krajewski et al., 1994).

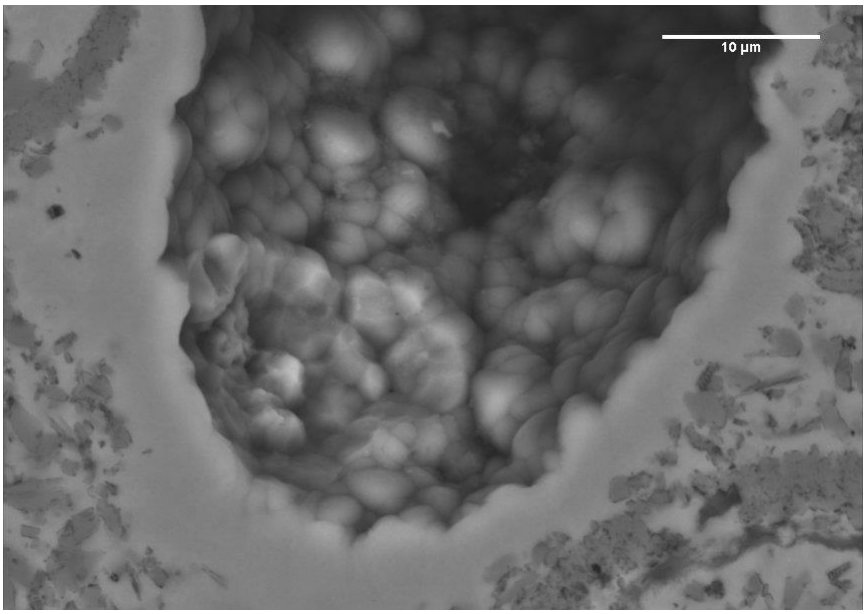

Figure 38. Back-Scattered electron SEM image of the globular ultrastructure of CFA. This indicates the rapid formation of a poorly ordered precursor phase involving a high concentration of nucleation sites.

However, all apatite mineralisations do not exhibit this globular ultrastructure. In similar settings, well-crystallised francolite is observed (figure 39). These two can be genetically linked by the observations of transitional forms (figure 40). This implies that some parts underwent a longer period of phosphatisation as it is known that growth and aging leads to a progressive improvement of the crystallinity of apatite (Kim and Burnett, 1986; Van Cappellen and Berner, 1991).

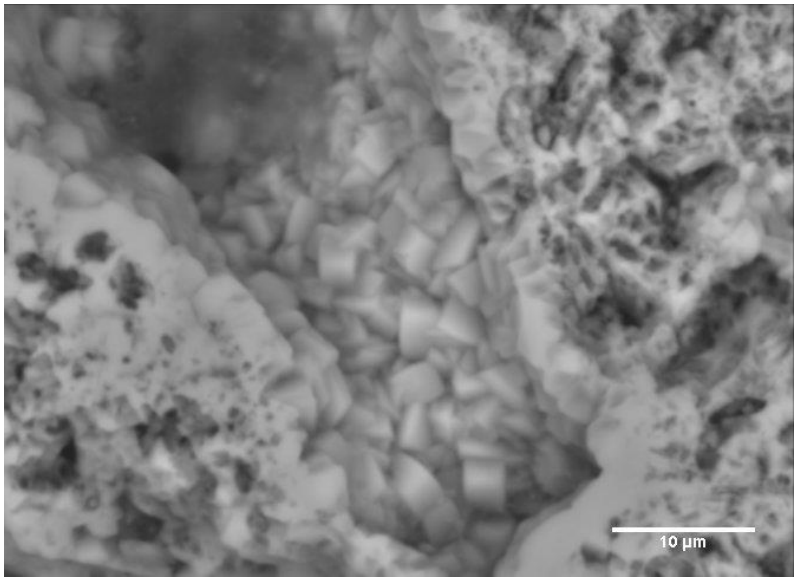

Figure 39. Back-scattered electron SEM image of well-crystallised CFA.

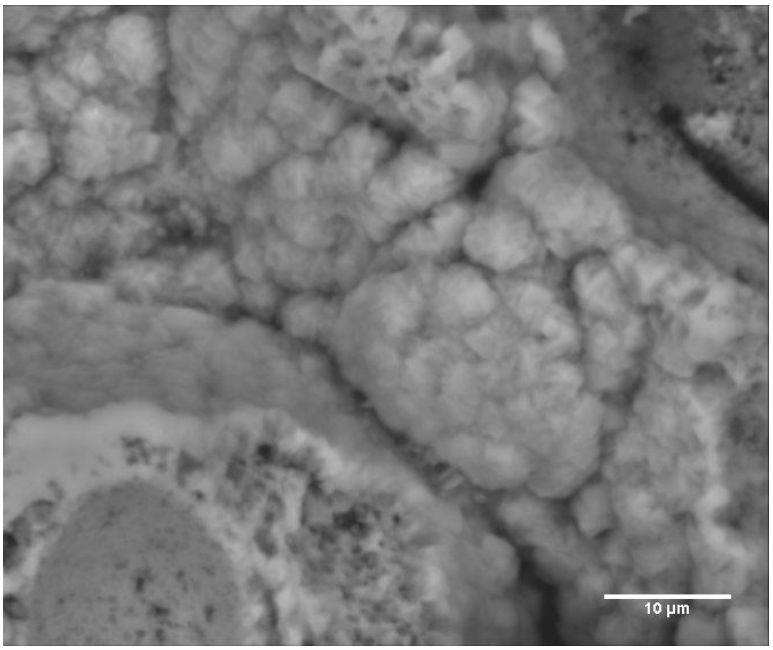

Figure 40. Back-scattered electron SEM image of moderately crystallised CFA. This represents the transition between the globular texture and the well-crystallised texture.

CFA does not preferentially precipitate on any particular substrate but uses the available surfaces (Krajewski et al., 1994). Nonetheless, it is recognised that microorganisms affect the production, storage and distribution of reactive phosphate in sediments, and that microbial reactions are largely responsible for the chemical composition of the pore water environment (Krajewski et al., 1994). Exchange of phosphate between bacteria and pore waters is also modulated by the redox conditions of the interstitial environment of the sediment (Gächter et al., 1988; Carlton and Wetzel, 1988; Ingall et al., 1993). As a result, upon depletion of oxygen, the bacterially stored phosphorus is used as an energy source and eventually released as dissolved phosphate (Krajewski et al., 1994). Dissolution of Fe-oxyhydroxides also releases adsorbed phosphate upon reduction in the sediment.

In some grains, laminated CFA mineralisation is accompanied by dissolution traces throughout the laminae (figure 41). This could be the result of the dissolution of remnants of microbial mats during or after CFA precipitation. This would not be surprising given that it is widely held that microbial activity is linked with phosphatisation (e.g. Jarvis, 1992; Krajewski et al., 1994; Föllmi, 1996). It is crucial to recognise that this association does not necessarily imply that phosphatisation is a biogenic process. However, it does mean that microbial activity may be indirectly responsible for precipitation of CFA by massive release of phosphate in the sediment porewaters (see Krajewski et al., 1994).

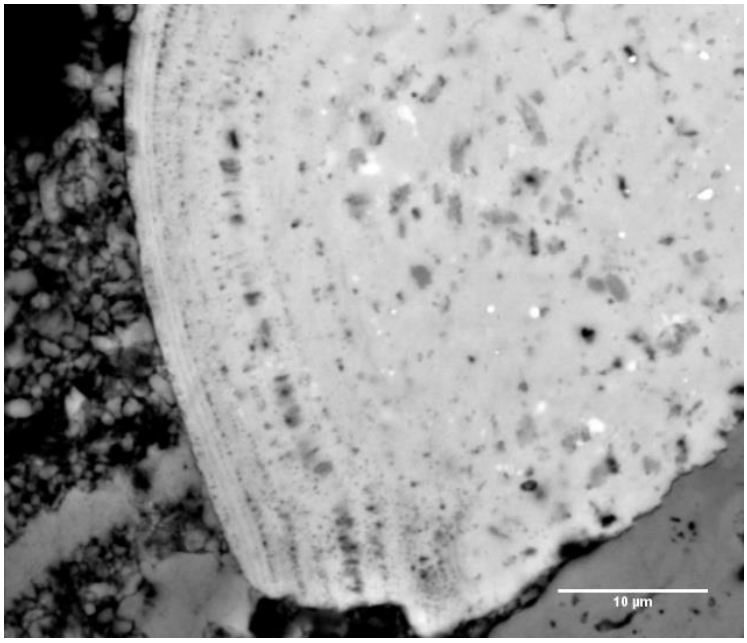

Figure 41. Back-scattered electron SEM image of laminated CFA mineralisation. The pores are contained within individual laminae.

Even though it is not possible to determine all the processes that could have occurred to release dissolved phosphate in the interstitial pores of the sediment, it seems that a high concentration of phosphate was achieved to precipitate CFA via a metastable precursor, which is kinetically favoured over direct apatite precipitation. It has been shown that moderate concentration of phosphate leads to precipitation of apatite (Krajewski et al., 1994). However, this is a slow process and cannot account for the unusually high concentrations found in phosphorites (Krajewski et al., 1994; Van Cappellen, 1991).

8.2. CFA and elements distribution:

It was determined by XRD analyses that CFA is the phosphate mineral present in all the samples of the Hyon borehole and La Malogne (see sections 6.1 and 6.2). Furthermore, observations using SEM coupled with EDS consistently yielded the same outcomes for phosphorus-bearing phases. This is consistent with the results obtained previously by Robaszynski and Martin (1988) who identified CFA as the phosphorus-bearing mineral for the samples of the Hyon borehole.

As it was already mentioned in section 2.2, CFA is capable of making numerous substitutions and host many elements. The very good correlations of Y, U, Th, Pb, Zr, Ga, Ge, Sr, Rb, and Cr with P_2O_5 indicate that these elements are hosted in CFA, most likely as substitutes of Ca^{2+}. The fact that the correlations are not higher indicate that these elements are not only present in CFA.

The excellent correlation between ΣREEs and P_2O_5 (figure 42) shows that most of the REEs are hosted in CFA. The REEs usually substitute for Ca^{2+} in CFA (cf. section 2.2). All the Hyon boring samples plot closely to a line (figure 42) while the La Malogne samples show some deviations. The deviation for the 'phosphatic sands' (i.e. sample ECH3) is due to post-depositional weathering. De Putter et al. (1999) concluded that the cryptodolines of the Mons Basin were formed by a recent weathering process of weak intensity resulting in U mobilisation. However, the mobilised U was readily trapped in neoformed (Y,REE)-phosphates, neoformed on high-surfaced iron oxyhydroxides (De putter et al., 1999). The deviations of the other La Malogne samples can be due to their unique characteristics which are caused by unique formation processes compared to the other samples. The REEs enrichment in the sediments is discussed below.

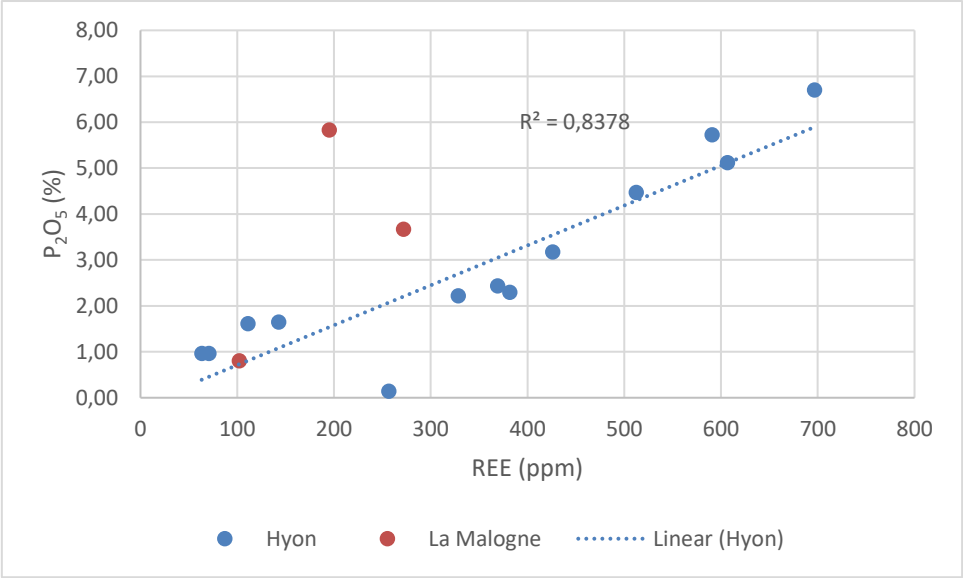

Figure 42. Plot of ΣREEs and P. The sample ECH3 is not represented in the graph.

8.3. Ce anomaly: a proxy of ancient conditions of oxygenation?

The REEs can give interesting information regarding the conditions of deposition. It has been suggested that negative Ce anomaly indicates that phosphorites gained their REEs under oxic conditions while positive Eu anomaly indicates reducing conditions (MacArthur and Walsh, 1984). However, some authors (e.g. Shields and Stille, 2001) conclude that Ce anomalies in phosphorites primarily record the influences of local diagenesis.

Except for the 'phosphatic sands' (i.e. ECH3), all the samples analysed possess a negative Ce anomaly within a narrow range (0.25 – 0.28; see table 5 and 6). In order to determine if the Ce anomalies are significant, we can use the method of Bau and Dulski (1996) using $(Ce/Ce^*)_{SN}$ and $(Pr/Pr^*)_{SN}$ defined as:

$$(Ce/Ce^*)_{SN} = Ce_{SN}/(0.5\ La_{SN} + 0.5\ Pr_{SN})$$

$$(Pr/Pr^*)_{SN} = Pr_{SN}/(0.5\ Ce_{SN} + 0.5\ Nd_{SN})$$

The graph of figure 43 indicates true Ce anomalies. Shields and Stille (2001) proposed that a good correlation between $(Ce/Ce^*)_{SN}$ and $(Eu/Eu^*)_{SN}$ ($(Eu/Eu^*)_{SN} = Eu_{Sn}/(0.5\ Sm_{SN} + 0.5\ Gd_{SN})$, taken from German et al. (1991)) confirms that diagenetic processes altered the Ce anomalies. However, no such correlation can be found for the samples of the Hyon boring (figure 44).

Furthermore, Shields and Stille (2001) also proposed that a good correlation between $(Ce/Ce^*)_{SN}$ and total REE indicates that alteration was the cause of progressive REE scavenging after deposition. The samples of the Hyon boring exhibit an antithetic correlation which is not the criteria set forth by Shields and Stille (2001) characteristic of diagenetic influence.

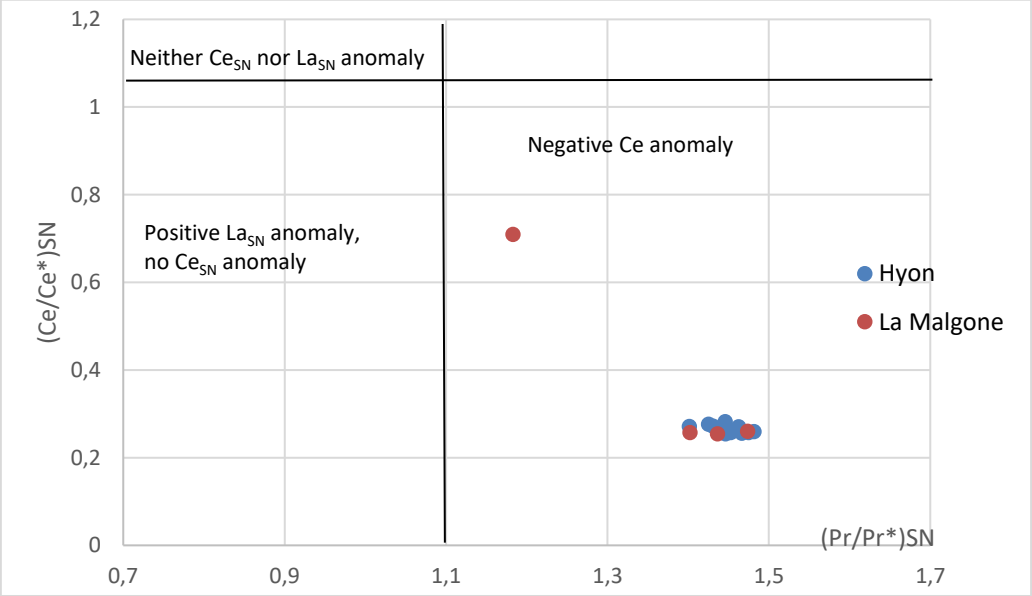

Figure 43. All the samples of the Hyon boring exhibit true negative Ce anomaly. The graph is adapted from Bau and Dulski (1996). The samples from La Malogne all have negative Ce anomaly but the 'phosphatic sand' does not plot near the other samples.

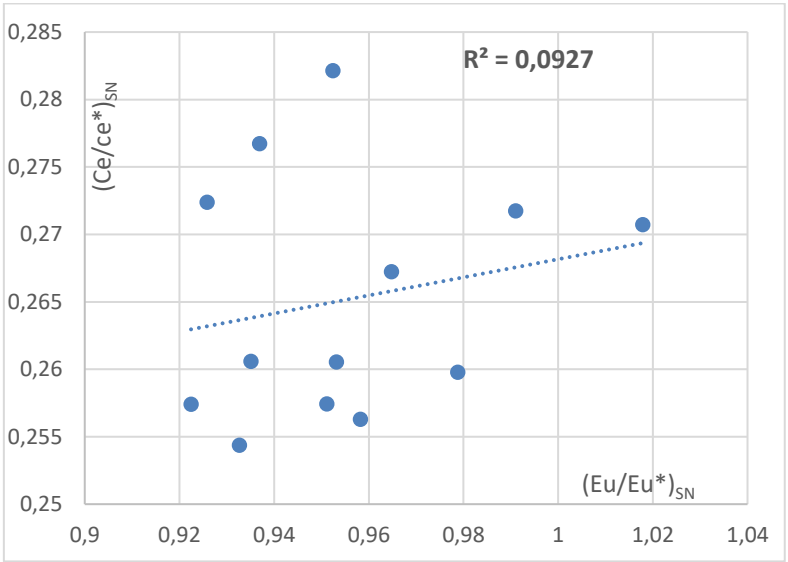

Figure 44. The lack of good correlation between $(Ce/Ce^*)_{SN}$ and $(Eu/Eu^*)_{SN}$ indicates that diagenetic processes did not play a major role in the REEs patterns. The La Malogne samples are not represented.

We can conclude that the negative Ce anomalies present at the Mons Basin are inherited from the redox conditions of the bottom waters because no significant diagenetic alteration occurred (except for the 'phosphatic sand'). The presence of bioturbation is an excellent indicator that the bottom waters of the Mons Basin were indeed oxygenated.

8.4. The origin of the peloids:

The similarity between the carbonate elements of the peloids and the matrix has already been noted (see section 6.1). This suggests that phosphatisation occurred in the sediment with CFA precipitating in the pore spaces. Even though there is clear centripetal trend of phosphatisation in some peloids, it is important to recognise that phosphatisation occurred in the core of the peloids to some degree. Extremely important are the observations of phosphatic peloids which show homogenous phosphatisation as interparticle cement (figure 45). Homogenous precipitation of CFA would be expected if the sediment were somewhat homogenous during CFA precipitation. However, this would not be expected if the peloids were already formed and later phosphatised. In this case, only centripetal phosphatisation should be expected because precipitation would occur on the surface of the grain, rendering more difficult the access to the inner parts of the grains.

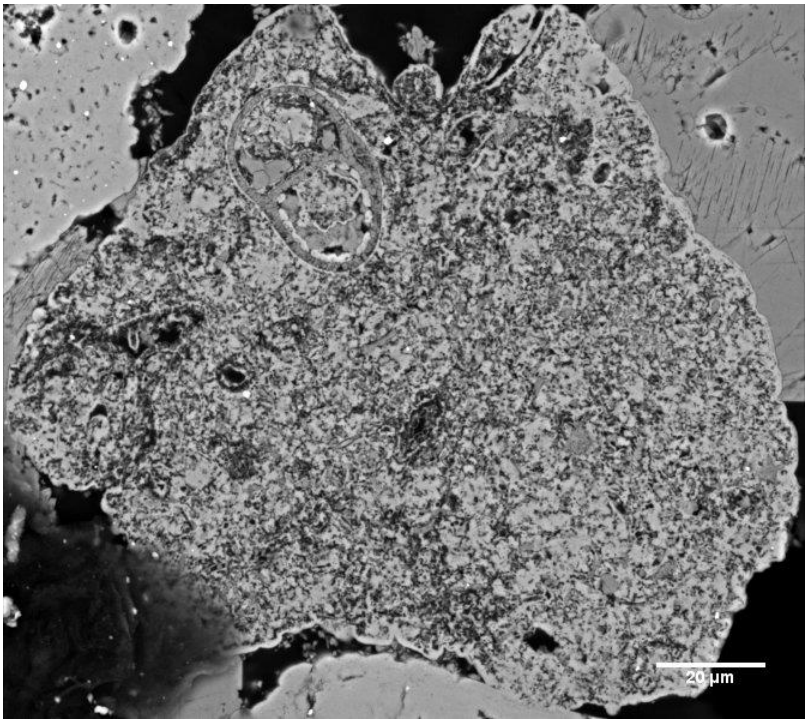

Figure 45. Back-scattered electron SEM image of a homogeneously phosphatised peloid. A thin cortex envelops the grain. The centripetal trend is clearly lacking here.

Therefore, in this case the cortex displayed by some peloids would be the testimony of another phosphatisation event after reworking of the phosphatised sediment. The centripetal phosphatisation is probably also a testimony of another phosphatisation event because there is no obvious reason why a centripetal trend of phosphatisation would occur in a rather homogenous sediment. However, there is clear evidence that phosphatisation may be very local (see figure 34). This could be due to other phosphatisation events.

The phosphatisation model proposed by Poels and Robaszynski (1988), where micritic peloids are phosphatised in a centripetal manner, should be revised for the following reasons:

- All the peloids are phosphatised in all their parts although it may be varying in intensity. Even weakly phosphatised peloids possess CFA in their core, binding the carbonate particles together. This contrasts with the model of Poels and Robaszynski (1988) where the micritic particles are solely phosphatised in a centripetal manner. According to this model, only the strongly phosphatised peloids should have CFA in their core. But the observations do not agree with this mechanism (figure 45).
- Not all peloids display a centripetal trend of phosphatisation (figure 45). This is to be expected if phosphatisation occurred rather homogenously in the sediment, filling the pore spaces and no further phosphatisation event took place for those peloids.
- Poels and Robaszynski (1988) do not consider reworking processes. While they do mention that phosphatisation is influenced by the time of the phosphatisation event and the sedimentation rate, no explicit mention of reworking processes is made. It was demonstrated, however, that reworking processes did occur and that several phosphatisation events took place (see section 6.1 and figure 21).
- The formation of purely carbonate peloids is problematic for the samples studied. It seems that there was no calcite cement that could have hold together the particles to form the peloids in the first place. The fact that no pure carbonate peloids have been found argues against the model proposed (i.e. that phosphatisation is fundamentally centripetal in already formed peloids). Even though Poels and Robaszynski (1988) did report micritic peloids, it is not evident to judge from the images published by the authors, and the observations of the present study do not corroborate this.

The new major elements to add to the phosphatisation model of the Mons Basin are the following:

- Phosphatisation occurred in the sediment as interparticle cement. This cement binds the carbonate particles together. Phosphatisation probably occurred during microbial release of phosphorus to the pore spaces due to redox condition change. Fe redox cycling probably also played a role in the release of phosphorus.
- Reworking processes lead to the formation of the peloids that subsequently resettled on the seafloor. Whatever the reworking processes involved, they did not leave traces of primary phosphorites.
- Subsequent phosphatisation events precipitated CFA on the peloids. This explains the presence of a cortex in some peloids and the centripetal trend of phosphatisation often observed. This is supported by the difference in REEs between the cortex and the core of the peloids evidenced by CL (cf. figure 18), that indicates that they originated from different phosphatisation events.
- Other phosphatisation and reworking events succeeded one another (cf. figure 21).

Given these elements, it is suitable to name those 'peloids' by the term 'intraclasts' as Jarvis (1992) did. Even though there might be debate as to where exactly phosphatisation occurred and where the peloids come from, it seems that it was not far away from the final site of deposition if not at the site of deposition itself given the limited extent of the Mons Basin. Therefore, the term 'intraclast' is a more satisfying one than 'peloid' which is strictly descriptive (see discussion in Trappe (2006)). Following the nomenclature of Trappe (2006) for the phosphatic grains, these intraclasts can be more precisely termed 'phosintraclasts'. This term is used for structureless grains of various shape formed in the same environment where they are deposited and are derived from reworking of phosphatic sediments (Trappe, 2006).

8.5. REEs patterns of the Ciply Phosphatic Chalk:

Many authors interpret normalised REEs patterns that resemble modern seawater as primary (Elderfield and Pagett, 1986; Wright et al., 1987; Piper et al., 1988; Picard et al., 2002; Martin and Scher, 2004). For the patterns that exhibit deviations, two possibilities emerge. The first is that they represent diagenetic processes such as post-depositional

alteration (McArthur and Walsh, 1984; Ilyin, 1998; Shields and Stille, 2001; Shields and Webb, 2004; Bright et al., 2009). Alternatively, those deviations may be interpreted as the result of secular variations in ocean chemistry (Wright et al., 1987; Picard et al., 2002; Lécuyer et al., 2004).

Seawater is characterised by a HREE enriched shale-normalised pattern with a pronounced Ce anomaly (Elderfield, 1988; Piepgras and Jacobsen, 1992). The Mons Basin samples present a slight MREE enrichment and a depletion of HREE (see figure 37 section 7.3). Dissolved riverine REE patterns are typically MREE enriched (e.g. Stolpe et al., 2013). Depletions of HREE have been reported in bottom sediments from estuarine settings (e.g. Censi et al., 2007) and riverbeds (Sholkovitz et al., 1999). A riverine origin of REEs seems unlikely given the very limited terrigenous supply attested by the scarcity of detrital material in the Ciply Phosphatic Chalk (see section 8.7).

Some authors have associated MREE enrichment with phosphates formed by phosphorus enrichment within the sediment caused by iron-redox cycling (Föllmi, 1996; Schenau et al., 2000; Haley et al., 2004; Crosby and Bailey, 2012). However, Auer et al. (2017) argue that redox iron cycling can be excluded as a mechanism for the formation of phosphates that are characterised by a negative Ce anomaly because REEs released from iron oxides during anoxic conditions would also liberate Ce which would be incorporated into the phosphates. However, this would not be the case if Ce was removed prior to the burial of iron oxyhydroxides. Upon dissolution under anoxic conditions REEs are released and would inherit their pattern from seawater if no diagenetic overprint occurs. This mechanism would still produce the negative Ce anomaly. This hypothesis also assumes that only iron oxyhydroxides are responsible for the REEs pattern while it seems much more complicated when considering all the possible sources (see Jarvis et al., 1994).

Moreover, the REEs and Y correlate with both P_2O_5 and Fe_2O_3 (figure 46). According to several workers (e.g. Elderfield and Greaves, 1982; de Baar et al., 1988; Sholkovitz and Elderfield, 1988) these correlations support the idea that the REEs were initially scavenged by ferric oxyhydroxides associated with biogenic detritus and were subsequently incorporated into francolite during early diagenesis. However, the correlation between P_2O_5

and Fe_2O_3 may also indicate that iron is present in CFA even though such substitutions are limited (Jarvis et al., 1994).

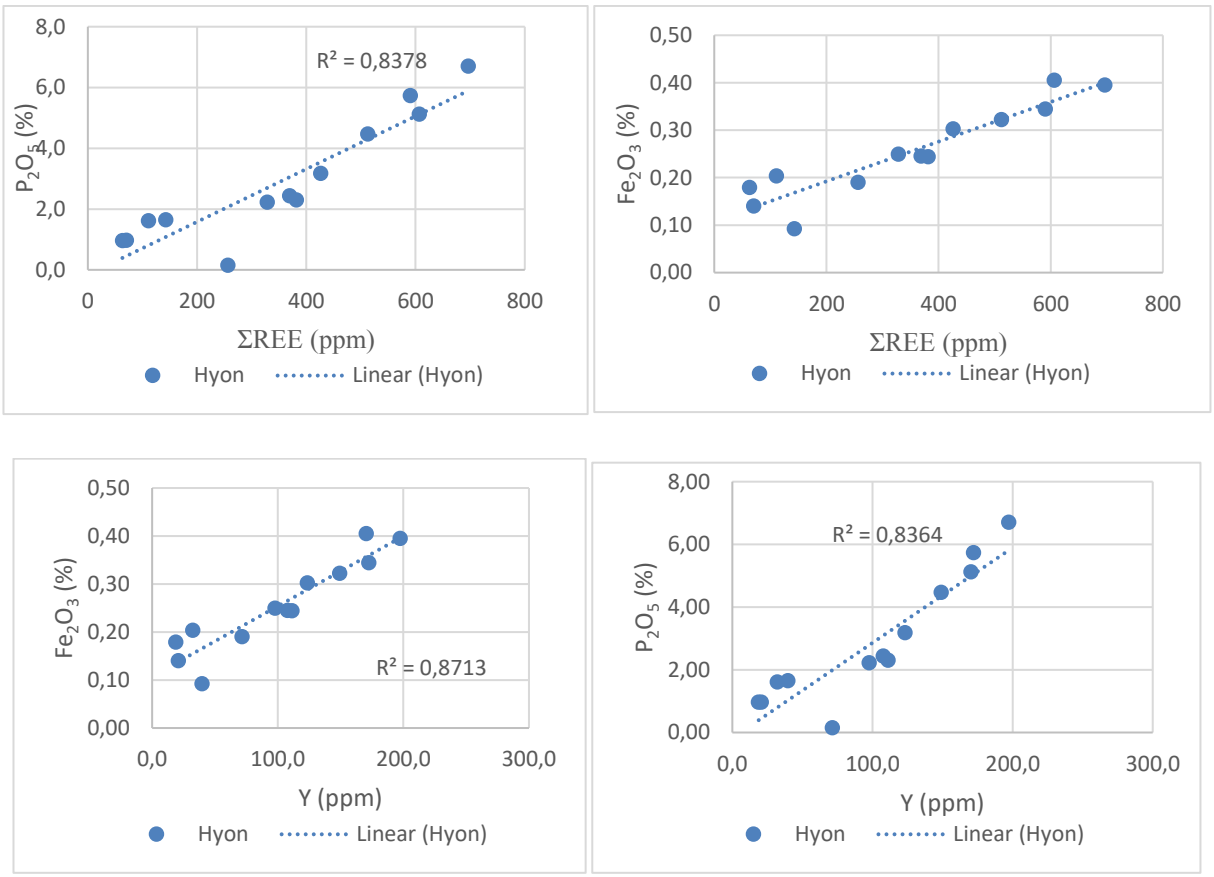

Figure 46. Plots of ΣREE vs P, ΣREE vs Fe, Y vs Fe and Y vs P. These relationships suggest that the REEs were associated with ferric oxyhydroxides and incorporated into francolite during early diagenesis upon dissolution of the iron oxyhydroxides.

Jarvis (1992) suggested that seawater is the ultimate source of the REEs for the French phosphorites because the REEs patterns are similar to those documented from open ocean seawater (Elderfield and Greaves, 1982; de Baar et al., 1985a, b) and are comparable to many other marine phosphorites (Kolodny, 1983; McArthur and Walsh, 1984; Tlig et al., 1987; Piper et al., 1988; Bonnot-Courtois and Flicoteaux, 1989). The Ciply Phosphatic Chalk exhibits similar REE patterns than that of the French phosphorites (figure 47). It is noteworthy to point out that the HREE depletion of the phosphatic chalk of Mons has much more similarity with South China Cambrian phosphorites (figure 47). It is not clear why the Ciply Phosphatic Chalk exhibit a more important HREE depletion than the French phosphorites. However, pre-Cenozoic sedimentary phosphorites are commonly reported to be HREE depleted (Shields and Webb, 2004). The depletion is not usually very important

$(Dy/Yb)_{SN}$ between 1.1 and 2.0 for Early Cambrian phosphorites of South China (Shields and Stille, 2002). The values are from 1.3 to 1.5 for the Ciply Phosphatic Chalk of the Hyon borehole. Shields and Webb (2004) concluded that HREE depletion and other unseawater-like features in ancient phosphate REE patterns are likely to be derived from post-depositional REE exchange with non-detrital components and non-quantitative uptake of REE from host sediments while REE seawater composition remained essentially the same throughout the Phanerozoic.

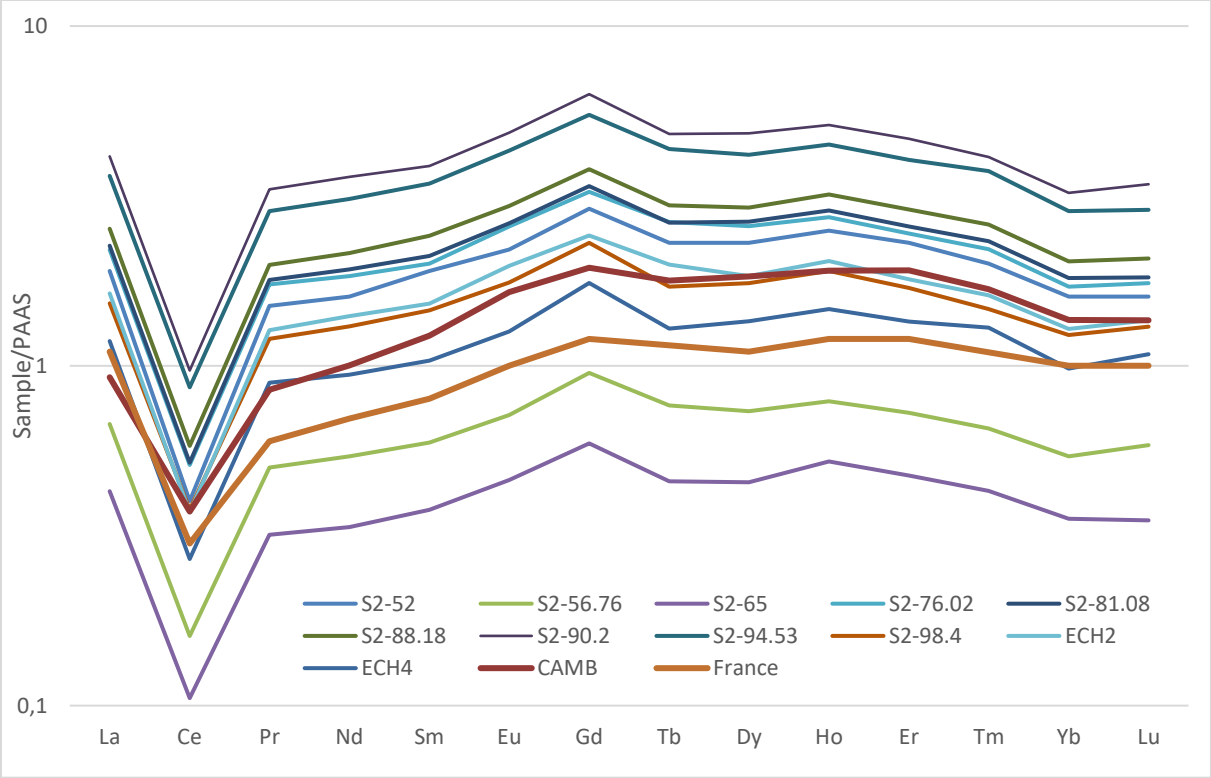

Figure 47. Shale-normalised REE patterns for some samples of the Ciply Phosphatic Chalk and the phosphatic chalk of France (labelled France; taken from Jarvis, 1992)) and a Cambrian phosphorite from South China (labelled CAMB; taken from Shields and Stille, 2001).

Emsbo et al. (2015) interpret REE patterns as secular variations in ocean chemistry. Figure 48 supposedly shows the variations of REE patterns as ocean chemistry changed through time. However, as figure 47 shows there is not much difference between the Late Cretaceous Mons Basin and the Lower Cambrian Chinese phosphorites regarding REE patterns. Questions can be raised concerning the representativeness of such data as well.

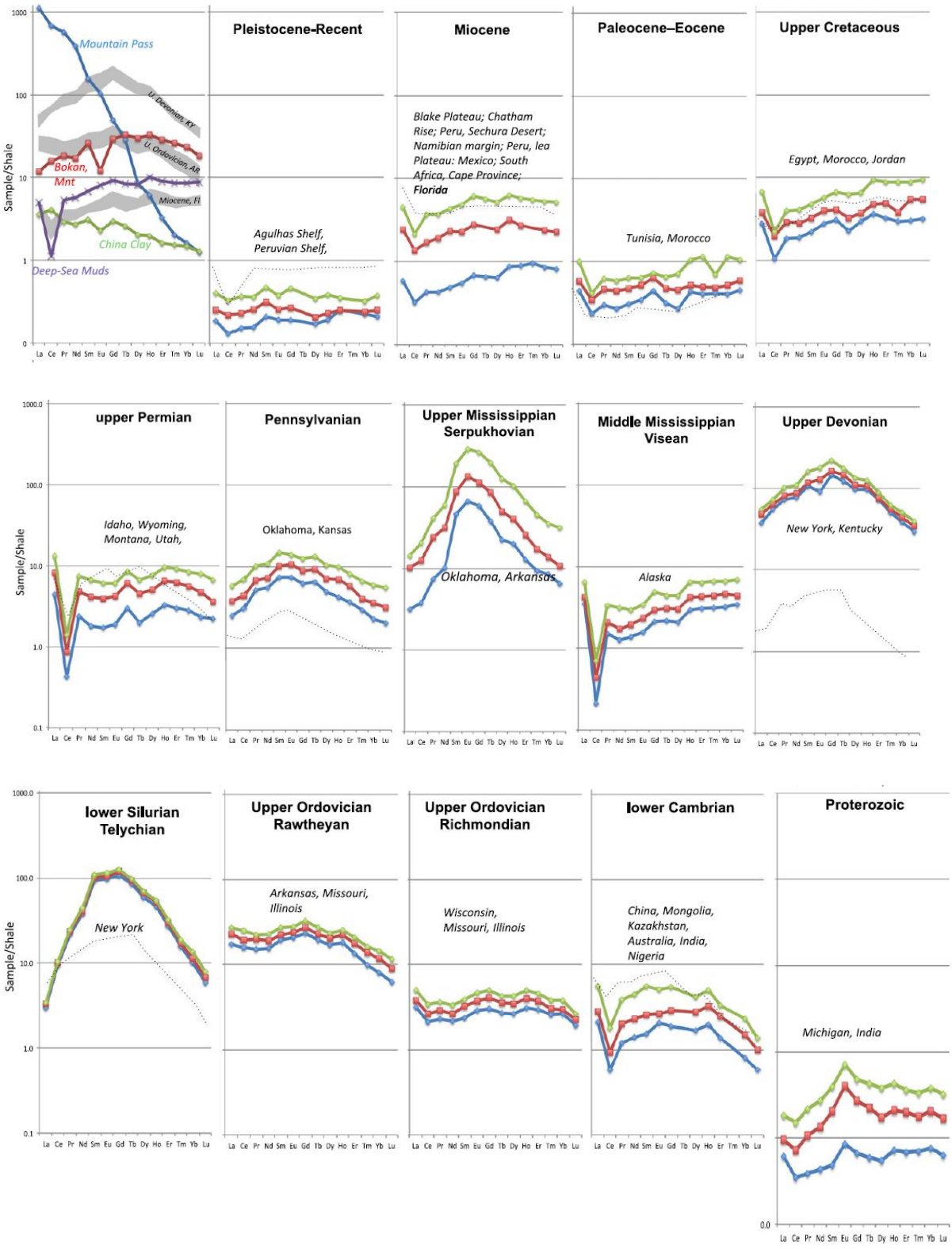

Figure 48. Shale-normalized REE (NASC, McLennan (1989)) plots for francolite from sedimentary phosphorites grouped by geologic age. From Emsbo et al. (2015). The different trends, according to Emsbo et al., (2015) reflect the secular variations in ocean chemistry regarding REEs. It would represent a powerful predictive tool for the exploration of HREES.

Given the wealth of information and hypotheses on this subject, it is difficult to single out all the processes that lead to the present REE patterns observed for the Ciply Phosphatic Chalk. However, many authors (Elderfield and Pagett, 1986; Wright et al., 1987; Piper et al., 1988; Picard et al., 2002; Lécuyer et al., 2004; Martin and Scher, 2004) agree that REE are incorporated into francolite during the earliest diagenesis, which faithfully records the REE composition of seawater at the time of deposition in modern environments. Moreover, it is suggested that granular phosphorites rarely depart from the seawater norm and tend to undergo less diagenetic alteration of REE spectra than skeletal apatite and other phosphate-types (Shields and Stille, 2001).

Because no significant diagenetic alteration affected the Ciply Phosphatic Chalk (except for the 'phosphatic sand' of La Malogne), we can be confident that the REE patterns were recorded to some extent in the francolite. However, it would be too extrapolative to state that the REE patterns of the Ciply Phosphatic Chalk record perfectly the seawater REE signature. It is more likely that some processes altered to some extent the REE patterns as explained above, and that REE seawater composition was roughly the same throughout the Phanerozoic. This is further shown by the comparison between the French phosphorites, the phosphatic chalk of the Mons Basin and the Chinese phosphorites (figure 47) which differ to a small extent.

8.6. Biogenic or inorganic origin of CFA?

Phosphatic grains with numerous microspheres similar in shape and size to coccoid-like bacteria (figure 27) have been interpreted by Salama et al. (2015) as remnants of microbial mats after reworking in Egyptian phosphorites. Coccoid cyanobacteria have been reported in phosphorites (Krajewski, 1984; Soudry and Lewy, 1988; Soudry, 1992). Many phosphatic matrices and grains are composed of minute apatite particles morphologically resembling bacteria (e.g. Baturin and Dubinchuk, 1979; Baturin et al., 1985; Mullins and Rasch, 1985; Lamboy, 1994). Some authors thus supposed that the apatite particles represent phosphate-replaced bacterial cells (O'Brien et al., 1981; Lamboy and Monty, 1984; Lamboy, 1990a, 1990b). As a result, bacterial activity would control the distribution of apatite. It is evident that such structures are not the dominant phosphate fabric for the phosphatic chalks of the Mons Basin, but that CFA mineralisation occurs as interparticle cement in

phosintraclasts. Therefore, bacterial activity does not directly control CFA mineralisation for the Mons Basin.

It is much more likely that CFA precipitation was itself an inorganic process probably influenced by microbial processes for the Ciply Phosphatic Chalk. Only the laminated CFA mineralisation is a candidate to bacterial precipitation in the Mons Basin.

8.7. High-productivity vs low-productivity system:

To better understand the formation of the Ciply Phosphatic Chalk, it is important to characterise the system in which these phosphate rocks formed. Two end-member types are usually put forward: high-productivity and low-productivity systems. In the first one, coastal upwelling plays a major role in supplying nutrients to surface waters causing primary productivities, and high organic carbon and phosphate fluxes into the sediments. A modern example of such system is the Peru-Chile shelf (see Arning et al., 2009). Such occurrence, along with others, provides the best analogues for ancient granular phosphorite – black shale – chert associations (Jarvis, 1992). According to Pufahl (2010) phosphate, biogenic chert and black shale constitute the upwelling triad, a diagnostic lithofacies assemblage for recognising high nutrient settings in the Phanerozoic.

The second type also has modern occurrences such as the east Australian continental margins (Heggie et al., 1990). This type is characterised by weak seasonal upwelling, organic carbon-poor (< 0.3 %) glauconitic foraminiferal sands, relatively low annual primary productivities, weak oxygen-minimum layers, and well-oxygenated bottom waters with low nutrient concentrations (Heggie et al., 1990; Jarvis, 1992; Jarvis et al., 1994). In these environments, Fe-oxyhydroxides scavenge the phosphate that is released by oxidation of organic matter. They are then dissolved as anoxic conditions develop during early burial, and ferrous Fe diffuses back to the oxic-post-oxic interface (1-2 cm depth) where it is reprecipitated (Schaffer, 1986; Froelich et al., 1988).

The lack of organic C-rich sediments, such as black shales, is an important element that seems to render unlikely the scenario in which the Mons Basin was a high-productivity system subjected to major coastal upwellings. This feature is also lacking in the phosphatic chalks of France (cf. Jarvis, 1992). This contrasts with other Late Cretaceous phosphorites

such as the Late Cretaceous phosphorites of Egypt (e.g. Baioumy and Tada, 2005; Salama et al., 2015). Upwelling, high productivity and intensification of the oxygen minimum zone were probably caused by the prevailing westerly wind direction in Tethys during the Late Cretaceous (Gordon, 1979; Germann et al., 1987).

It seems that the ultimate source of phosphorus is the seawater. Even though fluvial input may be one of the possible sources of phosphorus (e.g. Glenn and Arthur, 1990; Zanin et al., 1990), it is implausible in the case of phosphatic chalks. During Late Cretaceous, north-western European paleogeography was dominated by an extensive epicontinental sea bordered by restricted, arid, low-lying massifs (Hancock, 1975, 1990; Ziegler, 1982; Barron, 1987; Tyson and Funnell, 1987; Hart, 1990). Therefore, little siliciclastic material was delivered and there is no evidence of significant fluvial input anywhere in north-western Europe (Jarvis, 1992).

For either the high-productivity system or the low-productivity one, upwelling is still a requirement. However, major ones are not necessary as evidenced by the modern examples of low-productivity systems. No modern deposits where upwelling is totally absent have been described (Jarvis, 1992).

The Ciply Phosphatic Chalk likely represents a low-productivity system characterised by a weak or absent oxygen-minimum layer as evidenced by well-oxygenated bottom waters (as demonstrated in section 8.3) and the absence of black shale. The presence of glauconite in the CPC also fits the low-productivity system. Robaszynski and Martin (1988) suggested that phosphate sedimentation occurred under anoxic conditions based on the observations by Cornet (1909) of the grey colour of phosphatic grains (reduced iron) and the presence of pyrite. However, strong negative Ce anomalies and bioturbation do not support this hypothesis. Moreover, pyrite and reduced iron are produced in the sediments upon redox conditions changes (see section 2.5.1). In these settings, Fe redox cycling was probably acting alongside bacterial processes leading to the sediment porewater enrichment in phosphorus. The respective importance of these processes is hard to evaluate.

8.8. Spatial and temporal controls:

Because of the scarcity of paleoenvironmental information for the Mons Basin, it is difficult to establish an exact scenario for the reconstruction of the history of the Ciply Phosphatic Chalk. However, given the close spatial and temporal relationship with the French deposits (figure 49), it is possible to infer important factors influencing the phosphatisation in the Maastrichtian. Jarvis (1992) especially contributed to much of the information available for the French deposits.

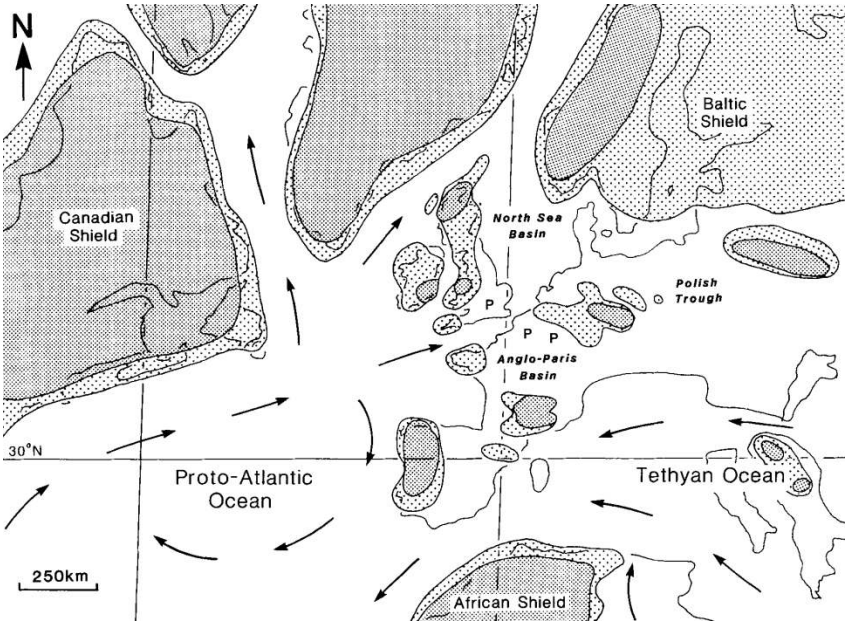

Figure 49. Late Cretaceous paleogeography of the north-eastern Atlantic and Western Europe showing the palaeoceanographic setting of the Anglo-Paris Basin. P indicates position of phosphatic chalk deposits. Taken from Jarvis (1992).

The Maastrichtian Ciply Phosphatic Chalk has many similarities with the Santonian – Lower Campanian phosphatic chalks of northern France. They are lithologically similar. Well-oxygenated waters bathed the seafloor of the French deposits (Jarvis, 1992) as it was the case in the Mons Basin where both bioturbation and negative Ce anomaly indicate oxic conditions of deposition.

According to Jarvis (1992), prior to the mid-Cretaceous, the water depths were insufficient in the Anglo-Paris Basin to allow the influx of nutrient-rich waters and the initiation of significant phosphatisation. The phosphatisation of the Anglo-Paris Basin was probably controlled by a critical environmental window which was, in part, related to eustatic sea

level (figure 50; Jarvis, 1992). Both the Santonian – Lower Campanian deposits and the Lower Maastrichtian deposits accumulated during eustatic sea level fall, although of different amplitude (figure 50). The two periods of phosphatic chalk deposition in the Anglo-Paris Basin lie within a very narrow range of sea levels (230-240 m above present) predicted by the long-term eustatic curves of Haq et al (1987).

It has long been recognised that the Late Cretaceous was one of the major periods of eustatic sea level highstand (Suess, 1875). Therefore, deposition of pelagic sediments on continental areas took place as broad epicontinental seas, restricted siliciclastic deposition and warm equable climates prevailed (Hancock and Kauffman, 1979). Warm climate would have caused more intense chemical weathering of continental areas and increased the supply of phosphorus and other nutrients to the oceans, promoting global productivity (Jarvis, 1992). Lower polar-equatorial thermal gradients would have caused the development of warmer, less-oxygenated deep-water masses, which would have acted as more effective phosphorus reservoirs and ultimately resulted in more productive upwelling regimes (Jarvis, 1992). Moreover, epicontinental seas would have been exposed to pelagic sediment deposition as sea level highstands prevailed.

The phosphatic chalks were interpreted as being predominantly transgressive deposits (the transgression is of a higher-order cycle than the regression already mentioned; see figure 50; Jarvis, 2006). Study of boreholes in the Mons Basin showed that transgressions prevailed during phosphate sedimentation. This is evidenced by several levels of pelagic organisms such as belemnites. According to Robaszynski and Martin (1988), rises of sea level must have favoured inflow of chemical elements such as phosphorus and silicon. This hypothesis would agree with the existence of a Proto-Gulf Stream in the Cretaceous Atlantic Ocean (Hart, 1976) from which upwelling currents might have flowed onto a shelf spreading from Southern England to Picardy and to the Mons Basin.

While the French deposits are primarily erosional structures whose location may have been influenced by synsedimentary tectonics (Monciardini, 1989), the Mons Basin seems to have been more significantly tectonically controlled. The tectonic evolution characterised in the Mons Basin may be partly related to the global geodynamic evolution of north-western Europe (Vandycke et al., 1991).

No paleobathymetric data is available for the phosphatic chalks of the Mons Basin. The French deposits were interpreted as having been deposited between 70 m and a few hundred metres (Jarvis, 2006). Given the numerous similarities between the French and Belgian deposits, we would expect analogous depths of deposition.

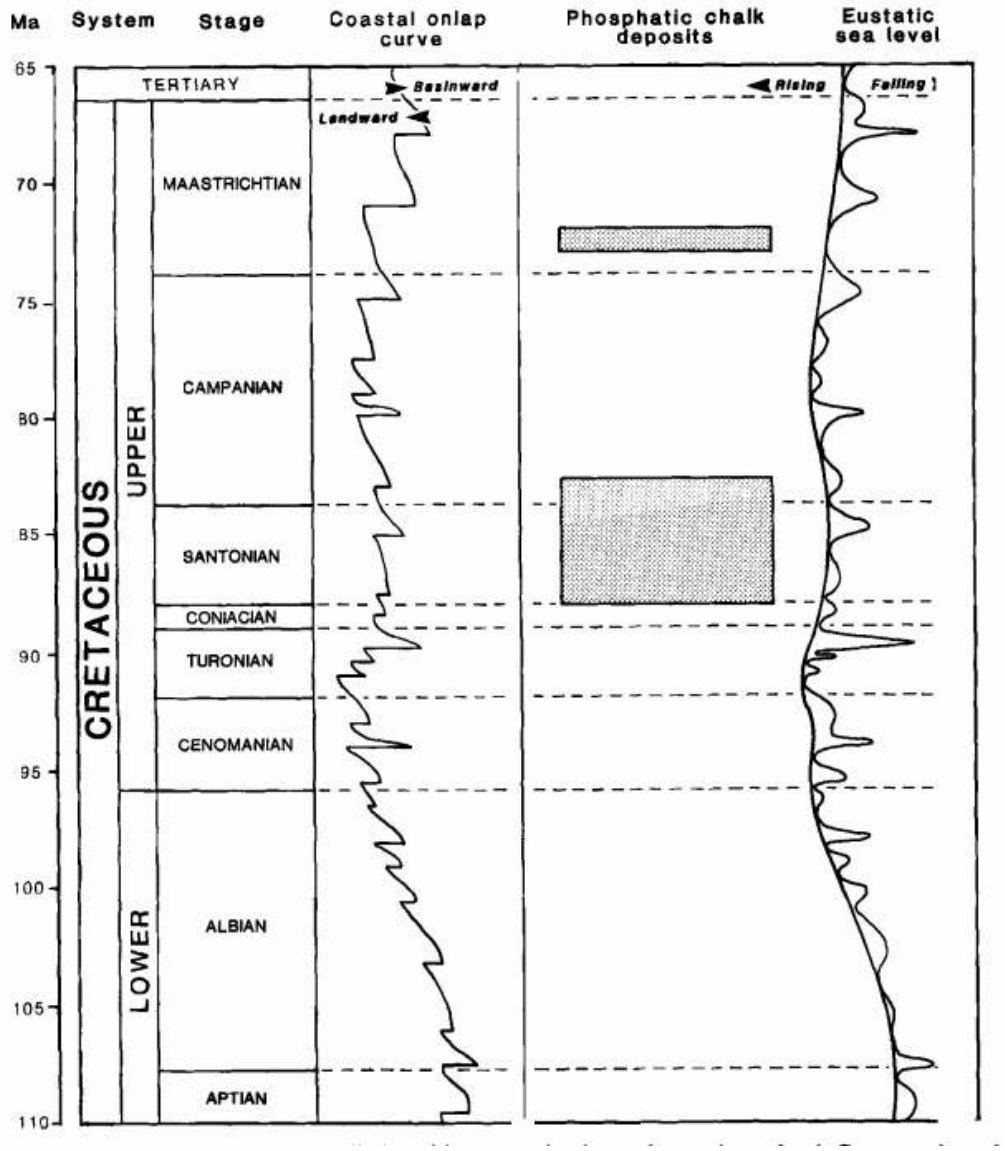

Figure 50. Relationship between phosphatic chalk deposition, coastal onlap and eustatic sea level. Curves and geochronology after Haq et al. (1987). Taken from Jarvis (1992).

8.9. Silicification and chert beds:

The presence of chert beds in the Hyon boring and the absence of silicification at the La Malogne underground quarry have already been noted (see Robaszynski and Martin, 1988). The source of silica is most likely biogenic as it is the case in most carbonate rocks (Hesse, 1989).

It can be argued that silicification was an early diagenetic phenomenon because studies showed that the Campanian chalks of the Mons Basin were not affected by burial diagenesis (Richard et al., 2005). It can be extrapolated that if the Campanian chalks of the Mons Basin did not undergo burial diagenesis, then the Maastrichtian phosphatic chalks of the Mons Basin did not either. It is also noteworthy to point out the low diagenetic potential of chalks in general (Flügel, 2004).

There appears to be different energy levels between La Malogne underground quarry and the Hyon boring. Indeed, the conglomeratic beds of La Malogne points to higher energy levels. It is recognised that different rates of subsidence characterised the Ciply Phosphatic Chalk of La Malogne and the Hyon boring given that the thickness of the phosphatic formation is highly variable, from a few metres to about 70 metres respectively (Robaszynski and Martin, 1988). The absence of chert at La Malogne may also be a sign of elevated energy level compared to the Hyon boring. It has been suggested that if the chert forming process within the sediment is disturbed by reworking, then the nucleation process is halted, and the silica disseminated (Mortimore et al., 2017).

The chert beds of the Hyon boring were not studied thoroughly and their origin is not certain. However, the elements mentioned above may provide important information regarding the conditions required for silicification. If silicification was an early diagenetic process, then it is reasonable to postulate that a frequent reworking of the sediment would prevent the porewater sediment to be supersaturated with respect to silica. However, in deeper parts of the basin, given that the sediment is exposed to lower energy levels, it is possible for silica to accumulate in the porewater sediment. Because of the lithological, mineralogical and chemical similarity of the La Malogne underground quarry and the Hyon boring, it is difficult to invoke any other major difference that would explain the presence or absence of chert beds. But this matter is far from being settled.

8.10. Genetic model for the Ciply Phosphatic Chalk:

All the information gathered thus far allow for the proposition of an updated genetic model for the formation of the Ciply Phosphatic Chalk.

A high sea-level covered the Mons Basin and caused pelagic sedimentation (attested by the presence of belemnites). It also brought nutrients to the Basin. Because the waters were well-oxygenated, as evidenced by bioturbation and negative Ce-anomalies, Fe-redox cycling likely played an important role in the concentration of P in the sediment by scavenging P from the water column and being buried in the sediment. As the redox conditions shift from oxic to suboxic, Fe-oxyhydroxides dissolve and liberate the adsorbed P in the sediments (figure 51). Bacterial processes might have been important in order to trap the liberated P. Microbial breakdown of organic matter was also likely a process leading to P enrichment in the sediment. However, as the water column was essentially oxygenated, less organic matter reached the seafloor because it was readily recycled. It is difficult to appreciate the relative importance of these processes.

As a result of the enrichment of the pore water in P, francolite precipitated rapidly as interparticle cement via an amorphous precursor (see section 8.1). The rapid character of phosphatisation is demonstrated by the presence of coccoid-like bacteria CFA moulds (see figure 27). It is also demonstrated by the globular ultrastructure of some phosphatic fabric (see section 8.1). There is also evidence that CFA precipitated in a laminar fashion (figure 21 and 26). The presence of phosphatic ooids is puzzling. They might be linked to microbial phosphate precipitation (Trappe, 2006). In any case, laminated CFA represents only a small percentage of the total CFA mineralisation.

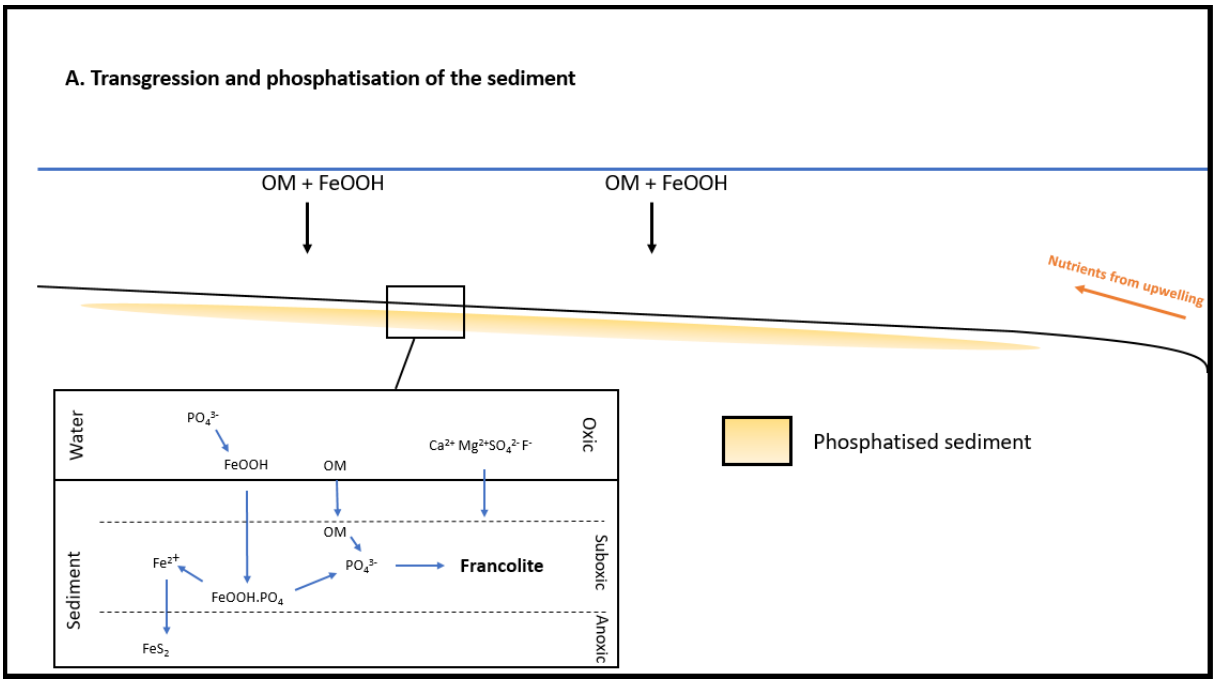

Figure 51. Representation of the first stage of the formation of the CPC.

Soon after the formation of this phosphatised sediment, reworking processes took place and reworked the sediment (figure 52). As a result, the sediment ripped up causing the formation of the phosintraclasts. The location of the formation of these grains cannot be known for sure but it certainly originated from the basin, not far from the site of deposition. It could be argued that the site of origin of the phosintraclasts was relatively shallow and thus more exposed to reworking. This is suggested by the presence of chert beds in the Hyon borehole which might indicate lower energy levels (see section 8.9). Therefore, we would expect trace of primary phosphorites if this site was subject to less reworking, but none is found.

The cause of reworking is difficult to establish. It may be linked to wave action during storm events (Trappe, 2006) because the sediment was relatively soft. It may also be linked to sea-level fluctuations but there is no evidence yet for the CPC. Whatever the reworking process, it did not leave primary phosphate rock in all the samples studied. Therefore, reworking was frequent. Consequently, wave action during storms is more likely the main reworking process.

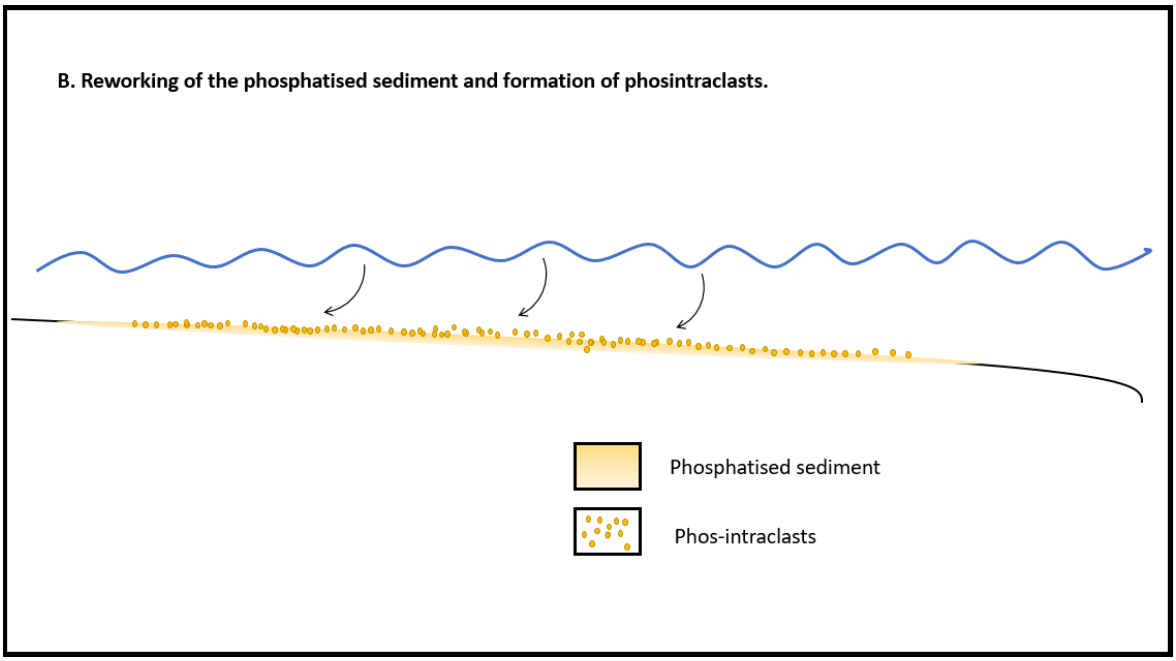

Figure 52. Representation of the second stage of the formation of the CPC.

Further phosphatisation took place in calmer periods. Some phosphatised grains underwent several phosphatisation events as evidenced by the presence of a cortex and the centripetal trend of phosphatisation (see section 8.4). Subsidence to the north of the basin created room for sediments which produced a thicker sequence of phosphatic chalk (see section 3.1 and 8.9) at the site of the Hyon borehole relative to the La Malogne underground quarry.

The hardground capping the Ciply Phosphatic Chalk separates the phosphatic chalks from the overlying white chalks devoid of phosphatic grains except for the lowermost part. It represents a period of non-deposition produced either by a rising or falling of the sea-level. It could represent the maximum flooding surface during transgression, corresponding to the highest stand of eustatic sea level. On the other hand, the hardground could also represent a sea level fall, swell-wave action and tidal currents precluding sediment accumulation on the seafloor (Christ et al., 2015). The end of the phosphatic sequence corresponds to a sea level fall according to the curves of Haq et al. (1987; figure 50). As a result, the hardground capping the CPC probably represents a period of sea-level fall during which no sediment accumulated. The cause for the cessation of phosphatisation is not known.

8.11. Economic potential of the Ciply Phosphatic Chalk:

Robaszynski and Martin (1988) estimated the resources of the Ciply Phosphatic Chalk at 960 million tons at a grade comprised between 5 and 10 % P_2O_5. The P_2O_5 contents of the samples of the Hyon borehole and the La Malogne underground quarry rarely exceed 5 % (cf. table 3). Only the "phosphatic sands" reach concentrations slightly over 10 %. However, in other parts of the Mons Basin, relatively high P_2O_5 contents are reported ranging from 7% to 13.5 % (Robaszynski and Martin, 1988). By taking 5 % P_2O_5, around 47 million tons could be retrieved from the Mons Basin while 96 million tons could be recovered by taking 10 % as the average value.

The REE contents average is around 350 ppm (cf. table 5) for the Hyon borehole and 660 ppm for the La Malogne borehole. However, this number is not representative for the La Malogne underground quarry because phosphatic sands are not very common.

By taking 350 ppm as the average value of the Mons Basin, the total REE that could be recovered amount to approximately 33 600 tons of REE based on the estimation of the resources of Robaszynski and Martin (1988). For the LREE, taking the average of the Hyon borehole, 19 584 tons are potentially retrievable while for the HREE, taking the Hyon borehole average, 14 112 tons.

Because Europe is mainly relying on non-European sources to meet its needs in REE (European Commission, 2017), the REE of the Mons Basin could potentially diminish Europe's dependency on these countries.

9. Conclusion:

The phosphatic calcarenite of the Mons Basin was probably formed under the influence of upwelling that brought nutrients, such as phosphorus and silicon, to the shallow epicontinental sea of the Mons Basin during transgressive events. The formation of the phosphatic chalk is linked to an overall period of eustatic sea-level highstand. The Ciply Phosphatic Chalk of the Mons Basin may represent a cycle of transgression-regression where nutrients are brought as the sea-level rises. The hardground capping the sequence probably originates from the following regression which prevented sediment deposition. There were a set of conditions favourable for the development of phosphatic chalk that was not reproduced above the hardground where chalk sedimentation resumed. The reason for the absence of phosphatisation above the hardground is presently unknown.

Phosphogenesis occurred in the sediment mainly in the form of interparticle carbonate-fluorapatite cement. Microbial breakdown of organic matter along with Fe-redox cycling are the likely processes of phosphorus pore water enrichment. There is no direct evidence of microbial phosphatisation. However, some laminated mineralisation may have arisen from organic activity.

The primary phosphatic sediment was reworked in the form of phosintraclasts. Several phosphatisation and reworking events took place. The rare earth elements were incorporated in CFA during phosphogenesis. The source of REE in phosphorites is most likely seawater and the REE patterns recorded in the phosphatic chalk should retain to some extent the primary signature of seawater. However, it has been discussed that the original seawater signature was probably altered by syndepositional processes.

The Ciply Phosphatic Chalk represents a non-negligible source of phosphorus and REE for Europe. However, the direct proximity of urban areas renders the exploitation of the deposit very difficult.

Further studies should aim at better characterising the paleoenvironmental conditions (pore-water temperature, age of phosphogenesis…). Stable isotopic studies will give new insights into the formation of the deposit. LA-ICP-MS studies could describe the

compositional variability in the phosphatic grains and give new clues regarding the phosphogenetic processes.

References:

Altschuler, Z.S., 1980, The geochemistry of trace elements in marine phosphorites. Part 1. Characteristic abundances and enrichment. In: Marine phosphorites – Geochemistry, Occurrence, Genesis (Ed. By Y.K. Bentor), Spec. publs Soc, econ. Paleont. Miner. 29, p. 19-30.

Arning, E.T., Birgel, D., Brunner, B., Peckmann, J., 2009, Bacterial formation of phosphatic laminites off Peru, Geobiology 7, p. 295-307.

Auer, G., Reuter, M., Hauzenberger, C.A., Piller, W.E., 2017, The impact of transport processes on rare earth element patterns in marine authigenic and biogenic phosphates. Geochim. Cosmochim. Acta 203, p. 140-156.

Baele, J.M., Hennebert, M., 2016, La Malogne Underground Quarry – Field Trip Documents 5th International Geologica Belgica Congress.

Baioumy, H., Tada, R., 2005, Origin of Late Cretaceous phosphorites in Egypt. Cretaceous Research 26, p. 261-275.

Barron, E.J., 1987, Global Cretaceous paleogeography – International Geologic Correlation Program Project 191. Palaeogeogr. Palaeoclim. Palaeoecol. 59, p. 207-214.

Baturin, G.N., 1982, Phosphorites on the sea floor, Nature 232, p. 61-62.

Baturin, G.N., Bersenev, I.I., Gusev, V.V., Leliukov, E.P., Schechenko, A.J., Shkolnik, E.L., 1985, Ultramicroscopic investigation of the structure of phosphorites from the bottom of the Sea of Japan. Dokl. Akad. Nauk SSSR 281, p. 1169-1172 (in Russian).

Baturin, G.N., Dubinchuk, V.T., 1979, Microstructures of Oceanic Phosphorites. Atlas of Photomicrographs. Izd. Nauka, Moscow (in Russian).

Bau., M., Dulski, P., 1996 Distribution of yttrium and rare-earth elements in the Penge and Kuruman iron-formations, Transvaal Supergroup, South Africa. Precambrian Research 79, p. 37-55.

Benitez-Nelson, C.R., 2000, The biogeochemical cycling of phosphorus in marine systems, Earth-Science Reviews 51, p. 109-135.

Bentor, Y.K., 1980, Phosphorites – the unsolved problems. In: Y.K. Bentor (Editor), Marine Phosphorites – Geochemistry, Occurrence, Genesis, Soc. Econ. Paleontol. Mineral. Spec. Publ. 29, p. 3-18.

Berner, R.A., Ruttenberg, K.C., Ingall, E.D., Rao, J.L., 1993, The nature of phosphorus burial in modern marine sediments. In: Wollast, R., Mackenzie, F.T., Chou, L., (Editors), Interactions of C, N, P and S Biochemical Cycles and Global Change. NATO ASI Series, I4, Springer, Nerlin, p. 365-378.

Bertram, C.J., Elderfield, H., 1993, The geochemical balance of the rare earth elements and neodymium isotopes in the ocean. Geochim Cosmochim Acta 57, p. 1957-1986.

Bonnot-Courtois, C., Flicoteaux, R., 1989, Distribution of rare-earth and some trace elements in Tertiary phosphorites from the Senegal Basin and their weathering products. Chem. Geol. 75, p. 311-328.

Bright, C.A., Cruse, A.M., Lyons, T.W., MacLeod, K.G., Glascock, M.D., Ethington, R.L., 2009, Seawater rare-earth element patterns preserved in apatite of Pennsylvanian conodonts ? Geochimica et Cosmochimica Acta 73, p. 1609-1624.

Burnett, W.C., Gomberg, D.N., 1977, Uranium oxidation and probable subaerial weathering of phosphatized limestone from Pourtales Terrace, Sedimentology, 24, p. 291-302.

Burnett, W.C., Veeh, H.H., 1997, Uranium series disequilibrium series in phosphorites nodules from the west coast of South America, Geochim et Cosmochim Acta, 41, p. 755-764.

Carlton, R.G., Wetzel, R.G., 1988, Phosphorus flux from lake sediments: Affect of epipelic algal oxygen production. Limnol. Oceanogr. 33, p. 562-570.

Cayeux, L., 1939, Les phosphates de Chaux Sédimentaires de France I. France Metropolitaine. Etudes des gîtes Mineraux de la France, Imprimerie Nationale, Paris, 349 p.

Censi, P., Sprovieri, M., Saiano, F., Di Geronimo, S.I., Larocca, D., Placenti, F., 2007, The behaviour of REEs in Thailand's Mae Klong estuary : Suggestions from the Y /Ho ratios lanthanide tetrad effects. Estuar. Coast. Shelf Sci. 71, p. 569-579.

Chen, N., Pan, Y., Weil, J.A., 2002a. Electron paramagnetic resonance spectroscopic study of synthetic fluorapatite: part I. Local structural environment and substitution mechanism of Gd at the Ca2 site. Am. Mineral. 87, p. 37–46.

Chen, N., Pan, Y., Weil, J.A., Nilges, M.J., 2002b. Electron paramagnetic resonance spectroscopic study of synthetic fluorapatite: part II. Gd3+ at the Ca1 site, with a neighboring Ca2 vacancy. Am. Mineral. 87, p. 47–55.

Cherniak, D.J., 2000. Rare earth element diffusion in apatite. Geochim. Cosmochim. Acta 64, p. 3871–3885.

Christ, N., Immenhauser, A., Wood, R.A., Darwich, K., Niedermayr, A., 2015. Petrography and environmental controls on the formation of Phanerozoic marine carbonate hardgrounds, Earth-Science Reviews, Volume 151, Pages 176-226.

Comodi, P., Liu, Y., Stoppa, F., Woolley, A.R., 1999. A multi-method analysis of Si-, S- and REE-rich apatite from a new kind of kalsilite-bearing leucitite (Abruzzi, Italy). Mineral. Mag. 63, p. 661–672.

Cornet, J., 1909, Geologie T.I. Mons, 298 pp.

Crosby, C.H., Bailey, J.V., 2012, The role of microbes in the formation of modern and ancient phosphatic mineral deposits. Front. Microbiol. 3, p. 1-7.

De Baar, H.J.W., Bacon, M.P., Brewer, P.G., Bruland, K.W., 1985a, Rare earth elements in the Pacific and Atlantic Oceans. Geochim. Cosmochim. Acta 49, p. 1943-1959.

De Baar, H.J.W., Brewer, P.G., Bacon, M.P., 1985b, Anomalies in rare earth distributions in seawater; Gd and Tb. Geochim. Cosmochim. Acta 49, p. 1955-1963.

De Baar, H.J.W., German, C.R., Elderfield, H., Van Gaans, P., 1988, Rare earth element distributions in anoxic waters of the Cariaco Trench. Geochim. Cosmochim. Acta 52, p. 1203-1219.

De Putter, T., Charlet, J.M., Quinif, Y., 1999, REE, Y and U concentration at the fluid-iron oxide interface in late Cenozoic cryptodolines from Southern Belgium, Chemical Geology 153, p. 139-150.

Drummond, J.B., Pufahl, P.K., Porto, C.G., and Carvalho, M., 2015, Neoproterozoic peritidal phosphorite from the Sete Lagoas Formation (Brazil) and the Precambrian phosphorus cycle: Sedimentology 62, p. 1978–2008.

Duce, R.A., Liss, P.S., Merrill, J.T., Atlas, E.L., Buat-Menard, P., Hicks, B.B., Miller, J.M., Prospero, J.M., Arimoto, R., Church, T.M., Ellis, W., Galloway, J.N., Hansen, L., Jickells, T.D., Knap, A.H., Reinhardt, K.H., Schneider, B., Soudine, A., Tokos, J.J., Tsunogai, S., Wollast, R., Zhou, M., 1991, The atmospheric input of trace species to the world ocean, Global Biogeochem. Cycles 5, p. 193-259.

Dupuis, C., Robaszynski, F., 1986, Tertiary and Quaternary deposits in and around the Mons Basin, Documents for a field trip, Meded. Werkgr. Tert. Kwart. Geol. 23 (1), p. 3-19.

Elderfield, H., 1988, The oceanic chemistry of the rare-earth elements. Philos. Trans. R. Soc. London 325, p. 105-126.

Elderfield, H., Greaves, M.J., 1982, The rare earth elements in seawater. Nature 296, p. 214-219.

Elderfield, H., Pagett, R., 1986, Rare earth elements in ichtyoliths: variations with redox conditions and depositional environment. The Science of the Total Environment 49, p. 175-197.

Emsbo, P., McLaughlin, P.I., Breit, G.N., du Bray, E.A., Koenig, A.E., 2015, Rare earth elements in sedimentary phosphate deposits: Solution to the global REE crisis?, Gondwana Research, Volume 27, Issue 2, Pages 776-785.

European Commission, 2017, Critical Raw Materials, http://ec.europa.eu/growth/sectors/raw-materials/specific-interest/critical_en.

European Community, 2017. Special Publication No. 6 of the Society for Geology Applied to Mineral Deposits, vol 6. Springer, Berlin, Heidelberg.

Feely, R.A., Massoth, G.J., Baker, E.T., Cowen, J.P., Lamb, M.F., Krogslund, K.A., 1990, The effect of hydrothermal processes on midwater phosphorus distributions in the northeast Pacific, Earth Planet. Sci. Lett. 96, p. 305-318.

Felsche, F., 1972. Rare earth silicates with apatite structure. J. Solid State Chem. 5, p. 266–275.

Filippelli, G.M., 2008, The global phosphorus cycle: Past, present, and future, Elements 4, p. 89-95.

Filippelli, G.M., 2011, Phosphate rock formation and marine phosphorus geochemistry: The deep time perspective, Chemosphere 84, p. 759-766.

Fleet, M.E., Pan, Y., 1995. Site preference of rare earth elements in fluorapatite. Am. Mineral. 80, p. 329–335.

Flügel, E. ,2004. Flügel, E. Microfacies of Carbonate Rocks: Analysis, Interpretation and Application Springer Berlin.

Folk, R.L., 1959, Practical petrographic classification of limestones, Bulletin of the American association of petroleum geologists 43 (1), p. 1-38.

Föllmi, K.B., 1996, The phosphorus cycle, phosphogenesis and marine phosphate-rich deposits, Earth-Science Review 40, p. 55-124.

Froelich, P.N., Arthur, M.A., Burnett, W.C., Deakin, M., Hensley, V., Jahnke, R., Kaul, L., Kim, K.H., Roe, K., Soutar, A., Vathakanon, C., 1988, Early diagenesis of organic matter in Peru continental margin sediments: phosphorites precipitation. Mar. Geol. 80, p. 309-343.

Froelich, P.N., Bender, M.L., Heath, G.R., 1977, Phosphorus accumulation rates in metalliferous sediments on the East Pacific Rise, Earth Planet. Sci. Lett. 34, p. 351-359.

Froelich, P.N., Bender, M.L., Luedtke, N.A., Heath, G.R., De Vries, T., 1982, The marine phosphorus cycle, Am. J. Sci. 282, p. 474-511.

Froelich, P.N., Klinkhammer, G.P., Bender, M.L., Luedtke, N.A., Heath, G.R., Cullen, D., Dauphin, P., Maynard, V., 1979, Early oxidation of organic matter in pelagic sediments of the eastern equatorial Atlantic: Suboxic diagenesis, Geochimica et Cosmochimica Acta 43, p. 1075-1090.

Gächter, R., Meyer, J.S., Mares, A., 1988, Contribution of bacteria to release and fixation of phosphorus in lake sediments. Limnol. Oceanogr. 33, p. 1542-1558.

German, C.R., Holliday, B.P., Elderfield, H., 1991, Redox cycling of rare earth elements in the suboxic zone of the Black Sea. Geochimica et Cosmochimica Acta 55 (12), p. 3553-3558.

Germann, K., Bock, W.D., Ganz, H., Schroter, T., Troger, U., 1987, Depositional conditions of late Cretaceous phosphorites and black shales in Egypt. Berliner Goewissenschaftliche Abhandlungen Reihe A 57, p. 629-668.

Gilinskaya, L.G., 1991, A new type of PO43-centre in apatite, J Struct Chem, 31, p. 892-898.

Gilinskaya, L.G., Zanin, Y.N., Knubovets, R.G., Korneva, T.A., Fadeeva, V.P., 1993, Organophosphorus radicals in naturalapatites (Ca5(PO4)3(F,OH), J Struct Chem, 33, p. 1463-1467.

Glenn, C.R. & Föllmi, Karl & Riggs, S.R. & Baturin, G.N. & Grimm, Kurt & Trappe, J & Abed, Abdulkader & Galli-Oliver, C & Garrison, R.E. & Ilyan, A.V. & Jehl, C & Rohrlich, V & Sadaqah, Rushdi & Schidlowski, M & E. Sheldon, R & Siegmund, H., 1994, Phosphorus and Phosphorites: Sedimentology and Environments of Formation, Eclogae Geologicae Helvetiae. 87. 747-788.

Glenn, C.R., Arthur, M.A., 1990, Anatomy and origin of a Cretaceous phosphorites-greensand giant, Egypt. Sedimentology 37, p. 123-154.

Gordon, W.A., 1979, Marine life and ocean surface currents in the Cretaceous. Journal of Geology 81, p. 269-284.

Grimm, K.A., 2000, Stratigraphic condensation and the redeposition of economic phosphorite: Allostratigraphy of Oligo-Miocene shelfal sediments, Baja California Sur, Mexico, in Glenn, C.R., Prévôt-Lucas, L., and Lucas, J., eds., Marine authigenesis: from microbial to global: SEPM Special Publication no. 66, p. 325–347.

Grimm, K.A., Föllmi, K.B., 1994, Doomed pioneers: Allochthonous crustacean tracemakers in anaerobic basinal strata, Oligo-Miocene San Gregorio Formation, Baja California Sur, Mexico, Palaios 9, p. 313-334.

Haley, B.A., Klinkhammer, G.P., McManus, J., 2004, Rare earth elements in pore waters of marine sediments. Geochim. Cosmochim. Acta 68, p. 1265-1279.

Hancock, J.M., 1975, Petrology of the Chalk. Proc. Geol. Ass. 86, p. 499-535.

Hancock, J.M., 1990, Cretaceous. In: Introduction to the Petroleum Geology of the North Sea, 3rd edn (Ed. by K.W. Glennie), p. 255-272. Blackwell Scientific Publications, Oxford.

Hancock, J.M., Kauffman, E.G., 1979, The great transgressions of the Late Cretaceous. J. geol. Soc. Lond. 136, p. 175-186.

Haq, B.U., Hardenbol, J., Vail, P., 1987, Chronology of fluctuating sea levels since the Triassic. Science 235, p. 1156-1167.

Hart, M.B., 1976, The mid-Cretaceous successions of Orphan Knoll (North-west Atlantic): micropalaeontology and palaeo-oceanographic implications. Can J Earth Sci 13: 1411-1421.

Hart, M.B., 1990, Cretaceous sea level changes and global eustatic curves; evidence from SW England. Proc. Ussher Soc. 7, p. 268-272.

Heggie, D.T., Skyring, G.W., O'Brien, G.W., Reimers, C., Herczeg, A., Moriarty, J.W., Burnett, W.C., Milnes, A.R., 1990, Organic carbon cycling and modern phosphorites formation on the East Australian continental margin: an overview, in Noholt, A.J.G., Jarvis, I., eds., Phosphorite research and development, Geological Society of London Special Publication 52, p. 87-117.

Hess, R., 1989, Silica diagenesis: origin of inorganic and replacement cherts. Earth Science Reviews, 26, p. 253-284.

Hill, P.J., Jacobson, G., 1989, Structure and evolution of Nauru Island, Central Pacific Ocean, Australian Journal of Earth Sciences 36, p. 365-381.

Hoshino, M., Moritz, R., Ovtcharova, M., Watanabe, Y., Spangenberg, J., Putlitz, B., 2015. REE mineralization of the Blockspruit fluorite prospect, Bushveld granitic complex, South Africa: geochemical, mineralogical and fluid inclusion studies. In: Proceedings of the 13th Biennial SGA Meeting, "Mineral Resources in a Sustainable World", 2015, 2, p. 1513–1516.

Hughes, J.M., Cameron, M., Mariano, A.N., 1991. Rare-earth element ordering and structural variations in natural rare-earth-bearing apatite. Am. Mineral. 76, p. 1165–1173.

Ilyin, A.V., 1998, Rare-earth geochemistry of 'old' phosphorites and probability of syngenetic precipitation and accumulation of phosphate. Chemical Geology 144, p. 243-256.

Ilyin, A.V., Ratnikova, G.I., 1981, Primary, bedded, structureless phosphorites of the Khubsugul Basin, Mongolia, J. Sed. Pet. 51, p. 1215-1222.

Ingall, E.D., Bustin, R.M., Van Cappellen, P., 1993, Influence of water column anoxia on the burial and preservation of carbon and phosphorus in marine shales. Geochim. Cosmochim. Acta 57, p. 303-316.

Ito, J., 1968. Silicate apatites and oxyapatites. Am. Mineral. 53, p. 890–907.

Jarvis, I., 1992, Sedimentology, geochemistry and origin of phosphatic chalks: the Upper Cretaceous deposits of NW Europe, Sedimentology 39, p. 55-97.

Jarvis, I., 2006, The Santonian-Campanian phosphatic chalks of England and France. Proceedings of the Geologists' Association 117, p. 219-237.

Jarvis, I., Burnett, W.C., Nathan, Y., Almbaydin, F.S.M., Attia, A.K.M., Castro, L.N., Flicoteaux, R., Hilmy, M.E., Husain, V., Qutawnah, A.A., Serjani, A., and Zanin, Y.N., 1994, Phosphorite geochemistry—state-of-the-art and environmental concerns: Eclogae Geologicae Helveticae, v. 87, p. 643–700.

Jasinski, S.M., 2016, Mineral commodity summaries 2016: U.S. Geological Survey, p. 124-125, https://minerals.usgs.gov/minerals/pubs/commodity/phosphate_rock/mcs-2016-phosp.pdf

Kasakov, A.V., 1937, The phosphorites facies and the genesis of phosphorites, Trans. Sci. Inst. Fertil. Insecto-Fung. 142, p. 95-113.

Kim, K.H., Burnett, W.C., 1986, Uranium-series growth history of a Quaternary phosphatic crust from the Peruvian continental margin. Chem. Geol. 58, p. 227-244.

Kolodny, Y., 1983, Phosphorites. In: The Sea, Vol. 7 (Ed. by C. Emiliani), p. 981-1023. Wiley, New York.

Krajewski, K.P., Van Cappellen, P., Trichet, J., Kuhn, O., Lucas, J., Martin-Algarra, A., Prevot, L., Tewari, V.C., Gaspar, L., Knight, R.I., Lamboy, M., 1994, Biological processes and apatite formation in sedimentary environments, Eclogae geol. Helv. 87, p. 701-745.

Lamboy, M., 1976, Géologie marine et sous-marine du plateau continental au Nord-Ouest de L'Espagne. Genèse des glauconies et des phosphorites, Thèse Fac. Sc. Rouen, 285 p.

Lamboy, M., 1990a, Microbial mediation in phosphatogenesis: new data from the Cretaceous phosphatic chalks of northern France. In: Phosphorite Research and Development (Ed. By A.J.G. Notholt and I. Jarvis). Geol. Soc. Spec. Publ. London 52, p. 157-167.

Lamboy, M., 1990b, Microstructures of a phosphatic crust from the Peruvian continental margin: Phosphatized bacteria and associated phenomena. Oceanol. Acta 13, p. 439-451.

Lamboy, M., 1994, Nannostructure and genesis of phosphorites from ODP Leg 112, the Peru Margin. Mar. Geol. 118.

Lamboy, M., Monty, C., 1984, Bacterial origin of phosphatized grains (Abstr.). Terra Cognita 7, 207.

Lécuyer, C., Reynard, B., Grandjean, P., 2004, Rare earth element evolution of Phanerozoic seawater recorded in biogenic apatites, Chemical Geology 204, p. 63-102.

Lucas, J. Prévot, L., 1981, Synthèse d'apatite à partir de matière organique phosphorée (ARN) et de calcite par voie bactérienne. C.R. Acad Sc. Paris II 292, p. 1203-1208.

Martin, E.E., Scher, H.D., 2004, Preservation of seawater Sr and Nd isotopes in fossil fish teeth: bad news and good news, Earth and Planetary Science Letters 220, p. 25-39.

McArthur, J.M., Walsh, J.N., Rare-earth geochemistry of phosphorites. Chemical Geology 47, p. 191-220.

McConnell, D., 1973, Apatite Its crystal chemistry, mineralogy, utilization, and geologic and biologic occurrences, 111 pp.

McLennan, S.M., 1989. Rare earth elements in sedimentary rocks; influence of provenance and sedimentary processes. *Reviews in Mineralogy and Geochemistry*, *21*(1), pp.169-200.

Meybeck, M., 1993, C, N, P, and S in rivers: from sources to global inputs. In: R. Wollast, F.T. Mackenzie and L. Chou (Editors), Interactions of C, N, P and S Biochemical Cycles and Global Changes. NATO ASI Series, I4. Springer, Berlin, p. 163-193.

Monciardini,C., 1989, Profil “ECORS” nord de la France”: correlations biostratigraphiques entre quarante-six sondages sismiques intra-crétacé et implications structurales. Géol. France 4, p. 39-48.

Mortimore, R.N.,Gallagher, L.T., Gelder, J.T., Moore, I.R., Brooks, R., Farrant, A.R., Stonehenge—a unique Late Cretaceous phosphatic Chalk geology: implications for sea-level, climate and tectonics and impact on engineering and archaeology, Proceedings of the Geologists' Association, Volume 128, Issue 4, 2017, Pages 564-598,

Mullins, H.T., Rasch, R.F., 1985, Sea-floor phosphorites along the central California continental margin. Econ. Geol. 80, p. 696-715.

Nelson, G.J., Pufahl, P.K., and Hiatt, E.E., 2010, Paleoceanographic constraints on Precambrian phosphorite accumulation, Baraga Group, Michigan, USA: Sedimentary Geology, v. 226, p. 9–21.

O’Brien, G.W., Harris, J.R., Milnes, A.R., Veeh, H.H., 1981, Bacterial origin of East Australian continental margin phosphorites. Nature 294, p. 442-444.

O’Brien, G.W., Milners, A.R., Veeh, H.H., Heggie, D.T., Riggs, S.R., Cullen, D.J., Marshall, J.F., Cook, P.J., 1990, Sedimentation dynamics and redox iron-cycling: controlling factors for the apatite-glauconite association on the East Australian continental margin, Geol. Soc. London, Spec. Publ. 52, p. 61-86.

Picard, S., Lécuyer, C., Barrat, J.A., Garcia, J.P., Dromart, G., Sheppard, S.M.F., 2002, Rare earth element contents of Jurassic fish and reptile teeth and their potential relation to seawater composition (Anglo-Paris Basin, France and England). Chemical Geology 186, p. 1-16.

Piepgras, D.J., Jacobsen, S.B., 1992. The behaviour of rare earth elements in seawater: Precise determination of variations in the North Pacific water column. Geochim. Cosmochim. Acta 56, p. 1851-1862.

Piper, D.Z., Baedecker, P.A., Crock, J.G., Burnett, W.C., Loebner, B.J., 1988, Rare earth elements in the phosphatic-enriched sediment of the Peru Shelf. Marine Geology 80, p. 269-285.

Piper, D.Z., Medrano, M.D., 1995, Geochemistry of the Phosphoria Formation at Monpellier Canyon, Idaho: Environment of deposition. US Geol Surv, Bull, 2023-B: B1-B28.

Poels, J.P., Robaszynski, F., 1988, Les grains phosphates de la craie de Ciply (Maastrichtien, Belgique). Éléments d'interprétation pour la phosphatogenèse, Meded. Rijks Geol. Dienst 42, p. 51-75.

Pufahl, P.K., Groat, L.A., 2017, Sedimentary and Igneous Phosphate Deposits: Formation and Exploration: An Invited Paper. *Economic Geology* ; 112 (3): 483–516.

Pufahl, P.K., 2010. Bioelemental sediments. *Facies models*, *4*, pp.477-503.

Pufahl, P.K., and Grimm, K.A., 2003, Coated phosphate grains: proxy for physical, chemical, and ecological changes in seawater: Geology, v. 31, p. 801–804.

Reimers, C.R., Kastner, M., Garrison, R.E., 1990, The role of bacterial mats in phosphate mineralization with particular reference to the Monterey Formation, in Burnett, W.C., Riggs, S.R., eds., Phosphate deposits of the world, Volume 3, Neogene to Modern phosphorites: Cambridge, Cambridge University Press, p. 300-311.

Renard, A., Cornet, J., 1891, Recherches micrographiques sur la nature et l'origine des roches phosphatées, Bull. Acad. Roy. Belg. 3, p. 126-160.

Richard, J., 2005. Environmental and diagenetic records from a new reference section for the Boreal realm: The Campanian chalk of the Mons basin (Belgium). *Sedimentary Geology, 178*(1), pp. 99-111.

Riggs, S.R., 1979a, Petrology of the Tertiary phosphorites system of Florida, Econ. Geol. 74, p. 195-220.

Riggs, S.R., 1979b, Phosphorite sedimentation in Florida – a model phosphogenic system, Econ. Geol. 74, p. 285-314.

Robaszynski F., Martin M. (1988) Late Cretaceous Phosphate Stratiform Deposits of the Mons Basin (Belgium). In: Boissonnas J., Omenetto P. (eds) Mineral Deposits within the

Robaszynski, F., 1984, Les gisements de phosphates. Hainaut. In: Bartholomé, P. et al. (eds) Métallogénie de la Belgique, des Pays-Bas et du Luxembourg. Mém Expl Carte Métallogénique Europe et Pays Limitr UNESCO Paris, p. 174-180.

Robaszynski, F., Poels, J.P., Martin, M., 1988. Le gisement de craie phosphate de Ciply: données nouvelles. Bulletin de la Société belge de Géologie 97 (1), p. 9-24.

Roeder, P.L., MacArthur, D., Ma, X.P., Palmer, G.R., 1987. Cathodoluminescence and microprobe study of rare-earth elements in apatite. Am. Mineral. 72, p. 801–811.

Rønsbo, J.G., 1989. Coupled substitution involving REEs and Na and Si in apatites in alkaline rocks from the Illimaussaq intrusions, South Greenland, and the petrological implications. Am. Mineral. 74, p. 896–901.

Salama, W., El-Kammar, A., Saunders, M., Morsy, R., Kong, C., 2015, Microbial pathways and palaeoenvironmental conditions involved in the formation of phosphorite grains, Safaga District, Egypt. Sedimentary Geology 325, p. 41-58.

Schaffer, G., 1986, Phosphate pumps and shuttles in the Black Sea. Nature 321, p. 515-517.

Schenau, S.J., Slomp, C.P., De Lange, G.J., 2000, Phosphogenesis and active phosphorites formation in sediments from the Arabian Sea oxygen minimum zone. Mar. Geol. 169, p. 1-20.

Serret, A., Cabanas, M.V., Vallet-Regı´, M., 2000. Stabilization of calcium oxyapatites with lanthanum(III)-created anionic vacancies. Chem. Mater. 12, p. 3836–3841.

Shields, G., Stille, P., 2001, Diagenetic constraints on the use of cerium anomalies as palaeoseawater redox proxies: an isotopic and REE study of Cambrian phosphorites. Chemical Geology 175, p. 29-48.

Shields, G.A., Webb, G.E., 2004, Has the REE composition of seawater changed over geological time? Chemical Geology 204, p. 103-107.

Sholkovitz, E.R., Elderfield, H., 1988, The cycling of dissolved rare earth elements in Chesapeake Bay. Global Biogeochem. Cycles 2, p. 157-176.

Sholkovitz, E.R., Elderfield, H., Szymczak, R., Casey, K., 1999. Island weathering: River sources of rare earth elements to the Western Pacific Ocean. Mar. Chem. 68, p. 39-57.

Slansky, M., 1980. *Géologie des phosphates sédimentaires* (No. 114). Bureau de recherches géologiques et minières.

Soudry, D., 1992, Primary bedded phosphorites in the Campanian Mishash Formation, Negev, Southern Israel. Sedimentary Geology 80, p. 77-88.

Soudry, D., Lewy, Z., 1988, Microbially influenced formation of phosphate nodules and megafossil moulds (Negev, Southern Israel). Palaeogeography Palaeoclimatology Palaeoecology 64, p. 15-34.

Soudry, D., Nathan, Y., 2000, Microbial infestation: a pathway of fluorine enrichment in bone apatite fragments (Nagev phosphorites, Israel). Sedimentary Geology 132, p. 171-176.

Soudry, D., Southgate, P.N., 1989, Ultrastructure of a middle Cambrian primary nonpelletal phosphorites and its early transformation into phosphate vadoids: Georgina Basin, Australia, J. Sed. Pet. 59, p. 53-64.

Starinsky, A., Katz, A., Kolodny, Y., 1982, The incorporation of uranium into diagenetic phosphorites, Geochim Cosmochim Acta, 46, p. 1365-1374.

Stolpe, B., Guo, L., Shiller, A.M., 2013, Binding and transport of rare earth elements by organic and iron-rich nanocolloids in Alaskan rivers, as revealed by field-flow fractionation and ICP-MS. Geochim. Cosmochim. Acta 106, p. 446-462.

Suess, E., 1875, Die Entstehung der Alpen. Wein, 168 p.

Tlig, S., Sassi, A., Belayouni, H., Michel, D., 1987, Distribution de l'uranium, du thorium, du zirconium, du hafnium et des terres rares (TR) dans les grains de phosphates sedimentaires. Chem. Geol. 62, p. 209-221.

Trappe, J., 2006, Phanerozoic phosphorite depositional systems: a dynamic model for a sedimentary resource system (Vol. 76), Springer.

Trichet, J., Fikri, A., 1997, Organic matter in the genesis of high-island atoll peloidal phosphorites: The lagoonal link, Journal of Sedimentary Research 67, p. 891-897.

Tyson, R.V., Funnell, B.M., 1987, European Cretaceous shorelines, stage by stage. Palaeogeogr. Palaeoclim. Palaeoecol. 59, p. 69-91.

Van Cappellen, P., Berner, R.A., 1991, Fluorapatite crystal growth from modified seawater solutions. Geochim. Cosmochim. Acta 55, p. 1219-1234.

Van Cappellen, P., 1991, The Formation of Marine Apatite: A Kinetic Study. Ph. D. Thesis, Yale University.

Van Kauwenbergh, S.J., 2010, World phosphate rock reserves and resources, IFDC Publications, Technical Bulletin T-75, 48 p.

Vandycke, S., Bergerat, F., Dupuis, C., 1991, Meso-Cenozoic faulting and inferred palaeostresses in the Mons Basin, Belgium, Tectonophysics 192, p. 261-271.

Waychunas, G.A., 2002, Apatite luminescence. Reviews in Mineralogy and Geochemistry 48, p. 701-741.

Wright, J., Schrader, H., Holser, W.T., 1987, Paleoredox variations in ancient oceans recorded by rare earth elements in fossil apatite. Geochimica et Cosmochimica Acta 51, p. 631-644.

Zanin, Y.N., Zverek, K.V., Solotchina, E.P., 1990, Clay minerals and phosphorites genesis in the Upper Cretaceous of the northern Siberian platform. In: Phosphorite Research and Development (Ed. by A.J.G. Notholt, I. Jarvis), Spec. Publ. geol. Soc. Lond. 52, p. 223-235.

Ziegler, P.A., 1982, Geological Atlas of Western and Central Europe. Elsevier, Amsterdam, 130 p..